AUTONOMOUS GUIDANCE OF UNMANNED COMBAT AIR VEHICLES IN BASIC FIGHTER MANEUVERING

by

JEFFREY DEAN

Presented to the Faculty of the Graduate School of
The University of Texas at Arlington in Fulfillment
of the Requirements
for the Degree of

DOCTOR OF PHILOSOPHY

THE UNIVERSITY OF TEXAS AT ARLINGTON

December 2021

To my wife, Emilee, who gave me the confidence to accomplish this.

ACKNOWLEDGEMENTS

I would like to thank Professor Atilla Dogan for his guidance and support through this dissertation. His supervision helped me to refine the dissertation to a final product that I am proud to present, and his constructive criticism was invaluable. Additionally, I thank the rest of my dissertation committee: Professors Kamesh Subbarao, Bernd Chudoba, Animesh Chakravarthy, and Brian Huff.

I also need to thank the University of Texas at Arlington and the entire faculty of the Mechanical and Aerospace Engineering Department for supporting me as a distance student. There are still very few opportunities across the country to pursue a doctoral degree from a distance, particularly in such a complex field as aerospace engineering. The MAE Department at UTA was always helpful and accommodating to a very unique set of circumstances. I will be forever grateful to the support I received.

ABSTRACT

AUTONOMOUS GUIDANCE OF UNMANNED COMBAT AIR VEHICLES IN BASIC FIGHTER MANEUVERING

Jeffrey G. Dean, Ph.D.

University of Texas at Arlington, Arlington, 2020

Supervising Professor: Atilla Dogan

Basic fighter maneuvering, or BFM, is the dynamic engagement of two or more aircraft in close-range air combat. The relatively recent introduction of advanced unmanned combat air vehicles (UCAVs) has opened the possibility for automated systems to be players in this arena of air-to-air combat, which has thus far been limited to manned aircraft. In order to design an unmanned system that could fight and win a BFM engagement, the system must include an advanced system for guidance. This dissertation leverages techniques from gain scheduling and incorporates adjustable aimpoint guidance, in order to address the capability for UCAVs to execute autonomous BFM. It also redefines how success is measured for an autonomous fighter aircraft in BFM. Finally, this guidance method also incorporates a concept known as Vertical Energy-Maneuverability, which quantities an aircraft's specific power at various energy states when maneuvering nose high or nose low.

Table of Contents

List of Figures

List of Tables

Glossary of Terms

A/A	Air-to-Air
ATA	Antenna Train Angle
ATA_{ap}	Antenna Train Angle (Measured Fighter to Aimpoint)
ATA_{bdt}	Antenna Train Angle (Measured Fighter to Bandit)
α	Angle of Attack
BFM	Basic Fighter Maneuvering
BVR	Beyond Visual Range
C_{Dp}	Parasitic Drag Coefficient
D	Drag
E_s	Specific Energy
g	Gravity
γ	Flight Path Angle
h	Height (Altitude)
θ	Pitch
k_{nr}	Radial Acceleration Command Scheduling Factor
k_{φ}	Roll Command Scheduling Factor
$k_{\Delta v}$	Relative Velocity Command Scheduling Factor
MSL	Mean Sea Level
n_Z	Load Factor
n_{ZB}	Load Factor (Body Frame of Reference)
n_{ZR}	Load Factor (Radial Frame of Reference)
$n_{Z\,max}$	Maximum Load Factor
$\underline{r}_B$	Position Vector (Body Frame of Reference)
$\underline{r}_i$	Position Vector (Inertial Frame of Reference)
$\underline{r}_R$	Position Vector (Radial Frame of Reference)
$r_{i\,ap_{corr}}$	Aimpoint Correction (Inertial Frame of Reference)
$r_{ftr\text{-}bdt}$	Position Vector (Measured Fighter to Bandit, Fighter's Body Frame of Reference)
R	Radius
P_s	Specific Power
$\underline{\rho}$	Position Vector (Measured Aircraft to Control Zone)
S	Advantage
S_A	Angular Advantage
S_{BL}	Baseline Advantage
S_E	Energy Advantage
S_R	Range Advantage
t	Time
T	Thrust
T_a	Thrust Available
T_e	Excess Thrust
T_R	Roll Time Delay
TA	Target Aspect
T/W	Thrust-to-Weight Ratio
τ	Angle on Turn Circle (Measured Aircraft to Control Zone)

UCAV	Unmanned Combat Air Vehicle
V	Velocity
$V_{min\ vert}$	Minimum Vertical Airspeed
φ	Roll
W	Weight
WVR	Within Visual Range
ω	Turn Rate
ψ	Heading

1. INTRODUCTION

Since the first time that aircraft were used in combat for the purpose of gaining a military advantage, the world's armies and navies have each sought to maintain superiority in the sky. In the beginning of World War I, the primary purpose of military aircraft was observation and reconnaissance. By 1916, aircraft like the Fokker D.III were being specifically designed for air combat, with forward firing machine guns that were synchronized to avoid the forward-mounted propellers [1].

Fighter aircraft performance continued to increase dramatically between the two World Wars. By 1940, the fabric-winged biplanes of the early 20th century had been almost fully replaced by rigid-structure monoplanes like the Submarine Spitfire and P-40 Warhawk. As jet-powered aircraft became the norm in Korea and Vietnam, fighter pilots saw the first use of air-to-air missiles, which initially required the attacking aircraft to be behind the target [1]. Even as the weapons continued to become more advanced and allowed fighter pilots to shoot their adversaries in the forward-quarter, the highest probability of weapons effectiveness and follow-on employment of both guns and missiles has always been when the shooter was established in a stable position behind the target.

The future of air combat may very well include unmanned combat air vehicles, or UCAVs, which are currently limited to the roles of reconnaissance and air-to-ground strikes. But if UCAVs begin to fight in air-to-air combat like their currently-manned counterparts, then they will have to be designed with guidance and control laws based on the fundamental principles of Basic Fighter Maneuvering (BFM). A UCAV in this role will have to autonomously maneuver against the

adversary in order to gain a positional advantage and capitalize on weapons employment opportunities.

2. PROBLEM STATEMENT

The objective of this proposed dissertation is to develop a set of functional guidance laws for an autonomous fighter aircraft engaging in basic fighter maneuvering. How is this problem set unique? What makes autonomous BFM different than other autonomous systems in the world today? After all, computers have been beating humans at chess since the 1970s. But one big difference between a computerized chess game and autonomous BFM is that while chess is comprised of measurable and discrete players and movements, BFM can be conducted with an infinite number of starting conditions and aircraft trajectories. In other words, the game of chess is discretized, and each moment time can be viewed as a static condition. Other applications of autonomous systems are more dynamic and fluid, like BFM. For example, Google and Tesla have been designing and manufacturing self-driving cars for several years now. However, the autonomous control of self-driving cars is limited to a two-dimensional road surface, whereas BFM occurs in a three-dimensional sky. Even in the broad context of air warfare, some work has been done for air-to-air engagements, route planning, and cooperative UCAV swarming tactics. However, very little of this work directly addresses the performance, maneuverability, and guidance aspects that are specific to the dynamic, three-dimensional environment BFM. Therefore, autonomous BFM is still new territory to be explored.

3. BACKGROUND

1. Defining Basic Fighter Maneuvering

Fighter pilots have many different names for BFM. They sometimes call it air combat maneuvering, air-to-air (A/A) training, or dissimilar air combat training. Or for anyone who has seen the 1986 blockbuster movie *Top Gun*, it can be called 'dogfighting.' While the names may vary, the concepts remain relatively unchanged for fighter pilots flying combat aircraft. In order to keep terms consistent in this dissertation, the author will primarily use the term basic fighter maneuvering, or BFM.

What is BFM? BFM is defined here as the *aerial engagement of two high-performance combat aircraft in close proximity to one another*. The term *basic* refers to the fact that the engagement is between only two aircraft – the smallest number of aircraft that can oppose each other at any given time. The term *fighter* describes the type of aircraft involved – high performance combat aircraft, typically with a swept-wing configuration and high thrust-to-weight (T/W) ratio. Finally, the term *maneuvering* implies that when in close proximity to one another, the paramount factors in victory are the combination of aerodynamic performance and control of one aircraft relative to another.

This definition of BFM is deliberately specific, and it necessarily limits the scope of the discussion for the rest of the dissertation. This discussion of BFM does not cover supersonic intercepts, multi-plane scenarios, or long-range engagements. These scenarios are intercept problems and do not involve maneuvering in close proximity. There is also no room for discussion about any unmanned aerial vehicles that do not have the size and speed to carry munitions in sufficient capacity to threaten or affect other modern fighter aircraft.

2. Importance of Autonomous BFM for Future UCAVs

With the advance of modern, all-aspect, long-range missiles like the AIM-120 Advanced Medium Range Air to Air Missile (AMRAAM), is BFM obsolete amongst current fighter aircraft? Many people believe so. Contrary to such opinions however, BFM remains as important as ever for two reasons. First, many modern air power tacticians assume that the identification of aircraft as friend or foe will occur beyond visual range (BVR). The problem with this assumption is that the identification process relies exclusively on electronic identification capabilities and techniques, which are increasingly fragile with modern airborne systems [2]. And once the BVR identification process breaks down, fighter pilots are forced into within visual range (WVR) in order to identify aircraft before employing weapons. If the aircraft are WVR, then they are in a BFM engagement. The second reason that BFM remains important is that many air forces have learned throughout history of the failure of relying on BVR weapons. Since the implementation of radar guided air-to-air (A/A) missiles during the Vietnam War, through the Yom Kippur War, to Desert Storm and beyond, radar guided missiles (the only missiles even capable of being employed BVR) have only comprised of 17% of all weapons employment. The remaining 83% consisted of guns and heat-seeking missiles WVR. The small numbers of BVR weapons employment opportunities have historically averaged a probability of kill between 0-25% [3]. Overall, BVR engagements have failed to realize their advertised capabilities due to either lack of identification at extended ranges, or insufficient BVR missile performance. WVR engagements, along with the BFM principles required to defeat an adversary in a close-in A/A fight, will thus remain important for the foreseeable future.

While the proliferation of BVR weapons have failed to yield successful results, one area of combat aviation that has seen drastic improvements in recent years is UCAVs. The United States

Department of Defense currently has over 100 different types of UCAVs in its inventory, ranging in all shapes and sizes [4]. The vast majority were designed for intelligence, surveillance, and reconnaissance. Some are even armed with air-to-ground weapons. Thus far, none of the currently fielded UCAVs have been designed for A/A combat, even though that day will likely come. As it stands now, UCAVs have zero lethality against other airplanes and are equally defenseless to any A/A attacks. This was made evident by the downing of a Georgian UCAV by a Russian MG-29 in 2008, shown in Figure 1 below.

Figure 1.Russian MiG-29 Shooting Down a Georgian UCAV [5]

In the case above, the Georgian UCAV clearly lacked survivability against a manned adversary. When considering future UCAV designs, lethality – the ability to offensively engage enemy aircraft – will likely become just as important as survivability. Several concept of operations for future fighter aircraft designs include either an unmanned system or a pilot-optional system. But in order for either of these concepts to be effective for a military use, they must have a significant

Figure 2. Artist Rendition of 6th Generation Fighter Concept

capability for both survivability and lethality. In other words, they must be able to survive in a hostile environment and shoot down enemy aircraft.

Some UCAVs are beginning to take the form of either “loyal wingman” or “pilot-optional” fighter aircraft [6]. This concept has the potential to provide task relief to a manned flight lead aircraft in a fighter role. The concept has been demonstrated by different agencies of both industry and government [7], [8].

Two conclusions can be drawn from arguments made in this dissertation up to this point: a) BVR employment will remain a minority percentage of successful A/A engagements, and b) future UCAVs will be required to maintain lethality and survivability against other aircraft. Given these two assertions, future UCAVs must be designed and built with the capability to execute BFM. This requires the development of a set of autonomous guidance laws, leveraging a complete understanding of BFM principles.

3. Fundamentals of BFM

BFM is sometimes a difficult concept to understand, and even more difficult to master. Current fighter pilots may spend at least 500 to 1,000 hours in fighter aircraft before they are qualified to instruct BFM [9]. That relegates the available pool of knowledge to only a select group of pilots that come almost exclusively from a military background.

Without going into all the details of BFM, it is important for this dissertation to at least identify key principles. Below are some concepts and definitions required for an introductory understanding:

1. *Types of BFM*

BFM can be broken down into two categories: offensive BFM and defensive BFM. As the name implies, the primary objective of offensive BFM is to kill the opposing aircraft, referred herein as the 'bandit', by arriving at the proper position and angle in order to employ some type of weapon. The primary objective of defensive BFM is to survive by preventing the bandit from being able to employ weapons. The difference between offensive and defensive BFM is important, because it determines what strategy is most appropriate. Determining whether a fighter is in offensive or defensive BFM is based on a number of relative factors between the two aircraft, including energy advantage, angular advantage, and performance capability. Figure 3 illustrates this concept. In this figure, and throughout the remainder of the dissertation, the 'fighter' (friendly aircraft) is depicted in blue, and the 'bandit' (target aircraft) is depicted in red. The captions and observations for discussion are always centered around the fighter's frame of reference.

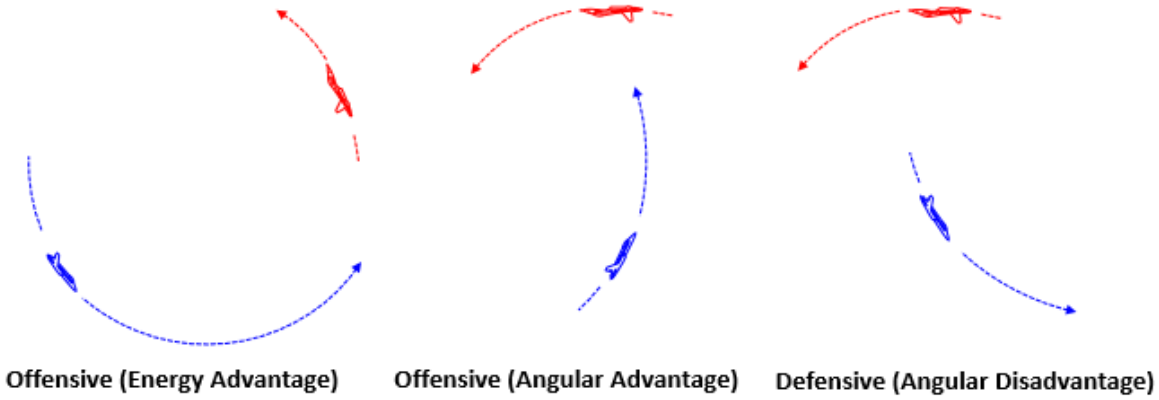

Figure 3. Examples of Offensive vs. Defensive BFM

2. *Antenna Train Angle and Target Aspect*

The angular relationship between the fighter and the bandit are defined by the antenna train angle (ATA) and target aspect (TA). The antenna train angle is the angular measurement from the

fighter's nose, to the bandit. The name is derived from the position of a radar antenna trained on its target. Target aspect (TA) is the angular measurement from the bandit's tail (or nose), to the fighter. Convention is important when defining TA. The convention of the United States Air Force is that 0° TA is defined off the bandit's tail [10]. The convention of the United States Navy is to define 0° TA off the bandit's nose [11]. The former definition is more widely adopted by other air forces, and will be used throughout the remainder of this dissertation. Setting 0° TA off the bandit's tail also simplifies the concept of defining offensive versus defensive BFM. Generally speaking, lower ATA and TA equate to an angular advantage (offensive), while higher ATA and TA equate to an angular disadvantage (defensive). Figure 4 below shows these concepts.

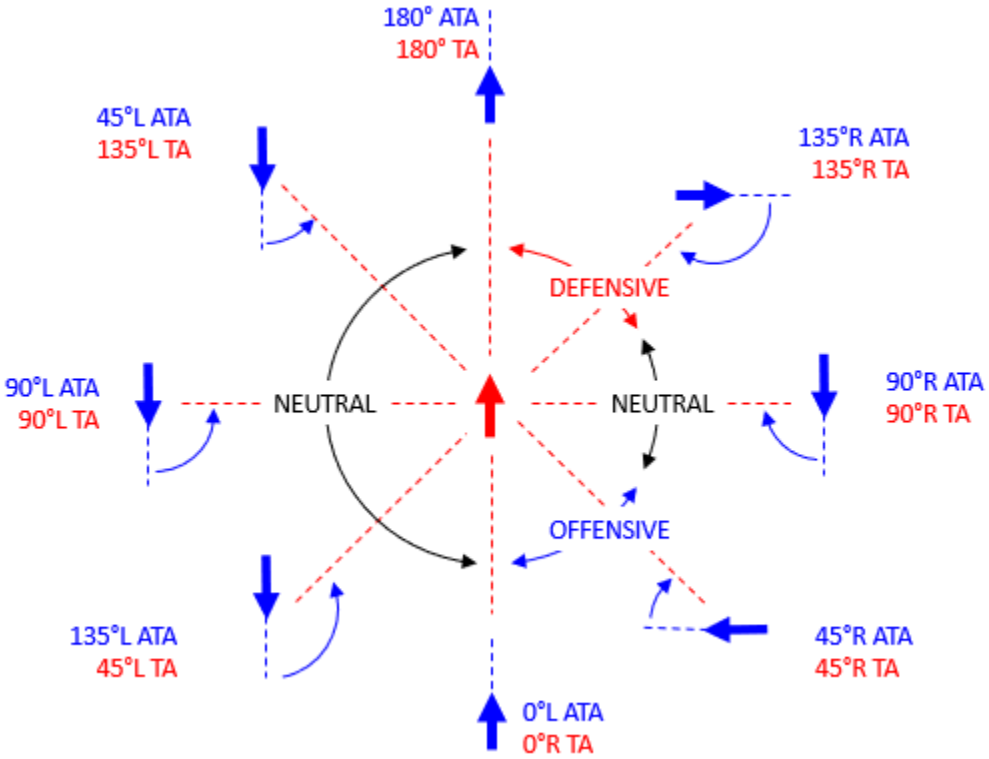

Figure 4. Antenna Train Angle and Target Aspect

3. *Turn Circle*

The turn circle is the invisible arc that an aircraft scribes through the sky given its orientation, airspeed, and load factor [11]. A slow aircraft that is able to generate a high load factor will have a small turn circle. Conversely, a fast aircraft or an aircraft that is unable to generate as much load factor will have a larger turn circle. A maximum performance turn circle occurs at either the maximum load factor (at higher airspeeds) or minimum turn radius (at lower airspeeds). The threshold between high airspeed and low airspeed is called the corner airspeed, which will be explained further below.

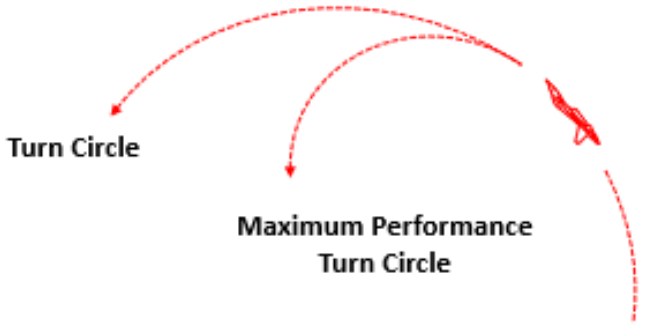

Figure 5. Turn Circle and Maximum Performance Turn Circle

One big takeaway is that whenever the fighter is established inside the bandit's maximum performance turn circle, that space is protected exclusively for the fighter. See Figure 6. It is a physical impossibility for the bandit to turn inside of his maximum performance turn circle. Therefore, the fighter should prioritize this opportunity to turn aggressively while inside the protected space. Outside of the maximum performance turn circle, the fighter should generally prioritize energy conservation over position (or angular) advantage. Inside of the bandit's

maximum performance turn circle, the fighter should generally prioritize position (or angular) advantage over energy conservation.

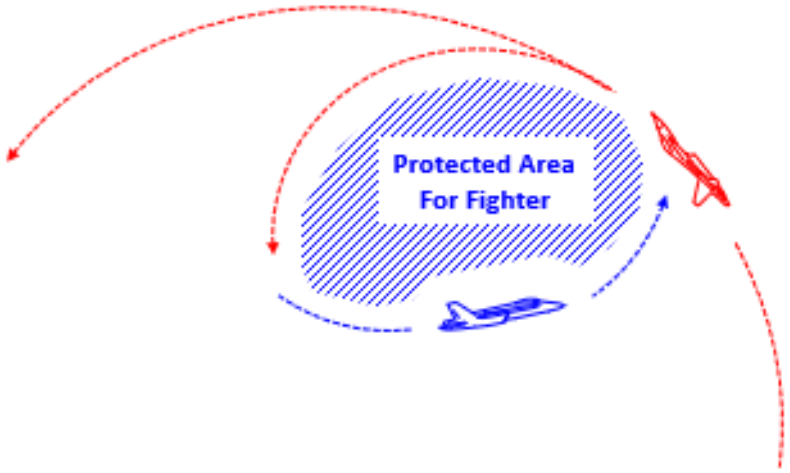

Figure 6. Protected Space Inside the Maximum Performance Turn Circle

4. *Control Zone*

The best place to maintain a positional and angular advantage is within an invisible, three-dimensional volume behind the bandit called the control zone. The position of the control zone's location behind the bandit varies with the fighter's weapons and the adversary's airspeed and load factor. Without getting into the multiple types and variants of weapons available, the control zone is located approximately at a distance of 1-2 times the bandit's minimum turn radius, and is longitudinally centered and symmetrical about the bandit's turn circle [11]. The reason the control zone is important in BFM is because once the fighter is stable inside the bandit's control zone, there is little that the bandit can do to deny a positional advantage to the fighter. Therefore, an offensive BFM strategy typically focuses on rendezvousing in the bandit's control zone, while a

defensive BFM strategy focuses on keeping the fighter's control zone as far away from the adversary as possible [10], [11], [12].

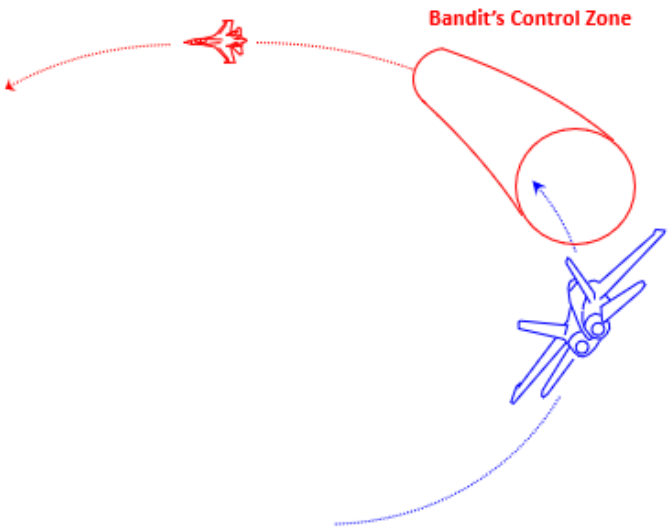

Figure 7. Control Zone

5. *Types of BFM Flow*

BFM can be broken down into three distinct types of flow: 1-circle flow, 2-circle flow, and out-of-plane flow.

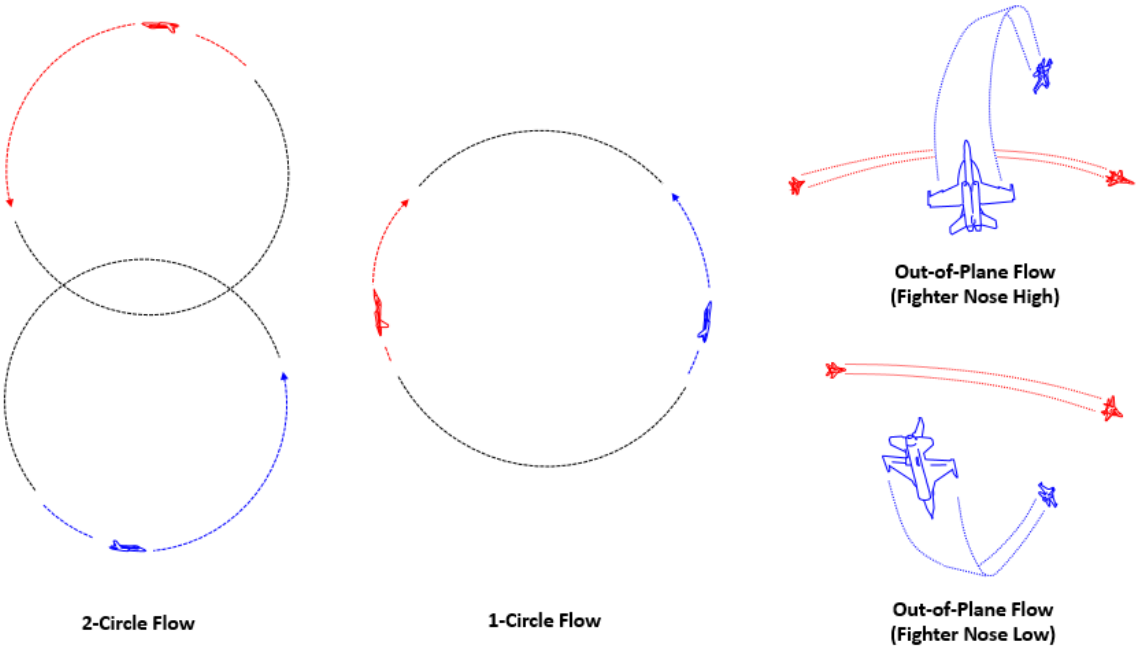

Figure 8. Types of BFM Flow

In 1-circle flow, the aircraft are turning different directions, i.e. one is turning left, while the other is turning right. This normally results in the aircraft being much closer to each other during the fight, while the aircraft appear to be flying opposite directions on the same turn circle. In 1-circle flow, relative turn radius is most important. Turn radius is defined by:

$$R = \frac{V^2}{a} \tag{1}$$

where R = radius, V = velocity, and a = acceleration.

Figure 9 shows why turn radius is paramount in a 1-circle fight. Assuming that the fighter and the bandit start abeam each other, and that the fighter has a smaller turn radius, the fighter can turn towards the bandit (decrease ATA) with less forward travel. This gives the fighter a predominantly positional advantage. As the bandit flushes out in front of the fighter, the fighter can then reverse its turn, again with a smaller turn radius than the bandit's, to decrease TA. This gives the fighter an angular advantage.

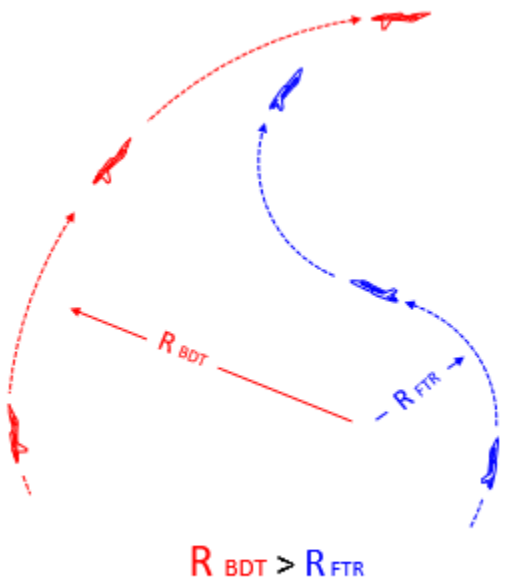

Figure 9. Turn Radius Advantage with 1-Circle Flow

The opposite of 1-circle flow is 2-circle flow, which occurs when both aircraft are turning the same direction – either both are turning left or both are turning right. In a neutral engagement, this often causes the aircrafts' individual turn circles to be displaced from each other. In 2-circle flow, relative turn rate is most important factor in achieving an advantage. Turn rate is defined by:

$$\omega = \frac{V}{R} \tag{2}$$

where ω is the turn rate.

Figure 10 shows the importance of turn rate in a 2-circle fight. Assuming the fighter can maneuver through more degrees of turn than the bandit in a given amount of time, the fighter's nose will come to bear on the bandit first. This can increase an angular advantage.

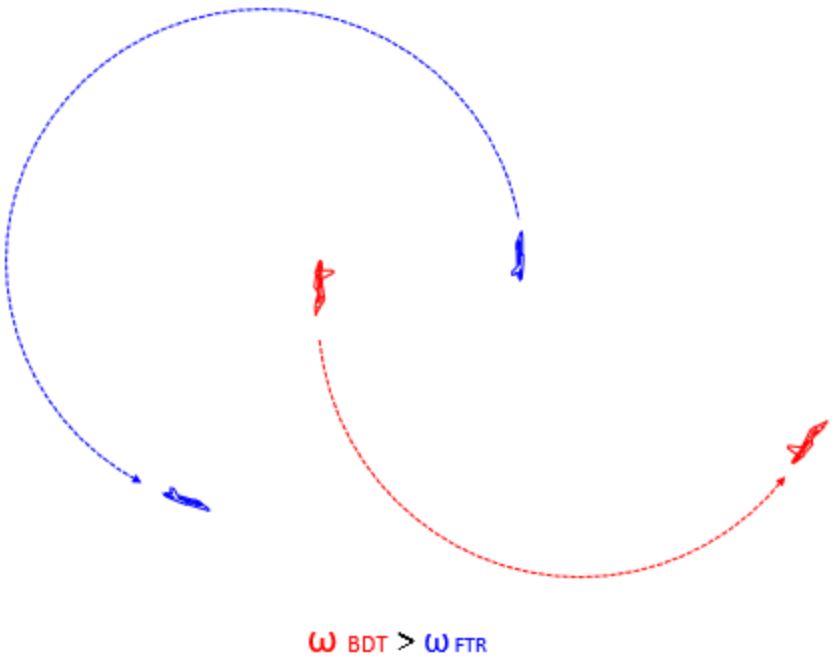

Figure 10. Turn Rate Advantage in 2-Circle Flow

The last type of BFM flow is out-of-plane flow, which can be any combination of nose high vs. level, nose low vs. level, or a flow with a significant oblique component.

6. *Pursuit Curves*

Three types of pursuit curves exist: lead, pure and lag. Each type of pursuit serves a different purpose. See Figure 11.

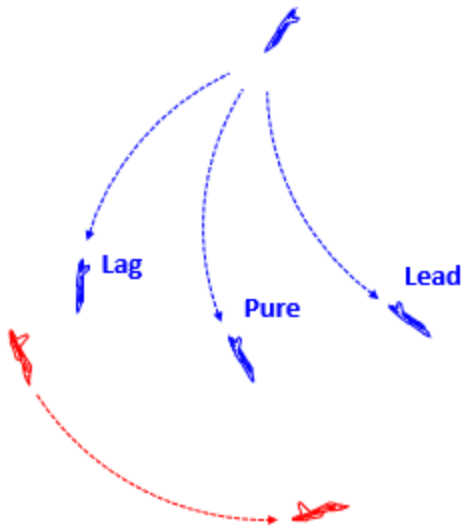

Figure 11. Lead, Pure, and Lag Pursuit

Lead pursuit is when the fighter's projected flight path is in front of the bandit. Maintaining lead pursuit causes the range to rapidly decrease without regard to angles between the fighter and bandit. This is generally used in one of two cases. First, lead pursuit can be used for shooting a forward-mounted gun or cannon. Second, it may be used in defensive BFM to create a range, angles, and closure problem for the bandit [11].

In pure pursuit, the fighter's projected flight path points directly toward the bandit. Like lead pursuit, pure pursuit also decreases range and create an angles problem for the fighter if maintained too long [11]. When picking a pursuit curve however, pure pursuit is a good starting point if no clear offensive or defensive roles have been established, or in order to quickly get into the bandit's turn circle.

Lag pursuit is when the fighter's projected flight path points aft of the bandit. Lag pursuit is used to maintain an offensive advantage and prevent range from decreasing (and angles from increasing) too rapidly. Pilots call this "managing the range, angles and closure problem." [11].

7. *Energy-Maneuverability Diagram*

One of the most important planning tools fighter pilots have in BFM is the Energy-Maneuverability (EM) Diagram. The EM Diagram provides a snapshot of an aircraft's specific energy (P_s), overlaid on a plot of aircraft velocity (V) versus turn rate (ω). Additionally, an aircrafts's maximum load factor ($n_{z\,max}$) and minimum turn radius (R_{min}) are depicted.

For a given aircraft in a standard atmosphere, each EM Diagram is constructed by assuming four constants: constant weight, constant drag index or parasitic drag coefficient (C_{Dp}), constant throttle setting, and constant altitude [13]. The constant weight is determined primarily by bare airframe design, fuel, and loadout. For example, fuel can be assumed to be either 50% or 75% of internal fuel, and loadout can be a specific combination of stores and weapons, like two A/A missiles and a full complement of gun rounds. A constant parasitic drag coefficient for each aircraft is determined exclusively by the loadout of external stores. Constant throttle setting usually implies either maximum rated thrust (afterburner) or military rated thrust (non-afterburner), but must be specified either way. Constant altitude is usually a tactically significant altitude, and multiple EM Diagrams can be produced to reflect aircraft performance at various altitudes. For example, a pilot might choose to produce EM Diagrams at 5,000 ft above mean sea level (MSL), 15,000 ft MSL, and 25,000 ft MSL.

The *x*-axis of the EM Diagram shows the aircraft velocity. This is usually in either ft/sec, knots true airspeed (KTAS), or knots calibrated airspeed (KCAS). The *y*-axis of the EM Diagram shows aircraft turn rate, usually in deg/sec. Embedded within the EM diagram are lines of constant turn

radius (R) and constant load factor (n_z) [14]. These lines are calculated from the relationship of V and ω using Eqs. (2) and (4) from earlier in this section.

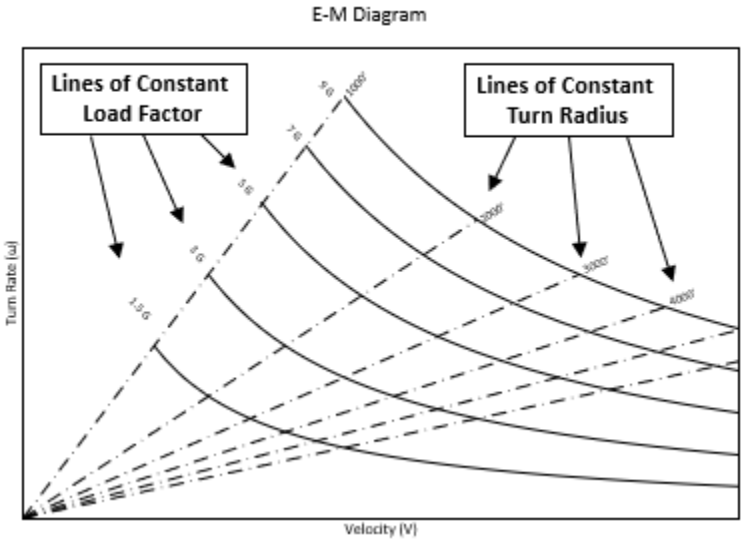

Figure 12. Blank EM Diagram

The specific power (P_s) is the change in specific energy (E_s) over time. Specific energy is the total mechanical energy (potential plus kinetic) per unit weight. Specific energy and specific power can be written as follows:

$$E_s = h + \frac{V^2}{2g} \tag{3}$$

$$P_s = \frac{dE_s}{dt} = \frac{dh}{dt} + \frac{V}{g}\frac{dV}{dt} \tag{4}$$

$$P_s = \frac{(T_a - D)V}{W} = \frac{T_e V}{W} \tag{5}$$

where:

h = Altitude

T_a = Thrust Available

T_e = Excess Thrust

D = Drag

W = Weight

By knowing the performance of a given aircraft, the P_s gradient can be overlaid onto an EM diagram. Figure 13 below shows an actual EM diagram of an F-15C Eagle [14]. Note the four constants listed in the legend in the top right: constant weight (40,095 lbs), constant drag index (23.80), constant throttle setting (maximum afterburner), and constant altitude (10,000 feet).

The P_s gradient loosely resembles the shape of a doghouse, albeit lopsided. Hence the EM diagram is affectionately known to fighter pilots as a "doghouse plot." In addition to the P_s gradient, other specific performance information can be derived from the doghouse. The right side of the doghouse is the maximum velocity, which is limited by dynamic pressure, q. The top right of the doghouse roof is the load factor limit, or $n_{z\,max}$, which is 7.33 G's in this case. The top left of the doghouse roof is the lift limit of the aircraft. The minimum turn radius occurs along the top left portion of the doghouse.

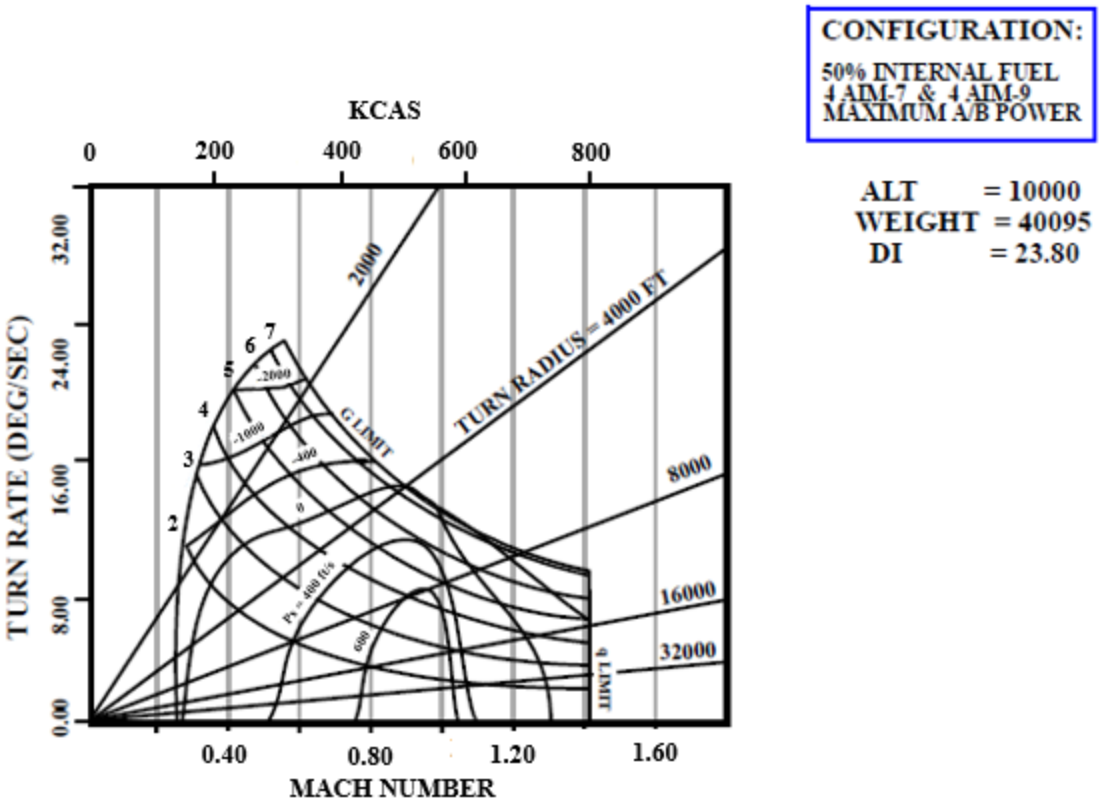

Figure 13. EM Diagram, F-15C at 10k ft [14]

At the top of the doghouse is the airspeed at which an aircraft simultaneously has both a maximum load factor and a minimum turn radius available. This is called the corner airspeed. This is normally not a static point, as most aircraft will suffer significant energy bleed rates at the corner airspeed with maximum load factor. In Figure 13 above, the F-15C's corner airspeed at this altitude and configuration occurs at approximately 310 KCAS (0.55 Mach), and the instantaneous turn rate is 23 deg/sec. But at this point, the loss of specific energy is greater than 2000 ft/sec!

Also note that above corner airspeed, the sustained turn rate is usually higher, and a 2-circle fight is usually more advantageous. The maximum sustained turn rate occurs at approximately 480 KCAS (0.87 Mach), at 15 deg/sec. While areas of positive P_s exist on both sides of corner

airspeed, as velocity increases, the area of maximum specific power resides to the right of corner airspeed. This is another characteristic of almost every fighter aircraft – increased velocity allows for an even greater rate of increase in energy (up to the point of transonic conditions). As velocity decreases below corner airspeed, the turn radius can be minimized, and a 1-circle fight is usually more advantageous. The minimum sustained turn radius of the F-15C depicted here occurs at approximately 220 KCAS (0.34 Mach), at a turn radius of 2200 feet.

8. *Vertical Energy-Maneuverability*

Vertical energy-maneuverability (VEM) is the analysis of the relationship between an aircraft's potential and kinetic energy, versus its maneuvering performance. This relationship is not widely understood among the fighter pilot community, but the concept has been developed and introduced previously through the author's original work. (This entire section is heavily derived from the author's work in reference [13].) The result is a more thorough understanding of energy advantage/disadvantage between different fighter aircraft.

While the EM Diagram is an analysis at a constant altitude, the VEM diagram is an analysis of fighter maneuvers in the vertical plane, i.e. pure nose high or pure nose low. In order to do this, the underlying assumptions are changed. Three of the four constants – thrust, weight, and configuration – still apply. The assumption of constant altitude however, is changed to an assumption of constant specific energy. (Obviously a vertical maneuver requires, by definition, a change in altitude.) But because aerodynamic performance is also a function of altitude, the assumption of constant specific energy requires to identify a specific starting point of kinetic and potential energy – a baseline altitude and velocity from which to analyze a vertical maneuver. An energy gradient plot on a diagram of altitude versus velocity shows this relationship. This is called

an h-V diagram, which includes lines of constant specific energy (E_s). A generic example is shown in Figure (14) below.

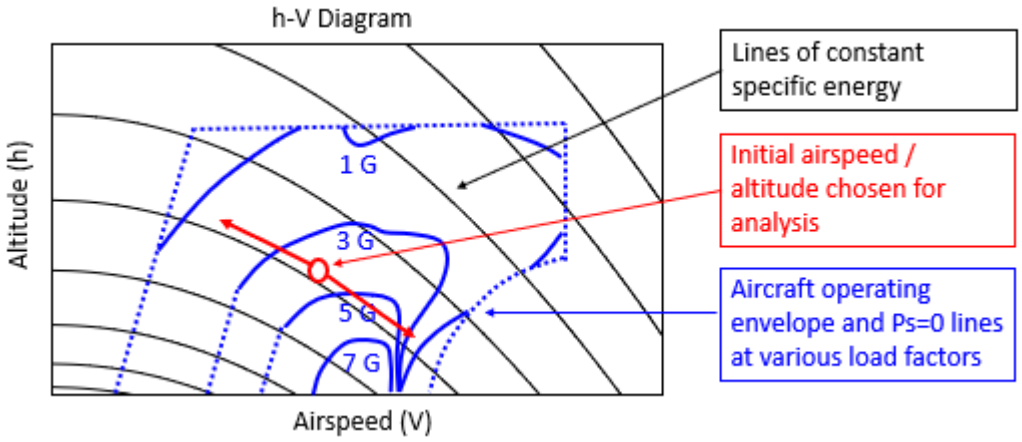

Figure 14. Generic h-V Diagram

By knowing the relationship between angular velocity (ω), flight path angle (γ), velocity (V), and load factor (n_z) at any time stamp (t_i), a template is created for the VEM diagram.

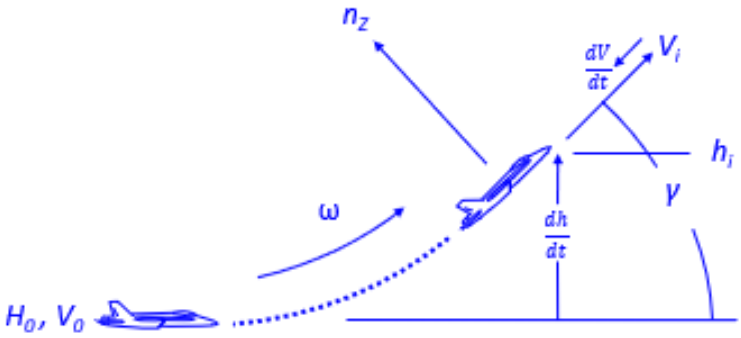

Figure 15. Vertical Maneuvering Relationships

$$\omega = \frac{g \cdot (n_z - \cos\gamma)}{V_i} \tag{6}$$

$$\frac{dh}{dt} = V_i \cdot \sin\gamma \tag{7}$$

$$\frac{dV}{dt} = -\frac{g}{V_i}\frac{dh}{dt} \tag{10}$$

In the VEM diagram, the trace of constant specific energy is represented by both altitude on the left and velocity on the right. On the bottom is a scale of load factor. Turn rate is also represented on the graph. The "sawtooth" effect on the lines of constant ω is a result of gravity's effect on radial acceleration. When pulling nose up, φ is assumed to be zero (wings level), and the radial acceleration (n_r) is less than the load factor (n_z). When pulling nose low, the aircraft is assumed to be at $\varphi = 180°$ (inverted), and therefore has the added assistance of gravity to increase the turn rate. Using Eqs. (8) through (10), it is possible to determine the total change in the flight path angle, γ. See Figure 16 below. In this case, the starting point of analysis is at 15,000 ft and 450 knots calibrated.

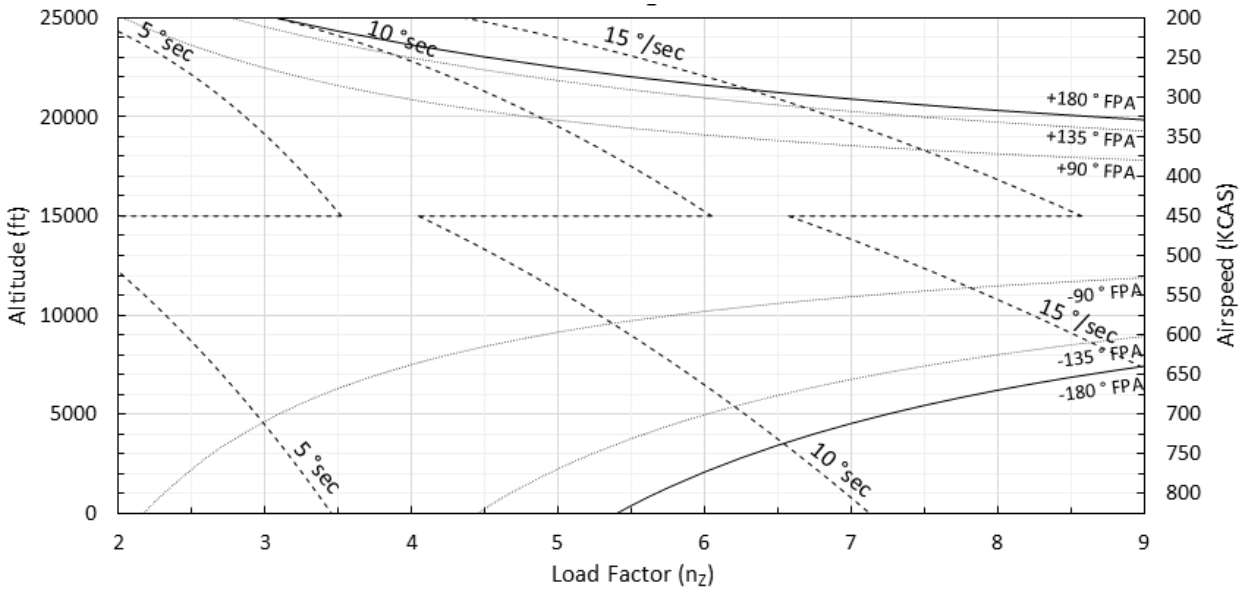

Figure 16. Blank VEM Diagram

By including a P_s gradient on the VEM diagram, aircraft performance can be evaluated along a domain of maneuvers at a constant specific energy. See Figure 17 for a notional fighter. (Actual VEM performance data can be derived from flight test data, but VEM diagrams are not yet readily available across multiple aircraft types.) Domains of positive, negative, and zero P_s are evident, as well as corner airspeed and load factor limits. In order to show some variation from the previous example, the initial conditions for the following diagram was 350 KCAS and 20,000 ft MSL. The P_s gradient of a notional fighter is shown in blue, and the P_s gradient of a notional bandit is shown in red.

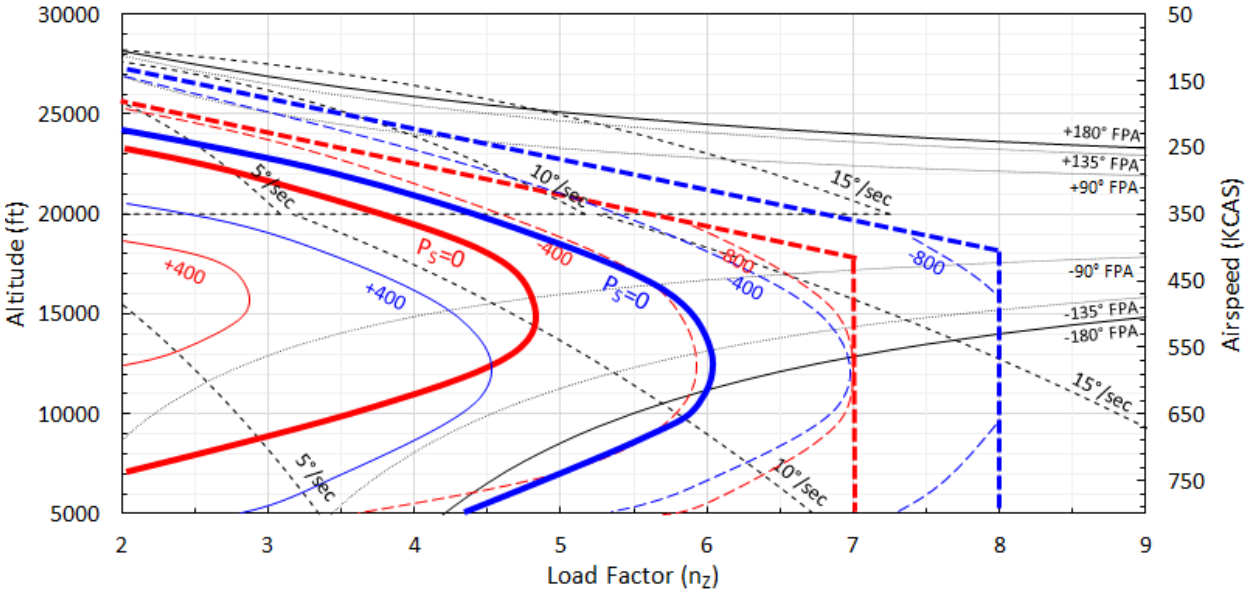

Figure 17. VEM Diagram w/ Notional Ps Data

One important piece of information that comes from the data on the VEM diagram is the minimum vertical airspeed ($V_{min\ vert}$). This is the lowest airspeed that an aircraft can execute a pure nose-high maneuver to 180° pitch attitude from a wings level starting position. It includes a specific margin of specific energy available throughout the maneuver. Anytime the fighter can execute a nose-high maneuver while the bandit cannot, this vertical turning room becomes a

protected area for the fighter, and vice versa. The importance of this concept will become evident in further sections on solution development. A more complete description of deriving the minimum vertical airspeed is available in reference [13].

4. LITERATURE SURVEY

The literature survey for this topic has four essential pillars. The first pillar is built by knowledge and understanding of basic fighter maneuvering. This includes much of the history of air warfare, basic concepts, definitions, and tactics – both old and new – that fighter pilots have used to achieve victory in air-to-air combat. These references are a combination of historical accounts of air combat and current military fighter pilot training manuals. The second pillar is built by works that fall outside the specific scope of the problem statement, but nonetheless contribute to the solution development. These works generally include multiple engineering topics from flight dynamics and aircraft design; to areas of guidance, navigation, and control; gain scheduling; and even fuzzy logic and game theory application. The third pillar is built by analyzing previous attempts to solve the problem of autonomous basic fighter maneuvering. Analyzing the full scope of other peoples' efforts achieves three important effects: one, previous successes can be leveraged and expanded upon. Two, previous failures can be identified and either avoided or improved upon. And three, the project as a whole can be validated against the criterion of "original contribution" by conducting a thorough literature survey of the topic. The fourth pillar is a survey of references that support accurate modeling and simulation. Figure 18 below is a graphical depiction of how this literature survey is organized.

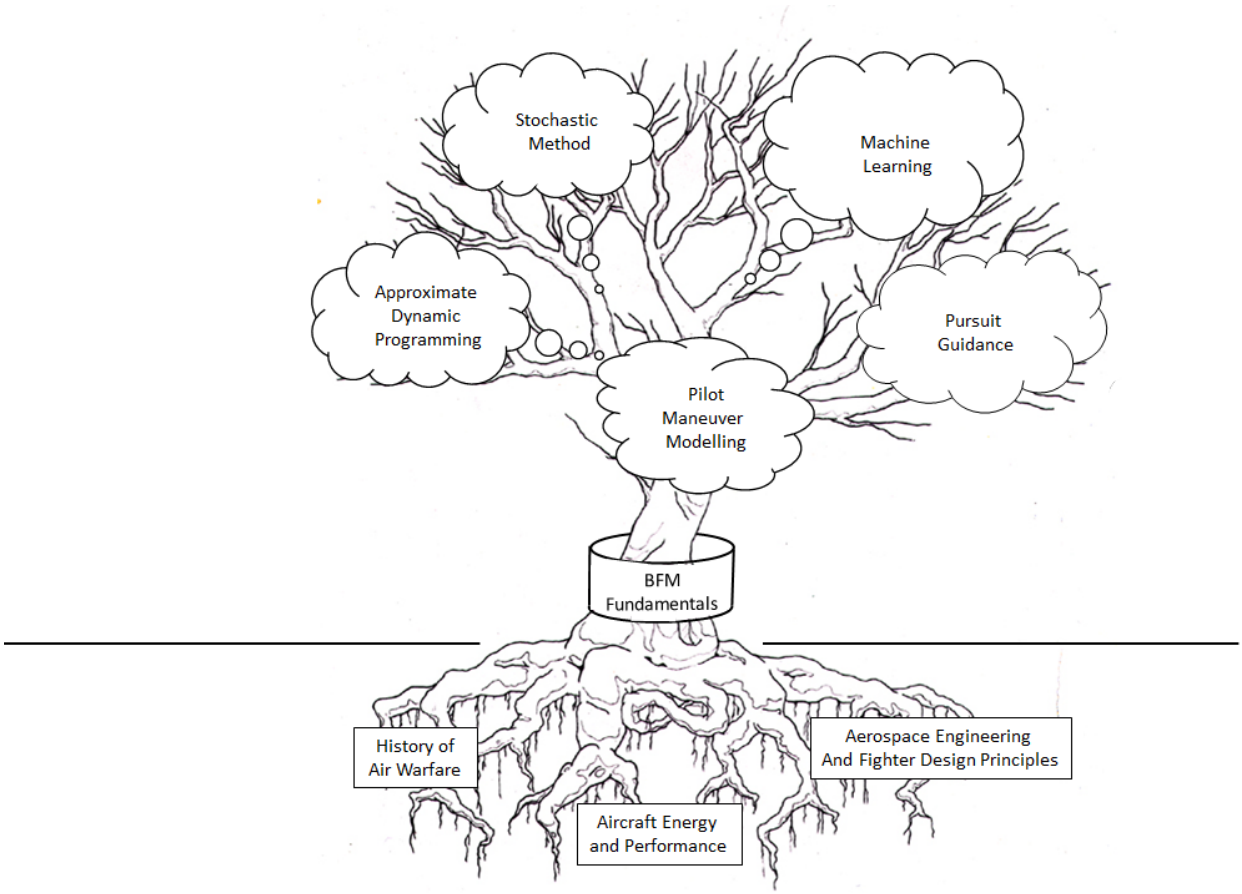

Figure 18. Organization of Literature Survey

Each of these four pillars has a collection of references to support it, and many of the cited references even overlap between pillars or cross-reference others. For example, reference [14] covers topics such as aircraft specific energy, specific power, and the Energy-Maneuverability Diagram. These topics are most appropriate in the first pillar of BFM fundamentals, but their application overlaps well into the second and fourth pillars. Other references that cover BFM fundamentals are often cited by works in the third pillar – proposed solutions to autonomous BFM.

Finally, this organization is arbitrary. In the end, the organization of the literature survey does not matter, so long as the literature survey accomplishes two main objectives: 1) sufficiently aids in solution development, and 2) adequately verifies the work's original contribution. However,

the author's division of the literature survey does make it easier to analyze each group of references in closer detail.

1. The First Pillar: BFM Fundamentals

The annals of air combat maneuvering are as old as the combat plane itself. Historical documents and training manuals can be traced back to the early twentieth century. And amazingly, since the invention of the interrupted forward-firing machine gun in 1915, the basic principles of BFM have not significantly changed. Baron von Richtofen, a.k.a. "The Red Baron," was taught by German pilot Oswald Boelke. Even as early as 1913, Boelke was quoted as saying "get in behind your enemy … get close before pulling the trigger, … and once engaged, remain committed to the battle" [12]. But what does the tactics of the Red Baron have to do with autonomous BFM?

When it comes to solving the problem of autonomous BFM, the purpose of studying BFM fundamentals is two-fold. First, the knowledge of BFM fundamentals helps to properly define the general objectives and environment of BFM. Otherwise, it would be like developing an autonomous driving car without knowing the rules of the road and traffic laws. The second reason that studying BFM fundamentals is important is because it helps eliminate regions of altitude, airspeed, and aircraft maneuvers that are inconsequential to a fighter's success in BFM. Therefore, the design space can be appropriately bounded before solution development begins.

The primary source references for understanding the BFM objectives and environment are a combination of several historical studies, a limited number of specific textbooks, and a variety of current military training manuals. Historical studies include studies and accounts of air combat through different air campaigns and battles. Keith Ayling, Edward Sims, and Major "Boots" Blesse were combat pilots in World War I [15], World War II [16], and Korea [12] respectively.

Each wrote their own contribution to air combat and BFM doctrine. The United States Department of Defense's Gulf War Air Power Survey accounted for air combat in Operations Desert Storm and Desert Shield [17].

Shaw's *Fighter Combat: Tactics and Maneuvering* [18] and Bonanni's *The Art of the Kill* [19] are the most relevant texts specific to BFM. Additionally, there are supporting references, like the *Energy* text from the U.S. Air Force Test Pilot School Syllabus, which are broader in scope, but still include very important background information [14]. Aircraft energy is fundamental to BFM because it describes the relationship of potential and kinetic energy per unit mass in the atmosphere, which is also directly related to turn rate and maneuverability (see Section 3.3.7 and 3.3.8). But the seminal work in aircraft energy management is widely viewed as *Energy Approach to the General Aircraft Performance Theory*, by Edward Rutowski [20]. This work is important because other works are heavily derived from Rutowski. In the 1960s, U.S. Air Force Colonel John Boyd extrapolated from Rutowski in order to create the Energy-Maneuverability Theory. Then-Captain Boyd's work even included his own treatise on specific BFM tactics and maneuvers [21]. Boyd's contribution was unique, because he uniquely combined his physical theories with his own vast experience as a fighter pilot. In the decades that followed Rutowski and Boyd, other academic contributions attempted to quantify fighter metrics via different means. David Johnson in 1972 tried to quantify metrics like throttle transient and climb rate as a way to compare relative fighter performance advantage [22]. Lane et al in 1982 evaluated results from multiple dogfight simulation scenarios in an attempt to find functional specifications for relevant performance measurements, but admitted the results were inconclusive [23]. And like Johnson, Paranjape et al searched for outlying parametrics, like roll reversal timing, power onset rate, and instantaneous turn rate [24]. But these parameters were insufficient measures of effectiveness to determine BFM

advantage in of themselves. The author made a contribution to this field as well. Just like Boyd's work built on Rutowski, the author's own previous work, *Vertical Energy Maneuverability* [13], built on the work of both Boyd and Rutowski, and expanded the relationship between energy and maneuverability into the vertical dimension. This concept was an original contribution to the field in its own right. VEM diagrams were added to the fighter syllabi at the Marine Corps Weapons and Tactics Instructor (WTI) course and the Navy Fighter Weapons School (TOPGUN).

The texts referenced above are balanced with current military training manuals like the United States Air Force's *F-16 Fundamentals* [10] and the United States Navy's *Basic Fighter Maneuvering / Section Engaged Maneuvering* [11]. Collectively, these references are where the concepts and definitions in this dissertation come from. The concepts and definitons are too numerous to be listed in a literature survey, but they were explained in further detail in Section 3.3. Additionally, the initial conditions for specific scenarios used to evaluate solutions in Section 5.4 come from reference [9], which specifies the current BFM training standards for U.S. Navy and Marine Corps fighter pilots.

When put together, what do all of these references reveal? The collective value of this first pillar of references is that they show in spite of changing technology, there is a continual need for BFM execution in air warfare. The consistency in BFM fundamentals, and aerial tactics and requirements is demonstrated through references [12, 15-18]. This consistency of BFM fundamentals spans across several decades. By extrapolating this consistency forward in time, the need for BFM will continue to exist. Because the fundamentals have not changed significantly over the past century, they are also not expected to change at any point in the foreseeable future, regardless of what the technology looks like on emerging UCAVs.

2. The Second Pillar: Supporting Engineering Topics

The second pillar of this literature survey contains references across a wide variety of topics: aircraft flight dynamics; guidance, navigation, and control; fuzzy logic control; and even game theory. This is such a wide variety of topics, that in many cases the contribution to the solution development is quite indirect. However, there are some specific references that have more direct contribution to solution development, and those references are covered here in greater detail.

The first reference to mention specifically is Tewari's *Atmospheric and Space Flight Dynamics* [25]. This textbook is not only a good source for basic flight dynamics and controls, it also has multiple examples and sample MATLAB codes that were used for modelling and simulation (see Section 5 and Appendix B). Another supporting reference on basic flight dynamics and control is Stevens and Lewis in *Aircraft Control and Simulation* [26]. This document also applies to the modelling and simulation section below because it includes supporting data on modern fighter aircraft like the F-16.

In addition to references that cover aircraft dynamics and simulation considerations, there are also a large number of references that cover different techniques for guidance of airborne vehicles. These are all references that do not address autonomous BFM specifically, but the references are specifically addressed here because they still have nuggets of contribution to the solution development in this dissertation. One concept that will be explained in further detail in Section 6 is called synthetic waypoint guidance. Reference [27] discusses the concept of synthetic waypoint guidance (SWG) for flight vehicle trajectories. The author's own previous work in reference [28] uses different frames of reference to define a synthetic waypoint on the target aircraft's turn circle. These two references will be covered in more detail in section 6.1. Another concept that is important below in solution development is gain scheduling. References [29] and [30] cover

different examples of gain scheduling techniques used for guidance and control. Reference [31] is a broad survey of gain-scheduling methods, including those applied to aircraft and missiles. Additionally, references [32], [33], and [34] investigate fuzzy logic as applied to guidance of airborne vehicles. Again, these topics will also be leveraged later during solution development in section 6.

Other topics were explored as part of the literature survey, but not all references had a direct contribution to solution development. Some topics, such as game theory, were explored early on as possible solutions [35]. Game theory showed potential, and many references even explored game theory as a solution to a pursuit/evasion type of air combat. Pursuit/evasion games are a fairly extensive class of literature in of itself, that seem to have gained popularity in the 1970s following the popularity of game theory. Works such as Othling's *Application of Differential Game Theory to Pursuit-Evasion Problems of Two Aircraft* [36], or Sprinkle et al's *Encoding Aerial Pursuit/Evasion Games with Fixed Wing Aircraft* [37] both investigate algorithms to optimize an aircraft's guidance logic through a discretized, two-dimensional environment – a checkerboard setup of sorts. And the titles, abstracts, and subjects alone may seem to have application here. Many more works join this fray: references [38], [39], [40], and [41]. But while these references were investigated and researched as part of the literature survey, the pursuit-and-evasion games do not qualify as BFM for two reasons. First, the roles are clearly established and maintained in pursuit/evasion, whereas in BFM the fighter bandit may constantly shift between offensive, neutral, and defensive roles. Second, the very nature of pursuit/evasion allows at least one aircraft to achieve "victory" at the departure of some arbitrary field or the expiration of some arbitrary time. No such escape clause exists in BFM. For these reasons, pursuit/evasion games are not analyzed further in this dissertation.

3. The Third Pillar: Previous Attempts at Autonomous BFM

A diligent literature search includes a handful of past attempts to develop a solution to autonomous BFM. A close analysis of this last group of references serves three purposes. First, the best aspects of previous attempts can be cherry-picked to create a better and more complete solution. Second, failures or shortcomings in previous works can be identified in order to avoid the same pitfalls. And finally, a full survey of previous work validates the original contribution of this dissertation.

The existing literature on autonomous BFM is divided into different generalized camps on how to solve the problem: Pilot and Maneuver Modelling, Stochastic Method, Dynamic Programming, and Pursuit Guidance. One goal of this literature survey – and the dissertation as a whole – is to identify the advantages and disadvantages of each method, and combine methods in such a way in order to contribute to the existing base of knowledge. This grouping is arbitrary, but it still helps analyze the literature in a deliberate manner.

There is also acknowledged overlap between these groupings. For example, the line between a stochastic process, reinforced computer learning, and approximate dynamic programming is thin, depending on the level of feedback used versus forward-path planning. Therefore, in this literature survey the classification of different approach methods rests largely on how the cited author(s) describe their own work. In the end, the classification of the literature is not as important as a thorough study of it all, because the objective is to take from the good parts and discard the bad. Each method has advantages and disadvantages, and within each group, some attempts are more successful than others. As stated previously, this dissertation seeks to build upon the advantages

of each of these previous methods into a more holistic and better solution, which will be explained in Section 6.

The first group of references to discuss – pilot and maneuver modelling – does not actually include "autonomous BFM" in the sense of a UCAV executing autonomous BFM decision-making. The first group of references under this second pillar of the broader literature survey covers multiple attempts to model fighter pilot behavior and BFM concepts. These efforts span multiple decades. In 1975, the National Aeronautics and Space Administration sanctioned a report titled *An Adaptive Maneuvering Logic Computer Program for the Simulation of One-to-One Air-to-Air Combat*. The title is misleading however, because this work does not actually provide a guidance method that shapes a fighter trajectory or response to BFM maneuvers. However, this document mathematically defined the target's plane of motion via rotation matrices [42], which is similar to the foundation laid in later in this dissertation. In Section 6.1, this dissertation expands on these rotation matrices to mathematically define the control zone within the bandit's plane of motion. Burgin et al also use a "test of maneuverability feasibility", which compares a fighter's desired maneuver to the maximum performance capabilities of the aircraft in question [42]. Hankins followed Burgin's work by trying to establish "IF…THEN" logic trees to select the optimal BFM maneuver [43]. But this work is purely theoretical, since the paper doesn't actually outline what the supposed available maneuvers are. Follow on works by Olsder et al, Lane et al, Ghasemi et al, Park et al, and Ure et al attempt to codify pilot behavior, specify lists of actual BFM maneuvers, and classify those maneuvers into a library available for program selection [23], [44], [45], [46], [47], [48], [49]. Reference [48] correctly identifies the primary pilot inputs for BFM – roll, load factor, and throttle. These are the guidance inputs used in solution development in Section 6.2. But again, most of these works do not actually include a guidance method or proposed

implement a solution. But in one exception, Pearce et al implement an open-loop guidance program for the UCAV to execute in reference [50]. One disadvantage of this entire group of work of a classifying approach of discrete BFM maneuvers is that limiting maneuvers to a discretized list inherently and necessarily limits the robustness of any solution development. Regardless of this self-evident disadvantage, this "look-up" library of available maneuvers is essential two other approaches to autonomous BFM: the stochastic method and the machine-learning method. These two methods are explained below in further detail.

The stochastic method approach includes all probabilistic and Markov methods, where autonomous fighter decisions and decision trees are based on assigned probability functions. The stochastic method is a common approach that has been used in previous attempts at autonomous BFM. The desired endstate in these cases is almost always a quantified reward condition. In 1974, the U.S. Navy's *Air Combat Conversion Model* report measured percentages of successful engagements from fighter pilot training missions and weapons school curricula [51]. This work was unique in how it theorized the possibility to predict success in aerial combat based on factors such as aircraft type, pilot proficiency, and weapon selection. Burgin et al expanded the previous pilot models and continued closer to autonomous BFM with a stochastic method approach [52]. Other works from Virtanen et al, Kaneshige et al, and Wang et al continue along this path [53], [54], [55], [56], [57]. But once again, the discretization of allowable maneuvers is a limitation. Even as late as 2016 in *Research on Unmanned Combat Aerial Vehicle Robust Maneuvering Decision Under Incomplete Target Information*, the maneuvers available for selection are limited to discrete options such as "left turn flight", "downward left turn flight", "downward flight", etc [57]. Regardless of the accuracy of the probability assigned to each decision path, such a basic discretization of available maneuvers and/or flight paths unnecessarily limits UCAV options to a

set of equally discrete trajectory options at any given time. Therefore, similar to the attempts to model pilot behavior, the stochastic method is not considered a robust solution to autonomous BFM. Yet there are cases where a library of pre-planned conditions can be beneficial. For example, when the U.S. Air Force started testing autonomous formation flying between two F-16s in 2013, the guidance algorithm was designed inside the same architecture as the Autonomous Airborne Collision and Avoidance System (AACAS) [58], [59]. While the test aircraft's flight control systems ran the autonomous formation program, the AACAS ran continuously in the background. Once a certain set of pre-defined conditions were met, the aircraft switched modes from formation flying to a collision avoidance maneuver [58], [59]. This same technique might be used in autonomous BFM, where the fighter aircraft maneuvers toward a positional advantage, while continuously assessing for a weapons employment opportunity based pre-planned conditions. Once the pre-planned conditions were satisfied, the guidance algorithm could change from maneuvering for positional advantage, to maneuvering for weapons employment. These conditions would be dependent on the weapons onboard, i.e. a missile-employment envelope versus a gun envelope [11]. These considerations for weapons employment are not applied in this dissertation, but are important to consider in follow on efforts.

Another approach to autonomous BFM is the machine-learning. This umbrella includes feedback learning systems such as artificial intelligence (AI), neural networks (NN), and reinforced learning (RL). This does not include optimal control, dynamic programming, or approximate dynamic programming, which will be addressed in greater detail below. AI and NN gained traction toward military strategy in the late 1980s. In 1992, Rodin and Amin outlined a strategy for computer-based learning in its application to BFM [60]. But like the stochastic methods, such machine-learning methods often require discrete maneuver libraries from which to

choose and learn from. In the case of Rodin and Amin, the aircraft's available maneuvers were limited to just nine combinations of velocity and acceleration commands [60]. Twenty years later in 2012, Teng et al allow only a total of 13 offensive and defensive maneuvers [61]. Other works with the same methodology include references [62], [63], and [64]. But a weakness in the entire methodology was summed up recently in 2020 by Wang et al, who stated in reference [65] that "RL algorithms are almost all one-sided optimization algorithms, which can only guide an aircraft to a fixed location or a regularly moving destination. However, the opponent in air combat has diversity and variability maneuver strategies, which are nonstationary, and the classic [RL] algorithms cannot deal with them." Therefore, reward definition is a limitation in any type of machine-learning method. In the solution development section of this dissertation, reward value is not assigned or used as desired endstate like it is in other references in this section. However, this dissertation still builds upon this idea. Instead of assigning a reward value, the solution in Section 6.3 assigns a quantitative value to relative energy and angular position between the fighter and the bandit.

The third group of references covers the method consisting of any combination of optimal control, dynamic programming, and/or approximate dynamic programming. This method requires knowing all current applicable states and estimating the effects on those states in the future, based on all possible actions. Optimal control and dynamic programming are different from the stochastic method because the former attempts to find an absolute optimum by solving it directy, while the latter relies on statistical probabilities of various solution options. The foundation of dynamic programming is the Bellman's equation, also known as the Hamilton-Jacobi equation in control theory [66]. This approach was predominantly applied to autonomous BFM by James McGrew at the Massachusetts Institute of Technology, beginning in 2008 [67], and again with

How et al in 2010 [68]. However, the use of either optimal control theory, or a discretized version like dynamic programming or approximate dynamic programming, increases the computational cost through the "curse of dimensionality" [69]. These methods are in fact so computationally expensive, that there has not been any successful demonstration to date of such a concept in a three-dimensional environment with accurate aircraft modeling, even in simulation. Therefore, one potential mitigation has been to constrain the testing environment, like McGrew's two-dimensional and constant-velocity domain experiment [67], [68]. Yaofei Ma et al also attempt to skirt this "curse of dimensionality" by holding the aircraft altitudes and velocities in their simulations [69]. Another option is to further limit and discretize the available maneuvers for the fighter, as Lopez et al describe in reference [70]. While this method has been attempted several times in autonomous BFM, the solution presented in this dissertation does not rely on trajectory optimization, because the curse of dimensionality is too costly.

The fourth and final approach to autonomous BFM that has been used in the past is pursuit guidance – or a trajectory that guides an object to a specific target or point in space. Variations of this method have been used for a long time in missile guidance. In the parlance of missile guidance and control, pursuit guidance generally refers to the missile guiding directly at the target's location [71]. More recently in both missile guidance and autonomous air combat, this method has been expanded to include techniques such as synthetic waypoint guidance [27], or virtual point pursuit guidance [72]. Unfortunately, some of the published applications and simulations are still limited in their usefulness. Gavilan, Vasquez, and Camacho design a trajectory for UAV path-following by just combining straight-line and circular-path segments in a two-dimensional plane [73]. Balampanis et al use a similar method of connecting waypoints along a trajectory, and implementing a guidance to minimize cross-track deviation(s), but their work is limited primarily

to long-range trajectory planning [74]. Another frequent downside of the pursuit guidance approach is sub-optimality, which means that there is no guarantee or expectation that the fighter's trajectory is the most efficient in terms of time or energy. But the pursuit guidance approach still has significant advantages. In the words of Medagoda and Gibbens, "mission performance can be enhanced by manipulating the trajectory taken by the pursuer to the targets." Medagoda and Gibbens also incorporate gain scheduling into the guidance solution, but only apply this to the line-of-sight rate signal [27]. You and Shim adjust the virtual pursuit point both laterally and vertically, which is a significant step forward in energy management [72]. But You and Shim still have three weaknesses in their guidance method. First, they show a fundamental misunderstanding of lead, pure, and lag pursuit in relation to offensive, neutral, and defensive BFM, because they define the objectives of these pursuit curves in contrast with current manuals and accepted BFM tactics. Second, their proposed switching function from lead, pure, and lag pursuit does not provide a smooth transition between each, which results in erratic endgame behavior during simulations. Third, their method only adjusts the vertical component of the virtual pursuit point as a function of relative velocity between the attacker and the target. This tactic becomes tactically unsound when range between attacker and target increases and ATA/TA decrease. Shin, Lee, and Shim (the same Shim from reference [72] above) attempt a similar method in *Design of Virtual Fighter Pilot and Simulation Environment for Unmanned Combat Aerial Vehicles* [75]. But their biggest weakness is their misapplication of BFM fundamentals. Sin et al choose corner velocity as the target command velocity and lead pursuit (based on projected target aircraft motion) as the desired aimpoint. First, corner velocity is rarely (if ever) sustainable at high load factors due to the high energy bleed rates. And lead pursuit, if maintained, will inevitably lead to either an in-close overshoot or role reversal [18], [10], [11].

Along with the good and bad of each individual approach method, there has also been a specific error that is frequently applied throughout the literature. The most common aimpoint is defined by 0° ATA and 0° TA, at a fixed range behind the adversary. This technique is actually so common, it has become the "de facto standard" [70] when quantifying the fighter's advantage over the bandit. Specifically, the most common formulas for the angular advantage (S_A) and range advantage (S_R), are:

$$S_A = 1 - \left[\left(1 - \frac{TA}{180°}\right) - \left(1 - \frac{ATA}{180°}\right)\right] \tag{11}$$

$$S_R = e^{-k\left(\frac{R-R_d}{180°}\right)} \tag{12}$$

where R is the measured range, R_d was the desired range, and k equals a constant chosen by the designer [70]. The baseline cost index, S_{BL}, is the product of S_A and S_R:

$$S_{BL} = S_A S_R \tag{13}$$

This method of setting the desired aimpoint at 0° ATA, 0° TA, and a fixed range is not the best solution, however. The first reason is that with the 0° ATA/0° TA/fixed range aimpoint, there is no consideration for airspeed differential. Perhaps this is just an oversight, or perhaps this is a byproduct of a willful (but common) simplifying assumption of constant velocity of both aircraft. Figure 18 depicts how a fighter with too much closing velocity (relative to the bandit) can overshoot its intended target or aimpoint.

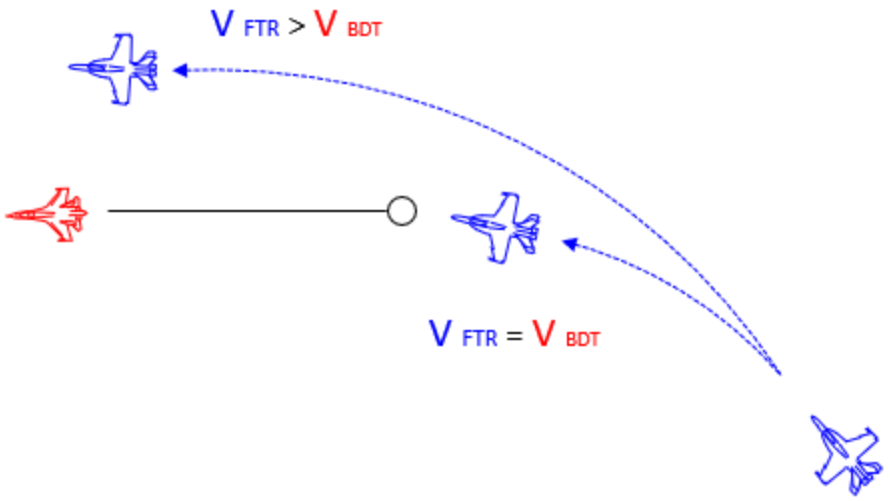

Figure 19. Problem with 0° ATA/0° TA/Fixed Range Aimpoint and Excessive Closure

Another problem is that it does not actually guide the fighter to the bandit's control zone in any condition other than level, 1-g flight. As described earlier, the control zone actually rests on the turn circle, where ATA and TA are not equal to zero. Figure 20 below is an example of why this is problematic. A straight black line is drawn to the bandit's six o'clock position. This represents the 0° ATA/0° TA/fixed range aimpoint solution. In the left frame, the fighter maintains an offensive position while steering towards a 0° ATA/0° TA/fixed range aimpoint. Because the aimpoint sweeps a larger arc through the sky than the bandit's aircraft, the fighter's turn circle is larger than the bandit's. By the end of one complete turn circle, the bandit has already neutralized the fighter's offensive advantage. In the right frame, the fighter executes the most basic pure-pursuit strategy. The difference in the fighter's offensive advantage is readily apparent.

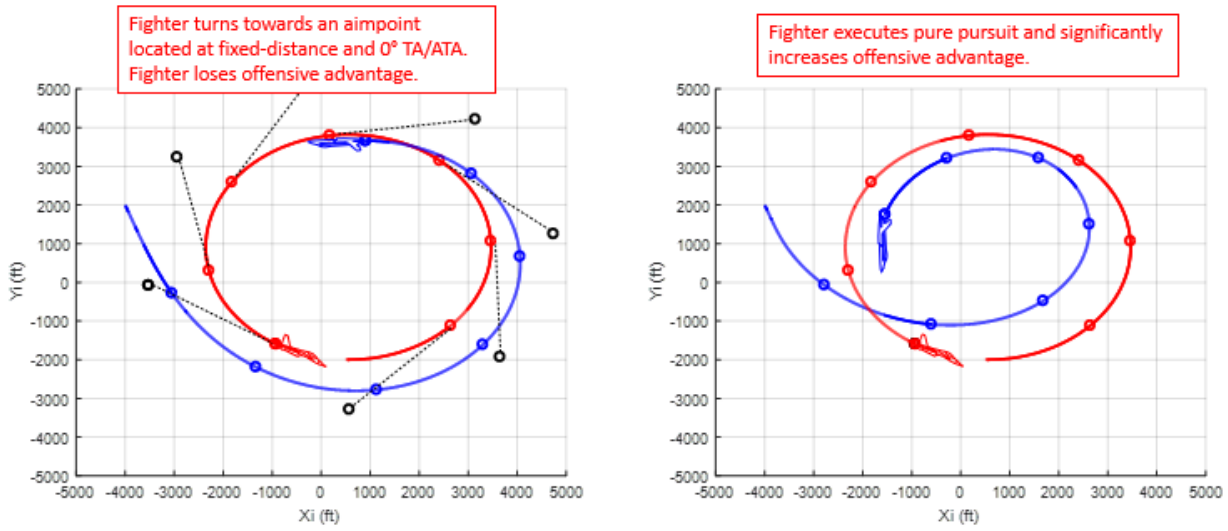

Figure 20. 0° ATA/0° TA/Fixed Range Aimpoint vs. Pure Pursuit in Offensive BFM

The third reason the 0° ATA/0° TA/fixed range aimpoint solution is not optimal is because the system does not allow for any defensive BFM considerations. In many cases, the aimpoint should not be behind the bandit – in lag pursuit – but rather, in front of the bandit – in lead pursuit. The scenario below paints a perfect example of how such a fixed aimpoint behind the bandit can work against a defensive fighter. Figure 21 shows a defensive scenario, when the bandit has just had an overshoot of the fighter's flightpath. The fighter could continue a left-hand turn, which would intuitively appear to be the shortest direction towards the desired aimpoint. Such a move however, would actually increase the bandit's offensive advantage while making the fighter even more defensive. The right side shows a basic fighter reversal while the fighter executes pure pursuit guidance. Again, the weaknesses of a 0° ATA/0° TA/fixed range aimpoint is readily apparent. Figure 21 is a top-down view.

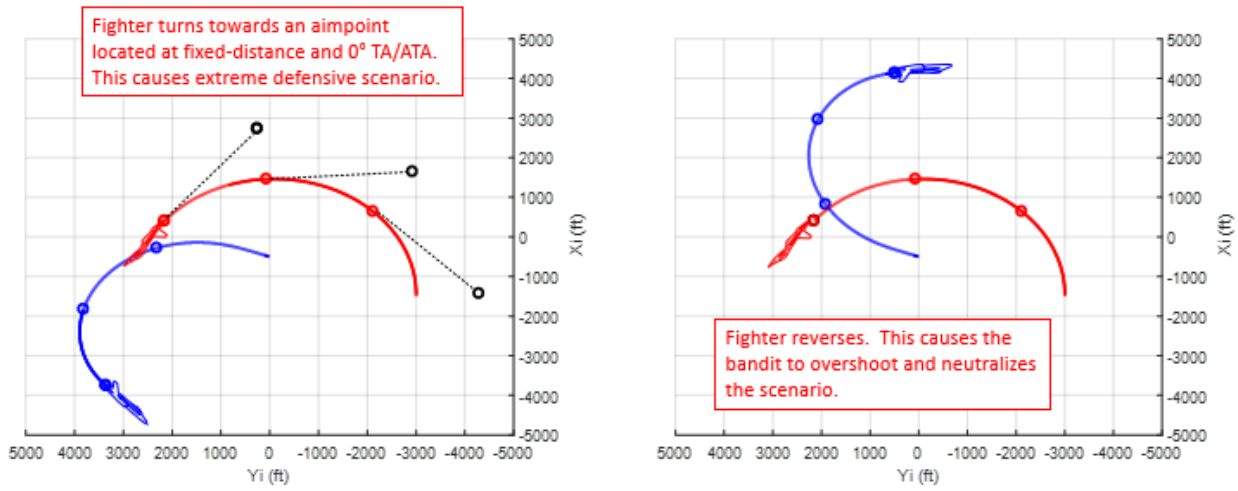

Figure 21. 0° ATA/0° TA/Fixed Range Aimpoint vs. Fighter Reversal in Defensive BFM

Where do these issues leave the current state of progress towards autonomous BFM? The most prevalent disadvantages are either too simplistic rule-based implementation or too much computational cost and complexity. Another frequent mistake is an improper reward definition or desired endstate for the fighter, as explained above. The third common mistake is either improper vertical guidance or even limiting the implementation to a two-dimensional environment. The best points of autonomous BFM found in the literature appear to include properly defining the bandit's plane of motion, defining roles and strategies based on offensive and defensive BFM, properly accounting for friendly aircraft energy management, and utilizing some type virtual point pursuit guidance or some type of adjustable aimpoint – laterally and vertically. In theory, the best solution to autonomous BFM combines all of these good points, while still honoring the basic BFM fundamentals and energy management.

4. The Fourth Pillar: Modeling and Simulation

Creating an accurate simulation environment is critical to validating the proposed guidance scheme. Since this project is centered primarily around high-performance fighter aircraft (defined in Section 3.1), a number of references were used to cover the design, performance, and modeling of modern fighter aircraft.

Another document that was heavily referenced for developing modelling and simulation was *MIL-STD-1797B: Flying Qualities of Piloted Aircraft* [76]. This document, produced by the Department of Defense, specifies the aircraft design requirements for flight control systems, aircraft response, and pilot handling qualities. By using the design specifications set forth in this reference, it can be reasonably assumed that future fighter aircraft – either manned or unmanned – will also meet these minimum standards. For example, modern fighter aircraft (category IV aircraft) are expected to have an effective time delay of less than 0.12 sec in response to a g-command input, and achieve g-onset rates of up to 15 g/sec with 80% control surface deflection [76]. Load factor limits are generally between 6.5 and 9.0 G'S [76], [77]. Roll rates for fighter aircraft are expected to be at least 180 °/sec with an effective time delay of less than 0.25 [76], [78]. This type of information is used to provide a basis for modelling and verifying the proposed solution in this dissertation.

Many previous references were also used in modelling and simulation, such as [25] and [79] for sample MATLAB coding of aircraft equations of motion. References [26], [76], [78], [80], and [81] were compared against in order to verify expected responses of roll and acceleration commands. Additionally, references such as [82], [83], and [84] were used to set the scope, constraints, and boundaries of the simulation environment based on the expected mission sets.

Finally, aircraft performance data used in this dissertation were very similar to modern 4th generation fighter aircraft, like the F-16. This data is readily available from aircraft flight testing,

and is usually included in an aircraft's performance manual. For example, the Air Force Tactics, Techniques, and Procedures 3-3.F16 manual has EM diagrams for multiple altitudes and configurations, but the distribution of this data is limited to Department of Defense personnel. Such is the case with most modern aircraft performance data; it is often either "export controlled", or it is classified to a higher level. Therefore, while the specific aircraft data cannot be used in this academic presentation, the modelling still closely resembles that of a modern fighter aircraft. This will be explained in more detail in the next section.

5. Literature Survey Summary

As stated at the beginning of this section, the first objective of a comprehensive literature survey is to assist in solution development. This literature survey has accomplished that objective by identifying the timeless fundamentals of BFM and evaluating the previous direct attempts of autonomous BFM and their supporting references. From the terrain of literature, six key elements were identified to be used in solution development: 1) incorporate original concepts of VEM in order to influence appropriate vertical maneuvers; 2) base the solution on sound BFM tactics and avoid the foreseeable weaknesses of previous attempts; 3) rely on primary guidance input commands of roll, load factor, and velocity; 4) quantify the relative BFM advantage between the two aircraft; 5) define a specific frame of reference and aimpoint on an aircraft's turn circle, instead of the commonly-used fixed-distance and 0° ATA/TA objective; and 6) use pursuit guidance to an adjustable aimpoint in inertial space. Figure 21 below depicts these individual elements of contribution, some pulled from existing knowledge, and combined in order to contribute an original and holistic approach to autonomous BFM.

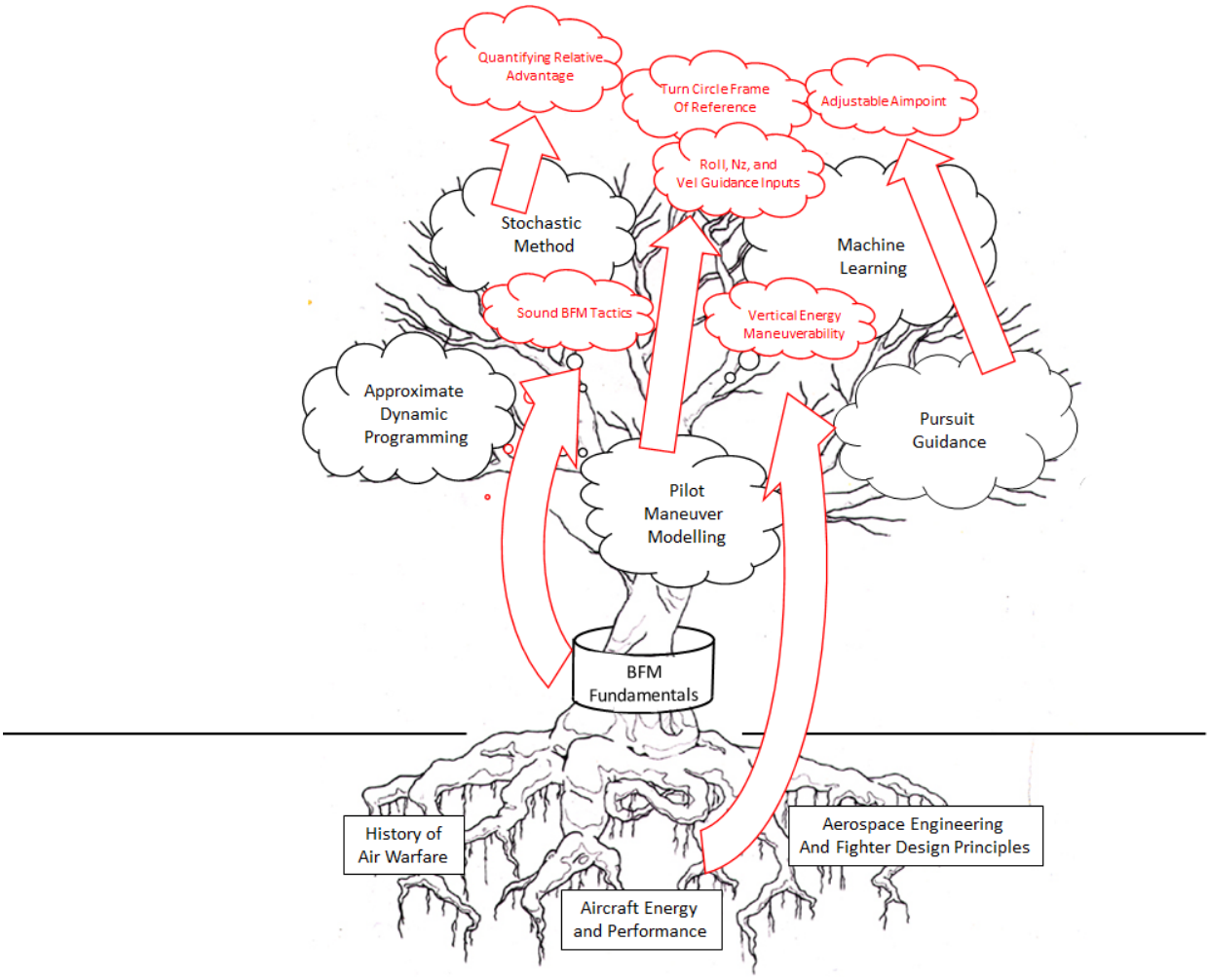

Figure 22. Elements Applied to Original Solution Development

The second objective of the literature survey is to validate original contribution. Combining the six elements above into a holistic solution is a new and original approach to autonomous BFM, because it specifically capitalizes on the strengths of other examples in literature and avoids the common pitfalls. Additionally, the testing and analysis of the proposed solution through the eyes of an experienced fighter pilot is unique in its own right. The author's own experience of over 2,500 hours in fighter aircraft and more than a decade as an air combat tactics instructor provides a new lens of analysis and contribution.

5. MODELING AND SIMULATION

The aircraft and environment modelling includes the aircraft performance, flight control characteristics, and flight path responses to guidance inputs. Definitions are important here, and the term *performance* specifically refers to the specific power of an aircraft as a function of altitude and velocity (energy), and acceleration (maneuverability). The term *control* refers the manipulation of forces and effectors to achieve a desired or commanded state, and *guidance* is the desired trajectory of an object [25]. The simulation environment is a three-dimensional inertial frame of reference in which the aircraft operate. Additionally, some simplifying assumptions are made regarding aircraft states and flight path responses to guidance inputs. Finally, specific initial conditions are identified in order to evaluate the proposed guidance scheme(s).

This section does not cover how the guidance commands are generated. That discussion is further below in Section 6. The intent here is to define the aircraft and environment modelling.

1. Modelling Aircraft Performance

In this dissertation, "aircraft performance" modelling refers the specific power gradient as a function of load factor and velocity. Recall from Eq. (6) that an aircraft's P_s gradient already accounts for the given load factor (or lift), drag, and thrust available as a function of altitude and velocity. As mentioned in the previous section, the aircraft performance model is based on a specific and realistic configuration, weight, and drag index of a modern fighter aircraft at maximum afterburning thrust. The entire set of data is included in Appendix C. The maximum turn rate for this model aircraft occurs at approximately 550 ft/sec true airspeed and 26.0 deg/sec at 5,000' MSL. These numbers closely resemble the F-15C [14].

The load factor, altitude, and velocity are modelled within the following ranges:

$$0 \leq n_{Z_B} \leq 9.0$$

$$0 \leq h \leq 25{,}000\ ft$$

$$200 \leq V \leq 900\ ft/sec$$

2. Modelling Aircraft Longitudinal Response to Guidance Inputs

Aircraft flight dynamics present somewhat of a challenge, only in the sense that some engineering judgement must be made on what level of fidelity is chosen for the model. The work in this dissertation does not require fine calculations at this level, because the trajectories are relatively coarse. Therefore, some freedom is allowed (and taken) in simplifying the aircraft flight dynamics in this model, specifically with regards to load factor (n_{Z_B}) and roll rate ($\dot{\varphi}$) response.

In this simplified model, the block diagram of an n_{Z_B}-command system can be represented as shown in Figure 33 below. This is derived from references [76] and [85].

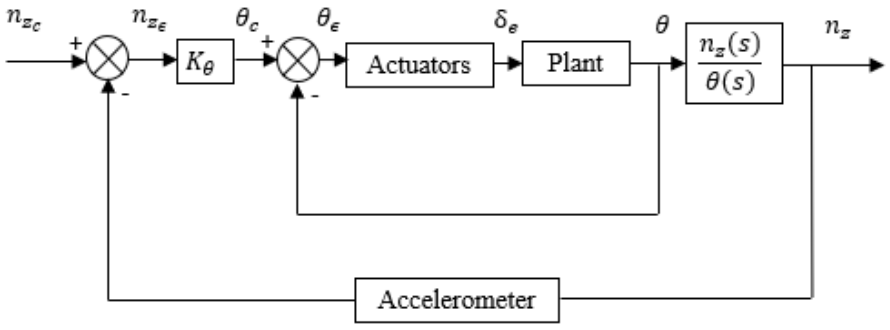

Figure 23. n_{Z_B} Command Block Diagram

Without knowing the specifics of each actuator, plant, sensor, and filter block, the n_{Z_B} response can be approximated by making the simple but realistic assumption that any modern fighter aircraft meets or exceeds the flying qualities specifications outlined by the Department of Defense in MIL-STD-1797B. Given a step input to the elevator, the resultant flight path response resembles Figure 22 below. For an aircraft that meets the MIL-STD requirements, the effective rise time and flight path delay from a step pitch input are less than 0.25 seconds, and the initial pitch rate time delay is less than 0.1 second.[1] This is a short amount of time compared to the entirety of a BFM engagement.

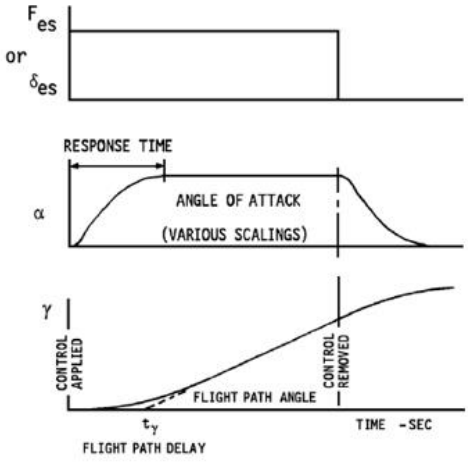

Figure 24. Flight Path Response to Elevator Input [76]

The exact response times and flight path delay is determined by the bare airframe, flight control system design, and atmospheric flight conditions. Keeping the aircraft and flight control

[1] MIL-STD-1797B has multiple requirements for pitch and flight path response. The measurements and standards presented here are a combination of Level 1 (best case) flying qualities of Category IV (fighter) aircraft. The specifications are found in Table XXIX for pitch rate time delay and effective rise time. Flight path time delay is represented in Figure 36, and driven primarily by short period dynamics requirements in Table XXVII [76]. NASA research and simulation has shown that modern fighters can go from 1.0 G to 7.0 G's with a rise time of less than 0.25 seconds, and a maximum G onset rate of over 20 G/sec [76].

model fixed, the biggest effects then come from atmospheric conditions. Dynamic pressure (q) is the main contributor. Therefore, it is beneficial to reflect this in the modeling with a Linear-Parameter Varying system, with q as the variable term.

The governing second-order approximation for an α response to a stick-force input is taken directly from reference [76] and is based on the aircraft's short-period characteristics.

$$\frac{\alpha}{F_s} = \frac{K_\alpha e^{-t_\alpha s}}{\left(s^2+2\zeta_{sp}\omega_{sp}s+\omega_{sp}^2\right)} \tag{34}$$

where, from references [80] and [81]:

$$\omega_{sp} = \sqrt{\frac{C_m \bar{q} S \bar{c}}{I_{yy}}}\ rad/sec \tag{35}$$

and from references [76], [78], [84], and [86]:

$$I_{yy} = 55{,}814\ slug \cdot ft^2 \tag{36}$$

$$\zeta_{sp} = 0.8 \tag{37}$$

$$C_m = 0.7 \tag{38}$$

$$t_\alpha = 0.1\ sec \tag{39}$$

$$S = 300\ ft^2 \tag{40}$$

$$\bar{c} = 30\ ft \tag{41}$$

Again, this is a simplification of the actual pitch and n_{Z_B} responses. In reality, several nonlinearities exist within the system, such as servo position saturation and rate limiting, changing aerodynamic coefficients as a function of attitude and flight control surface position(s), etc. The nonlinearity that is most important in this case however, is the n_{Z_B} saturation at $n_{Z_B max}$.

3. Modelling Aircraft Roll Response to Guidance Inputs

The generic roll response is simpler than the pitch response. A given aileron input (or lateral stick deflection, F_a) generates a roll rate ($\dot{\varphi}$) command, and the roll rate response from the simplified aircraft plant dynamics is usually characterized by a first order system.

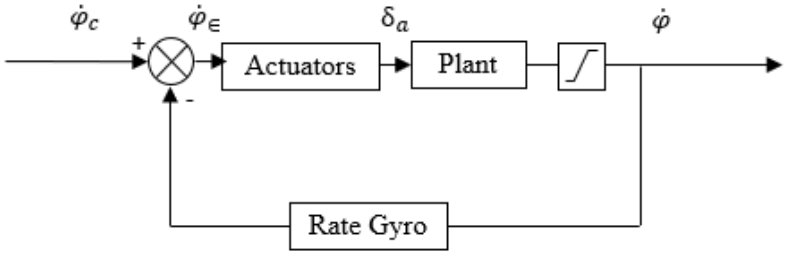

Figure 25. $\dot{\varphi}$ Command Block Diagram

Again referencing MIL-STD-1797B, the roll time delay (T_R) of a fighter aircraft have an absolute maximum of 1 second.

$$\frac{\dot{\varphi}}{F_a} = \frac{K_p}{\left(s+\frac{1}{T_R}\right)} \tag{42}$$

In most cases, the roll time delay is less than 0.1 second, and fighter aircraft can achieve 180° of roll within 1.6 seconds (or 360° of roll within 2.5 seconds) across the majority of the flight

regime.[2] These numbers reflect roll rates for unloaded rolls (≤ 1 G), because unloaded rolls are quicker and more efficient than loaded rolls (>1 G) [11], [76]. Relative to a BFM engagement, these are all small measurements of time.

What's the "so what"? The point of explaining some of these flight dynamics is not to design and build a flight control system for a modern fighter aircraft. The goal is just to explain some of the characteristic pitch and roll responses in order to make simplifying assumptions in this proposed model, which is an initial demonstration. From the Federal Aviation Administration's Reference Handbook of Flight Simulation Fidelity Requirements: "If decision-making skills and tactics are being evaluated, then high fidelity in vehicle handling characteristics are not critical [87]."

4. Simulation Architecture

The guidance commands and responses are a functions of bandit states, fighter states, the relative position between them, and the performance modelling characteristics as a function of velocity, altitude, and load factor. Figure 26 below depicts the simulation architecture. This is a graphical depiction of the MATLAB code in Appendix B.

[2] MIL-STD-1797B has multiple requirements for roll response. The measurements and standards presented here are a combination of Level 1 (best case) flying qualities of Category IV (fighter) aircraft. Target airspeed is $1.4V_{min}$ to $0.8V_{max}$, or 0.8M. The design specifications are found in Table LX for 1-g roll performance requirements, and Figures 165-168 for F-4, F-5, and F-18 flight test data in combat configurations [76].

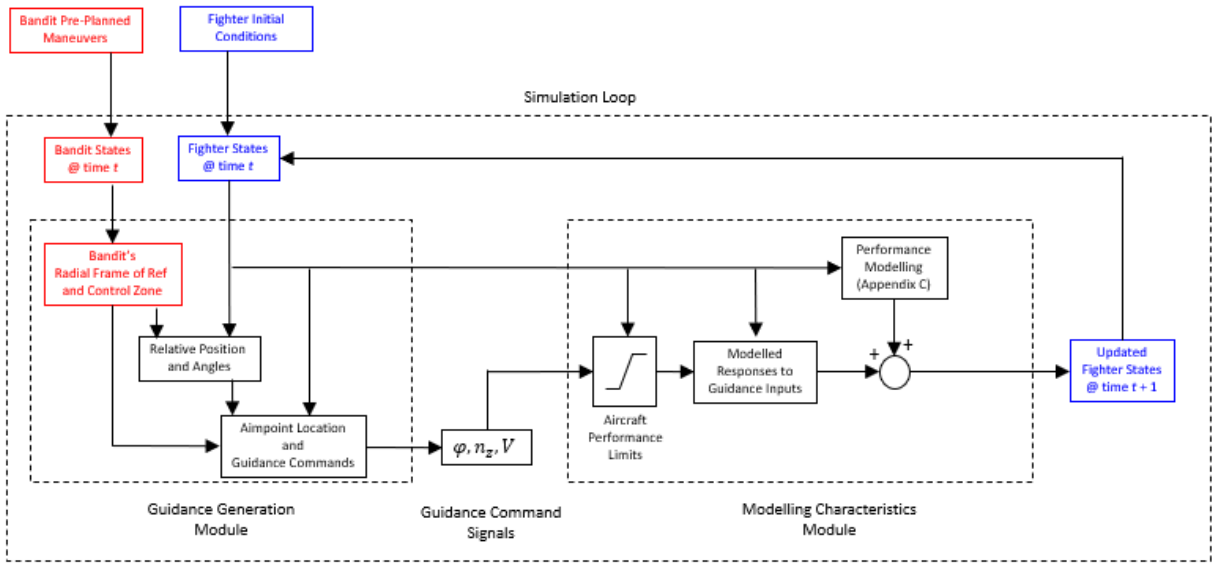

Figure 26. Simulation Architecture

5. Limitations and Constraints

This project focuses exclusively on guidance for an autonomous UCAV to gain and maintain a BFM advantage on the bandit. In order to accomplish this on a conceptual level, certain assumptions, limitations, and constraints are made.

The first assumption that needs to be made is that the position and velocity vectors of the adversary are known (or can be determined) by the UCAV. The dissertation will not address how, or with what sensors, this tracking process is accomplished. Nor will it go into an estimation or sensor-fusion process. Given that the concept of autonomous BFM is being researched for aircraft that have not even been designed yet, multiple possibilities exist for tracking the bandit. Radar is the most common tracking system on fighters today, but it is primarily limited to a portion of the forward hemisphere only. Therefore, it would not work well unless the fighter already had a significant positional advantage. Electrical-optical and infrared (EO/IR) systems have been incorporated with a full spherical observation capability in some aircraft already, like the F-35

Lightning II. Additionally, laser-ranging systems can be combined with an EO/IR sensor to provide a three-dimensional tracking capability. There are also passive systems that can track a bandit's electronic or radar emissions [88]. Finally, there are data-link systems to provide target information from offboard sources. But whatever sensor is used, the goal of this dissertation is not to develop new sensor technology or solve the tracking and estimation problem. Therefore, the assumption is made that, at a minimum, the position and velocity of the bandit relative to the fighter is a known and useable input for the guidance module. Based on initial demonstrations shown later in Section 6, tracking errors that fall within existing sensor specifications (radar, infrared, laser, datalink, etc.) should have negligible impact on system performance.

Certain limitations are also placed on the scope of the research, in order to keep the project manageable. The biggest limitation of this project is that only focuses on the relative position, angles, and velocity of the fighter and the adversary. It does not address any specifics regarding different weapons or weapons' capabilities for two reasons. First, to do so would create another set of near-infinite domain of variables, and expand the scope of the project to an untenable amount. Second, trying to address actual weapons' capabilities could potentially require classified information that is unsuitable for an academic dissertation.

6. Simulation Scenarios

Ten unique scenarios were chosen for analysis. The scenarios are:

1) 2,000 ft Abeam

2) 3,000 ft Perch (Fighter Offensive)

3) 6,000 ft Perch (Fighter Offensive)

4) 9,000 ft Perch (Fighter Offensive)

5) In-Close Overshoot

6) Rolling Scissors

7) 6,000 ft Perch (Fighter Defensive)

8) High Aspect (Fighter Energy Advantage)

9) High Aspect (Fighter Energy Disadvantage)

10) High Aspect (Bandit Pure Pursuit)

Each scenario is meant to test and analyze a specific fighter response in the BFM engagement. The first scenario is the abeam scenario. This is the only scenario presented here that is not a common training set for fighter pilots. However, it allows for a demonstration of the proposed solution. In the abeam scenario, the bandit is constant airspeed and non-maneuvering, i.e. wings level 1-G flight. This is the most benign case in order to examine the fighter's response in maneuvering toward the control zone. The initial conditions below indicate position vectors in the inertial frame, along with the Euler angles (φ, θ, ψ) and true airspeeds.

Table 1. Initial Conditions, Abeam Scenario

Fighter Initial States	Bandit Initial States
$r_{i\,ftr}$ = [-2000 -4000 5000] ft	$r_{i\,bdt}$ = [0 -4000 5000] ft
$\measuredangle_{ftr}$ = [0 0 90]°	$\measuredangle_{bdt}$ = [0 0 90]°
V_{ftr} = 550 ft/s	V_{bdt} = 500 ft/s

In the 3,000 ft perch scenario, the fighter begins at the edge of the bandit's control zone. However, the fighter's velocity is 800 ft/s compared to the bandit's velocity of 600 ft/s. The bandit's velocity is held constant for this scenario, and the fighter must manage a closure problem.

Table 2. 3,000 ft Perch Initial Conditions

Fighter Initial States	Bandit Initial Sates
$r_{i\ ftr}$ = [-2000 2200 5000] ft	$r_{i\ bdt}$ = [1000 2000 5000] ft
$\measuredangle_{ftr}$ = [0 0 0]°	$\measuredangle_{bdt}$ = [80.9 0 -40]°
V_{ftr} = 800 ft/s	V_{bdt} = 600 ft/s

The 6,000 ft perch scenario tests the fighter adherence to lag pursuit while in an offensive position. The fighter should delay any aggressive maneuvering until established within the bandit's turn circle, and then the fighter is expected to maneuver toward lag pursuit. The bandit's velocity is again held constant.

Table 3. 6,000 ft Perch Initial Conditions

Fighter Initial States	Bandit Initial Sates
$r_{i\ ftr}$ = [-3000 2200 5000] ft	$r_{i\ bdt}$ = [3000 2000 5000] ft
$\measuredangle_{ftr}$ = [0 0 0]°	$\measuredangle_{bdt}$ = [80.9 0 -40]°
V_{ftr} = 800 ft/s	V_{bdt} = 800 ft/s

The 9,000 ft perch scenario is similar to the 6,000 ft perch, except the bandit has more time to turn toward the fighter and create an angular problem. The fighter most likely overshoots the control zone (outside the bandit's turn circle). After the overshoot, the fighter is expected to have a "second entry" into the bandit's turn circle [11], [19]. This requires the fighter to manage energy conservation, while still trying to regain an angular advantage.

Table 4. 9,000 ft Perch Initial Conditions

Fighter Initial States	Bandit Initial Sates
$r_{i\ ftr}$ = [-6000 2200 5000] ft	$r_{i\ bdt}$ = [3000 2000 5000] ft
$\measuredangle_{ftr}$ = [0 0 0]°	$\measuredangle_{bdt}$ = [80.9 0 -40]°
V_{ftr} = 800 ft/s	V_{bdt} = 800 ft/s

The in-close overshoot scenario initiates with the fighter facing a high-angle pass behind the bandit, at a range closer than the near-side of the bandit's control zone. The fighter also has excess velocity to manage: 800 ft/s to the bandit's 600 ft/s. Therefore, this is a problem of range, angles, and closure. The fighter needs to solve all three.

Table 5. In-Close Overshoot Initial Conditions

Fighter Initial States	Bandit Initial Sates
$r_{i\ ftr}$ = [-2000 0 5000] ft	$r_{i\ bdt}$ = [-2700 -700 5000] ft
$\measuredangle_{ftr}$ = [0 0 120]°	$\measuredangle_{bdt}$ = [79.1 0 0]°
V_{ftr} = 800 ft/s	V_{bdt} = 600 ft/s

The rolling scissors is defined by a series of horizontal and vertical overshoots. See Figure 27 below.

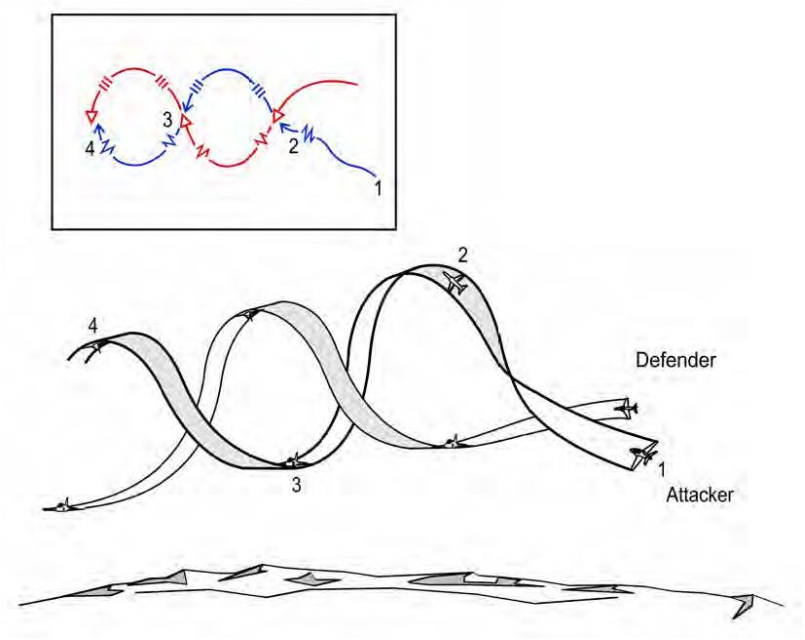

Figure 27. Rolling Scissors Example [11]

Even though the two aircraft are at significantly different positions and orientations in space, the rolling scissors is a completely neutral start by design. The bandit starts at a higher altitude, but the fighter starts with a greater velocity. The initial specific energy of both aircraft is the same.

Table 6. Rolling Scissors Initial Conditions

Fighter Initial States	Bandit Initial Sates
$r_{i\,ftr}$ = [-4000 2000 5200] ft	$r_{i\,bdt}$ = [-4000 2000 8500] ft
$\measuredangle_{ftr}$ = [0 0 0]°	$\measuredangle_{bdt}$ = [0 180 90]°
V_{ftr} =690 ft/s	V_{bdt} = 450 ft/s

The bandit's specific energy is constant, so the bandit's velocity changes as a function of the vertical maneuvering (Eq. (10)). For the rolling scissors, the bandit's roll and acceleration are pre-determined and governed by the following equations:

$$\begin{bmatrix}\varphi_{bdt}\\ \theta_{bdt}\\ \psi_{bdt}\end{bmatrix}_{t+\Delta t} = \begin{bmatrix}\varphi_{bdt}\\ \theta_{bdt}\\ \psi_{bdt}\end{bmatrix}_{t} + \begin{bmatrix}\dot{\varphi}_{bdt}\\ \dot{\theta}_{bdt}\\ \dot{\psi}_{bdt}\end{bmatrix}_{t} \cdot \Delta t + \begin{bmatrix}0.26 \cdot sin(\theta_{bdt}) \cdot \Delta t\\ 0\\ 0\end{bmatrix}_{t} \quad (34)$$

$$n_{z_{B\ bdt}} = 0.01 \cdot V_{bdt} \quad (35)$$

In the 6,000 ft defensive perch scenario, the fighter and bandit roles are switched from the previous 6,000 ft perch. The fighter is significantly defensive. At the start, the bandit executes a 3 second delay, followed by lag turn towards the fighter's control zone. The bandit maintains constant airspeed and level flight.

Table 7. 6,000 ft Perch (Fighter Defensive) Initial Conditions

Fighter Initial States	Bandit Initial Sates
$r_{i\ ftr}$ = [3000 0 5000] ft	$r_{i\ bdt}$ = [-3000 0 5000] ft
$\measuredangle_{ftr}$ = [0 0 -40]°	$\measuredangle_{bdt}$ = [0 0 0]°
V_{ftr} = 800 ft/s	V_{bdt} = 800 ft/s

The term "high-aspect" refers to high AOT and TA between the fighter and bandit. The high-aspect scenarios are divided into three different sets of conditions. First, the fighter is given a distinct energy advantage over the bandit.

Table 8. High Aspect (Fighter Energy Advantage) Initial Conditions

Fighter Initial States	Bandit Initial Sates
$r_{i\ ftr}$ = [0 3000 5000] ft	$r_{i\ bdt}$ = [0 3500 5000] ft
$\measuredangle_{ftr}$ = [0 0 0]°	$\measuredangle_{bdt}$ = [78.4 0 180]°
V_{ftr} = 800 ft/s	V_{bdt} = 600 ft/s

Second, the fighter starts at a distinct energy disadvantage from the bandit.

Table 9. High Aspect (Fighter Energy Disadvantage) Initial Conditions

Fighter Initial States	Bandit Initial Sates
$r_{i\ ftr}$ = [0 3000 5000] ft	$r_{i\ bdt}$ = [0 3500 5000] ft
$\measuredangle_{ftr}$ = [0 0 0]°	$\measuredangle_{bdt}$ = [78.4 0 180]°
V_{ftr} = 550 ft/s	V_{bdt} = 800 ft/s

Finally, the two aircraft begin at the exact same altitude and airspeed, but the bandit is given freedom to maneuver with exclusively pure pursuit against the fighter.

Table 10. High Aspect (Bandit Pure Pursuit) Initial Conditions

Fighter Initial States	Bandit Initial Sates
$r_{i\ ftr}$ = [0 3000 5000] ft	$r_{i\ bdt}$ = [0 3200 5000] ft
$\measuredangle_{ftr}$ = [0 0 0]°	$\measuredangle_{bdt}$ = [0 0 180]°
V_{ftr} = 800 ft/s	V_{bdt} = 800 ft/s

6. SOLUTION DEVELOPMENT

In this section, the solution development is broken down into three overlapping parts. First, the transformation matrices are developed to define the frame of the fighter's turn circle, the bandit's turn circle, and the bandit's control zone. Second, a system for guidance of autonomous BFM is shown in a three-dimensional environment. Finally, an adjustment to the system will include a moveable aimpoint, allowing a smooth transition between offensive and defensive BFM.

1. Understanding the Control Zone Through Frames of Reference

In addition to the background literature covered in the previous sections, the author also completed previous graduate work on defining the kinematic relationship between the adversary, the adversary's control zone, and the fighter. This work lays the foundation for solution development to the problem of three-dimensional autonomous BFM. The conclusion from this work was that the vector from the fighter to the adversary's control zone can be found by applying a series of rotation matrices from one frame of reference to another, including the inertial frame (I), the body frame (B), the wind frame (W), and the radial frame (R).

1. *Inertial Frame*

In this dissertation, the general frame of reference, $[\underline{\hat{X}}]$, will be denoted by the following matrix notation:

$$[\underline{\hat{X}}] = \begin{bmatrix} \underline{\hat{\imath}}_x \\ \underline{\hat{\jmath}}_x \\ \underline{\hat{k}}_x \end{bmatrix} \tag{14}$$

Therefore, a non-rotating inertial reference frame is represented by Eq. (15) below. The Earth and its atmosphere are assumed to be a flat, non-rotating frame of reference.

$$[\hat{I}] = \begin{bmatrix} \hat{\imath}_I \\ \hat{\jmath}_I \\ \hat{k}_I \end{bmatrix} \tag{15}$$

2. *Body Frame of Reference*

The origin of an aircraft's body frame of reference is fixed about certain point on the aircraft, usually close to its center of gravity (CG). For traditionally-configured aircraft, the x-axis (or $\hat{\imath}_B$ unit vector) points forward out the nose, the y-axis ($\hat{\jmath}_B$) points out the right wing, and the z-axis ($\hat{k}_B$) points out the bottom of the aircraft. Figure 28 illustrates the body frame of reference.

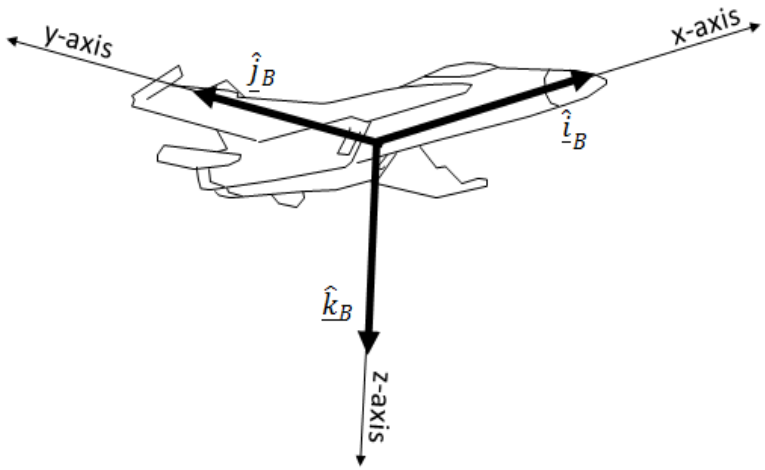

Figure 28. Aircraft Body Axis

To represent one vector in another frame of reference, the rotation matrix $\boldsymbol{R}$ is used. For example, $\boldsymbol{R_{BI}}$ is the rotation matrix from the inertial frame to the body frame, about the angles ψ (yaw), θ (pitch), and φ (roll).

$$\boldsymbol{R_{BI}} = \boldsymbol{R_3}(\phi)\boldsymbol{R_2}(\theta)\boldsymbol{R_1}(\psi)$$

$$= \begin{bmatrix} \cos(\theta)\cos(\psi) & \cos(\theta)\sin(\psi) & -\sin(\theta) \\ -\cos(\phi)\sin(\theta)+\sin(\phi)\sin(\theta)\cos(\psi) & \cos(\phi)\cos(\psi)+\sin(\phi)\sin(\theta)\sin(\psi) & \sin(\phi)\cos(\theta) \\ \cos(\phi)\sin(\theta)\cos(\psi)+\sin(\phi)\sin(\psi) & \cos(\phi)\sin(\theta)\sin(\psi)-\sin(\phi)\cos(\psi) & \cos(\phi)\cos(\theta) \end{bmatrix} \quad (16)$$

The identities in Eqs. (17) through (21) below are used for different rotation matrices throughout this dissertation.

$$[\underline{\hat{B}}] = \boldsymbol{R_{BI}}[\underline{\hat{I}}] \quad (17)$$

$$[\underline{\hat{I}}] = \boldsymbol{R_{BI}}^T[\underline{\hat{B}}] \quad (18)$$

$$[\underline{\hat{B}}]^T = [\underline{\hat{I}}]^T\boldsymbol{R_{BI}}^T \quad (19)$$

$$\boldsymbol{R_{IB}} = \boldsymbol{R_{BI}}^T \quad (20)$$

In the aircraft's body frame of reference, load factor can be further specified with notation n_{z_B}. This value is a magnitude, whereas the vector representation is $\underline{n}_{z_B}$. (Note: in true vector algebra, n_Z actually acts along the negative z-axis. However, the value of n_{z_B} is traditionally recognized as positive.)

$$\underline{n}_{ZB} = \left[\underline{\hat{B}}\right]^T \begin{bmatrix} 0 \\ 0 \\ -n_{ZB} \end{bmatrix} \tag{21}$$

3. *Wind Frame of Reference*

Now that the inertial and body frames of reference have been defined, next is the wind frame of reference. The wind frame of reference is characterized by the angle of attack, α, and the angle of sideslip, β. The rotation from the body frame to the wind frame, $\boldsymbol{R_{BW}}$, is:

$$\boldsymbol{R_{WB}} = \boldsymbol{R_1}(\beta)\boldsymbol{R_2}(-\alpha)$$

$$= \begin{bmatrix} \cos(\alpha)\cos(\beta) & \sin(\beta) & \sin(\alpha)\cos(\beta) \\ -\cos(\alpha)\sin(\beta) & \cos(\beta) & -\sin(\alpha)\sin(\beta) \\ -\sin(\alpha) & 0 & \cos(\alpha) \end{bmatrix} \tag{22}$$

The aircraft's velocity vector ($\underline{V}$) is entirely along the x-axis of the aircraft's wind frame, as shown in Figure 29.

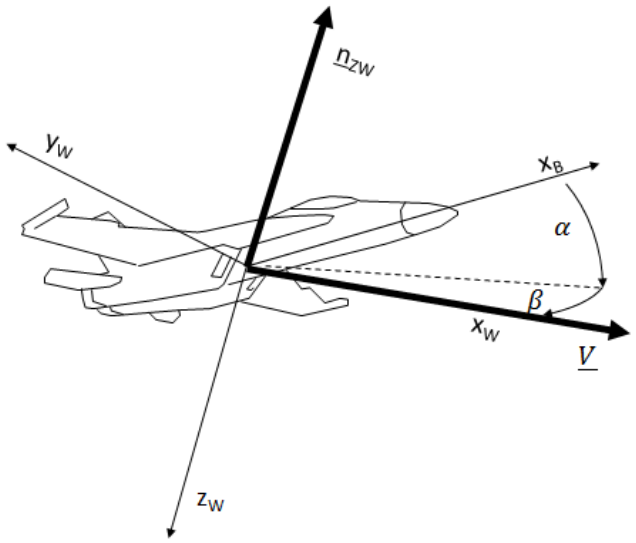

Figure 29. Wind Frame of Reference

Also note that in the body frame of reference, the z-axis acceleration was denoted by n_{z_B}. In the wind frame of reference, the z-axis acceleration is denoted by n_{z_W}. The vector $\underline{n}_{ZW}$ is directionally aligned with the force of lift and perpendicular to the x-axis of the wind frame. This makes sense because $\underline{V}$ is directionally aligned with the x-axis of the wind frame and opposite the relative wind. The term $n_{ZW\,max}$ applies when the aircraft is generating its maximum amount of lift.

4. *Radial Frame of Reference*

So far, the inertial frame, body frame, and wind frame have all been covered, as well as their ***R*** matrices. In BFM however, fighter pilots are most concerned with the turn circle of each aircraft. A trimmed aircraft that is at 1 n_{z_W} and wings level simply flies a straight line. In this case, the acceleration measured along the *z*-axis is equal and opposite to the gravity constant. But as the aircraft increases n_{z_W}, it results in a radial acceleration, n_{z_R}. The flight path that was a straight line then becomes a turn circle. The vector $\underline{n}_{z_R}$ is in-plane with the turn circle and directionally aligned towards its center.

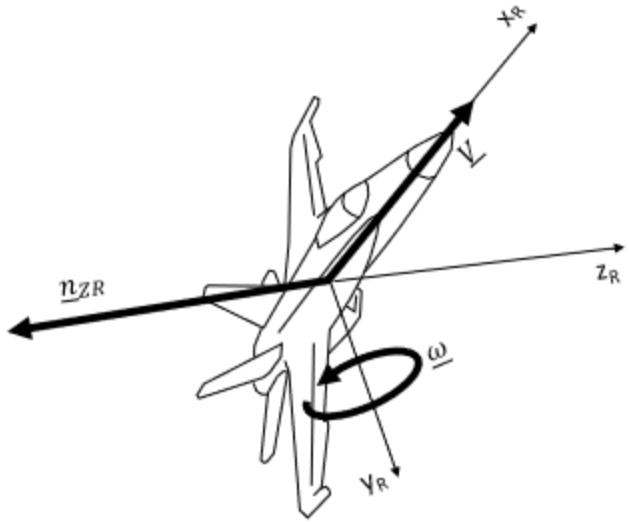

Figure 30. Radial Frame of Reference

In order to parameterize the turn circle, a new frame of reference is required, called the radial frame of reference. In the radial frame, the aircraft's velocity vector is still aligned with x-axis of the wind frame. The z-axis points away from the center of the turn circle, while the acceleration $\underline{n}_{z_R}$ points toward the center of the turn circle. The y-axis is orthogonal, using the right-hand rule.

The radial frame of reference is defined where $\underline{n}_{ZR}$ is the sum of the vector $\underline{n}_{ZW}$ and the vector representation of gravity. Since gravity is constant in the inertial frame:

$$\left[\hat{\underline{I}}\right]^T \underline{g} = \left[\hat{\underline{I}}\right]^T \begin{bmatrix} 0 \\ 0 \\ g/g \end{bmatrix} = \left[\hat{\underline{I}}\right]^T \begin{bmatrix} 0 \\ 0 \\ 1 \end{bmatrix} \tag{23}$$

The sum of $\underline{n}_{ZW}$ and $\underline{g}$ yields the following equations for the radial acceleration:

$$\underline{n}_{ZR} = \underline{n}_{ZW} + \underline{g} \tag{24}$$

$$\left[\hat{\underline{R}}\right]^T n_{ZR} = \left[\hat{\underline{W}}\right]^T \underline{n}_{ZW} + \left[\hat{\underline{I}}\right]^T \underline{g} \tag{25}$$

Graphically, Eq. (25) looks like Figure 31 below.

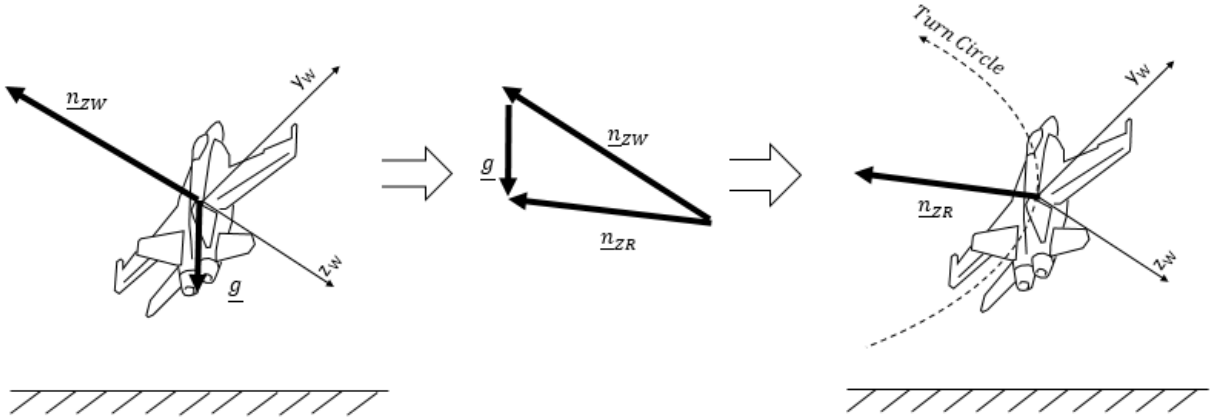

Figure 31. Radial Acceleration, $\underline{n}_{ZR}$

In order to complete Eq. (25) with all terms in the same frame of reference, a new rotation matrix must be identified to represent each term in the radial frame. The term $\underline{n}_{ZR}$ varies primarily as a function of flight path angle (γ) and roll angle (ϕ). To simplify the understanding of this, it is best broken down into two parts: first by analyzing the effect of γ, and then analyzing the effect of ϕ.

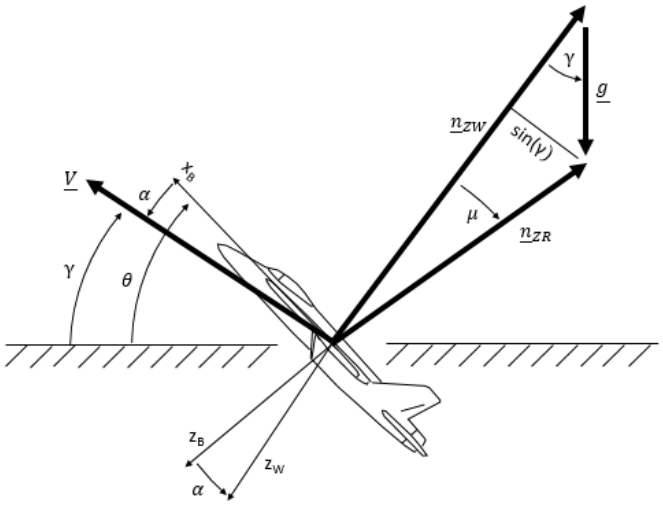

Figure 32. Effects of γ on $\underline{n}_{ZR}$

From Figure 32 above, as γ becomes non-zero, the angular difference between $\underline{n}_{ZW}$ and $\underline{n}_{ZR}$ is the angle μ, where:

$$\mu = \sin^{-1}\left(\frac{\sin(\gamma)}{n_{ZR}}\right) \tag{26}$$

Therefore, the rotation matrix from the wind frame to the radial frame, around the y-axis is:

$$\boldsymbol{R_2}(\mu) = \begin{bmatrix} \cos(\mu) & 0 & \sin(\mu) \\ 0 & 1 & 0 \\ -\sin(\mu) & 0 & \cos(\mu) \end{bmatrix} \tag{27}$$

Roll angle also has an effect on $\underline{n}_{ZW}$, shown in Figure 33.

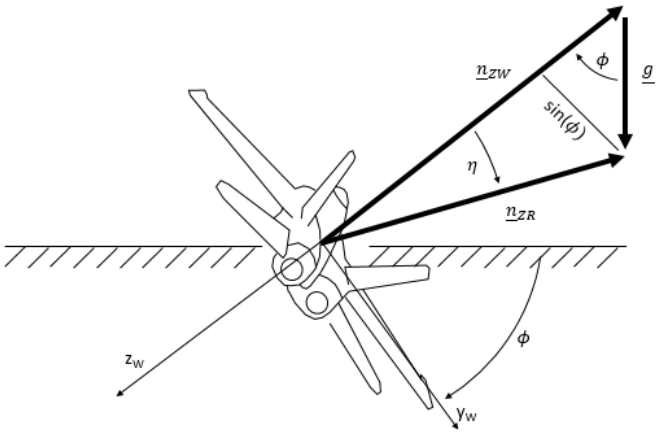

Figure 33. Effects of γ on $\underline{n}_{ZR}$

From Figure 33, as φ becomes non-zero, the angle η is:

$$\eta = \sin^{-1}\left(\frac{\sin(\varphi)}{n_{ZR}}\right) \tag{28}$$

And the rotation from the wind frame to the body frame around the x-axis is:

$$\boldsymbol{R_3}(\eta) = \begin{bmatrix} 1 & 0 & 0 \\ 0 & \cos(\eta) & -\sin(\eta) \\ 0 & \sin(\eta) & \cos(\eta) \end{bmatrix} \tag{29}$$

Going all the way back up to Eq. (25), the original problem in this section was how to find a rotation matrix from the wind frame to the radial frame. Putting Eqs. (27) and (29) together results in the rotation matrix $\boldsymbol{R_{RW}}$.

$$\boldsymbol{R_{RW}} = \boldsymbol{R_3}(\eta)\boldsymbol{R_2}(\mu) = \begin{bmatrix} \cos(\mu) & 0 & -\sin(\mu) \\ \sin(\eta)\sin(\mu) & \cos(\eta) & \sin(\eta)\cos(\mu) \\ \cos(\eta)\sin(\mu) & -\sin(\eta) & \cos(\eta)\cos(\mu) \end{bmatrix} \tag{30}$$

By plugging Eq. (30) into Eq. (25), the terms $\underline{n_{ZW}}$ and $\underline{g}$ can both be represented and summed in the radial frame.

$$\left[\underline{\hat{R}}\right]^T n_{ZR} = \left[\underline{\hat{R}}\right]^T \left[\boldsymbol{R_{WR}}\underline{n_{ZW}} + \boldsymbol{R_{IB}}\boldsymbol{R_{BW}}\boldsymbol{R_{WR}}\underline{g}\right] \tag{31}$$

5. *The Control Zone*

Finally, the rotation and translation can be made from either aircraft's orientation in the radial frame, to the control zone located on the aircraft's turn circle. Because the control zone is displaced by a certain arc length along the turn circle, the relationship between the two consists of another angular rotation. The angle τ can be calculated from the current turn radius (or current radial load factor), minimum turn radius (or maximum radial load factor), and a specified scaling factor (k_{cz}).

$$\tau = \frac{k_{cz} \cdot R_{min}}{R} = \frac{k_{cz} \cdot n_{ZR}}{n_{ZR\,max}} \tag{32}$$

Graphically, it looks like Figure 34 below.

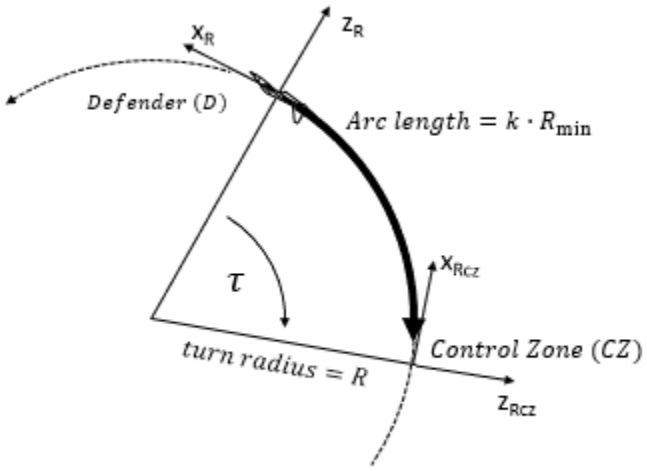

Figure 34. Arc Length from Aircraft to Control Zone

Because the control zone is located on the turn circle by definition, the rotation matrix from the aircraft's radial frame of reference ($[\underline{\hat{R}}]$) and the control zone's radial frame of reference ($[\underline{\hat{R}}_{CZ}]$) about the $\underline{\hat{j}}_R$ axis is denoted as $\boldsymbol{R}_{\boldsymbol{R_{cz}}}$.

$$\boldsymbol{R}_{\boldsymbol{R_{cz}}} = \boldsymbol{R_2}(-\tau) = \begin{bmatrix} \cos(\tau) & 0 & \sin(\tau) \\ 0 & 1 & 0 \\ -\sin(\tau) & 0 & \cos(\tau) \end{bmatrix} \tag{33}$$

Using all the information up to this point, combined with some trigonometry from knowing the arc length along the turn circle, a position vector ($\underline{\rho}$) is created from the aircraft to the center of its control zone. This position vector is represented in the radial frame of reference. See Eq. (34) and Figure 35.

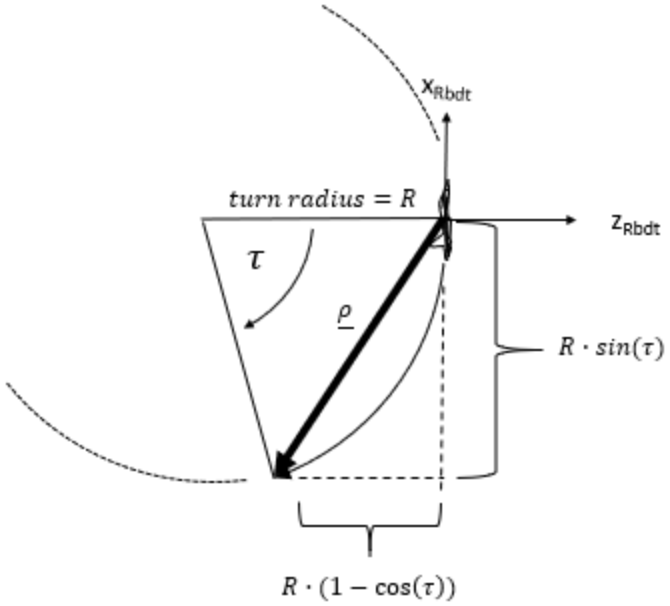

Figure 35. Relationship Between Aircraft and Control Zone

The vector $\underline{\rho}$ is defined as:

$$\underline{\rho} = \left[\underline{\hat{R}}\right]^T \begin{bmatrix} -R\sin(\tau) \\ 0 \\ -R(1-\cos(\tau)) \end{bmatrix} \tag{31}$$

Note, do not confuse the turn radius (R) with the radial frame of reference $\left[\underline{\hat{R}}\right]$.

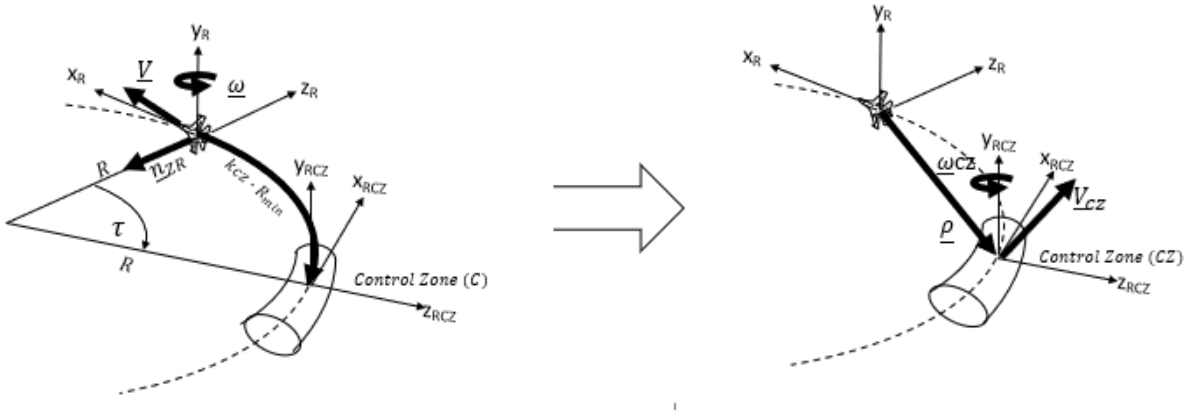

Figure 36. Range and Angle Components of the Control Zone

The magnitude of the velocity vector (V) is the same for both the aircraft and its control zone, and the direction of the velocity vector is simply rotated by the angle τ.

$$\underline{V_{cz}} = \left[\underline{\hat{R}}\right]^T \boldsymbol{R}_{\boldsymbol{R}_{cz}}{}^{\boldsymbol{T}} \underline{V} \tag{32}$$

While the relative orientation of the control zone frame with respect to the aircraft's radial frame is a function of τ, the angular velocity (ω) is equivalent for both frames, since the y-axes are aligned.

$$\underline{\omega} = \underline{\omega_{cz}} \tag{33}$$

Therefore, both the position and the rotation of the control zone have now been defined with respect to the bandit.

2. Variable Gain Scheduling for Generating Guidance Commands

In order to understand how the fighter's guidance commands are generated, it is important to understand in a broad sense what the aircraft needs to accomplish. Recall the objective of offensive BFM: to arrive at a specified distance and orientation behind the bandit in order to employ weapons. In other words, the fighter needs to intercept the control zone, on the bandit's turn circle, with reasonably low angles and closure relative to the bandit. Section 6.1 covered how to calculate the control zone. The previous section described very basic principles of aircraft dynamics and simplified acceleration control system. Next it is time to generate the guidance commands.

An ordinary fighter pilot uses an iterative three-step process in fighting BFM: 1) roll the aircraft to the desired orientation, 2) increase the longitudinal pull in order to move the aircraft's flight path toward the desired intercept point, and 3) manage energy and velocity, as required. In order

to address steps 1) and 2), the dissertation will first examine the guidance command signals for n_z and φ. Energy and velocity management will then be addressed afterwards.

The best way to start is to look at a generic relationship between the fighter, the bandit, and the control zone. In Figure 37 below, the fighter is 2,000 ft abeam the bandit's 9 o'clock position. In these initial conditions, the TA from the bandit to the fighter is 90°, and the ATA from the fighter to the bandit is 90°. Both aircraft are at an altitude of 5,000 ft. Assuming a non-maneuvering (wings-level, 1G) bandit at a velocity of 500 ft/s for this case, the bandit's control zone is behind the bandit's aircraft, at a distance equal to the minimum turn radius (1,035 ft). This is the fighter's desired point of intercept, and yields a different ATA from the fighter to the aimpoint. Thus, a distinction is made between ATA_{bdt} and ATA_{ap}. Figure 37 is a top-down view.

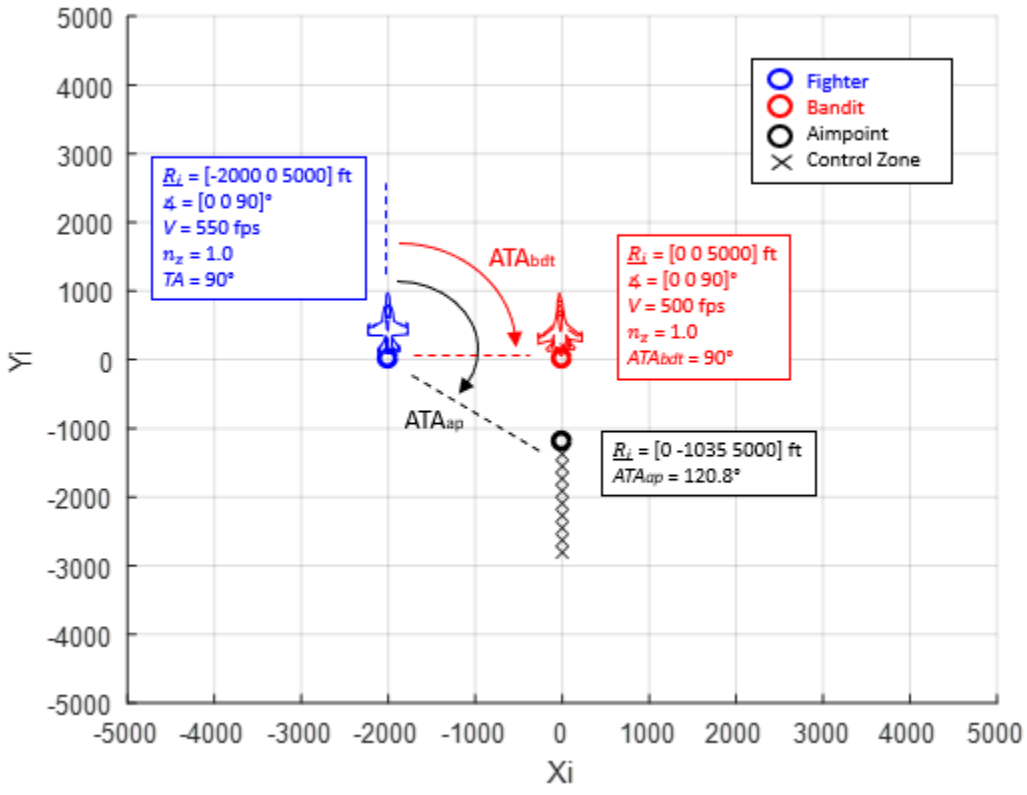

Figure 37. Abeam Initial Conditions

The fighter is abeam the bandit at 90° *TA* and ATA_{bdt}. The center of the control zone – the aimpoint where the fighter needs to intercept – is at 120.8° ATA_{ap}. Clearly the fighter needs to initiate a turn to the right in this case. The objective is to get the ATA_{ap} equal to zero. In the outer guidance command loop, ATA_{ap_c} is the command signal, which must be converted to a radial acceleration command via k_{n_R} in (G/°). The error (ATA_{ap_ϵ}) is the difference between the command signal and the amount of turn generated by the fighter's radial acceleration. See Figure 38.

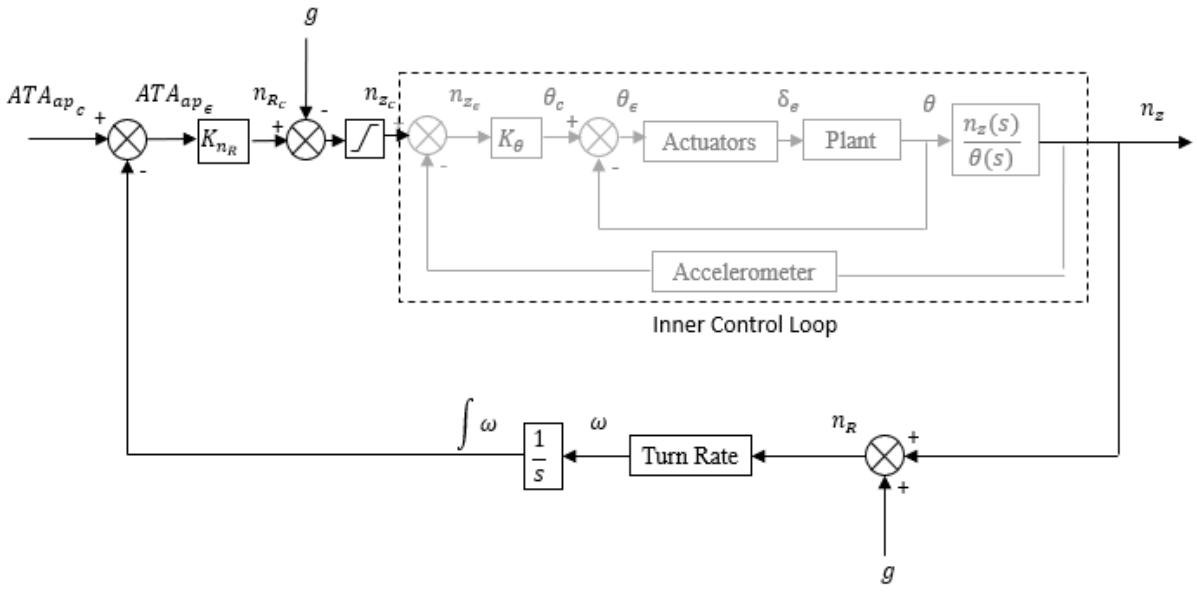

Figure 38. Guidance Command Loop

But what magnitude of radial acceleration is desired? Too much acceleration (i.e. lift and drag) will cause the fighter to bleed airspeed unnecessarily. Too little acceleration will delay the fighter's desired intercept, and potentially even allow a wily bandit to outmaneuver the fighter. The solution is a tradeoff for the fighter. At high ATA_{ap}, the fighter should aggressively maneuver in order to get the flight path vector pointing closer toward the aimpoint. At low ATA_{ap}, the fighter

can reduce the acceleration in order to preserve (or even gain) energy. A logical benchmark is 45° ATA_{ap}. Below 45° ATA_{ap}, the component of closure velocity towards the aimpoint's position is greater than the remaining orthogonal component. Above 45° ATA_{ap}, the opposite is true. See Figure 39.

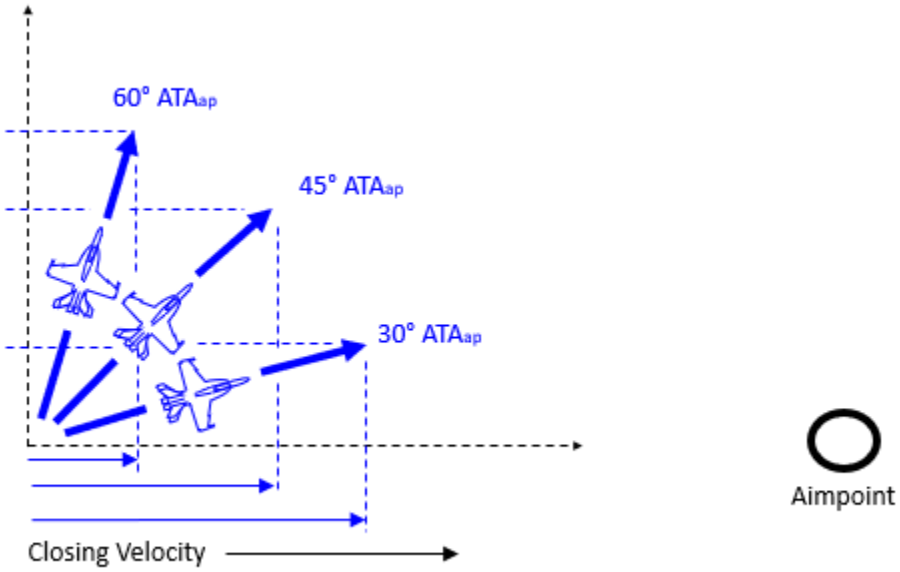

Figure 39. Closing Velocity Component Vs ATA_{ap}

Using 45° ATA_{ap} as a benchmark, k_{n_R} is set to allow maximum acceleration above, and reduced acceleration below this number. At a load factor limit of 7.5 G's:

$$k_{n_R} = \frac{n_{z\,max}}{45°} = 0.1667\ (G/°) \tag{36}$$

Additionally, recall from Section 3.3.3, once the fighter is inside of the maximum performance turn circle (or once the fighter is closer to the bandit than the bandit's minimum

turn diameter), the fighter should also be maneuvering more aggressively. This is where variable gain scheduling becomes useful. The term *gain scheduling* has many different implications, and is frequently included with the larger term *gain scheduling control*. This implies that gain scheduling, in of itself, is used in conjunction with control, vice guidance. In this case however, gain scheduling will be used as a method of managing guidance commands. The solution proposed here is similar to the "divide and conquer" technique in references [31], [32], where gains are chosen by the engineer in order to achieve specific design points, and then gains are interpolated between those design points by some scheduling function within the required domain.

Armed with that definition and the previously stated fundamentals of BFM, refer once again to the abeam scenario in Figure 37. The next objective is to adjust k_{n_R} as a function of range between the fighter and the bandit. In the abeam scenario, the bandit's minimum turn radius is 1,035 ft, and the minimum turn diameter is 2,070 ft. For simplicity, a round number of 2000 ft was used as a threshold about which to scale the gain. This began a seemingly arbitrary process, but it is important to understand what needed to be accomplished. First, the gain for radial acceleration (k_{n_R}) needed to increase when the range was less than 2000 feet, but had to be bounded on the high end. A gain scaling factor of 2.0 sufficed as the high end, in order to achieve maximum load factor at 23° ATA_{ap}. This was an intuitive decision by the author. Additionally, the gain needed to decrease at ranges greater than 2000 feet, but also had to be bounded on the low end. With a gain scaling factor of 0.5, maximum load factor occurred at 90° ATA. Shaping the gain scaling factor as a function of range to the bandit could be done one of several different ways, like a switching function, a saturated linear function, or a sigmoid.

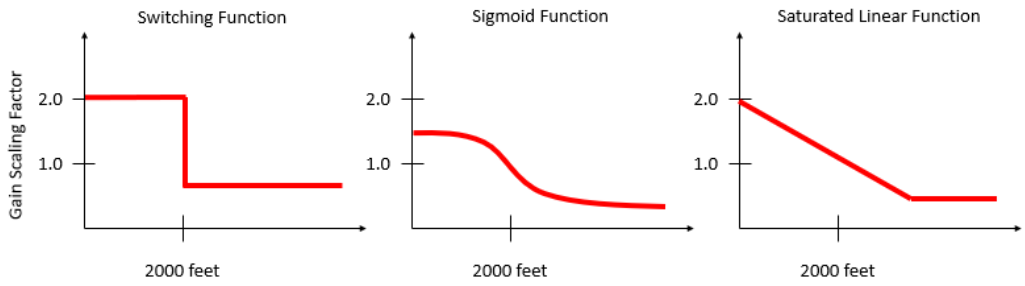

Figure 40. Gain Shaping Functions

The switching function is not practical for BFM, because the discrete gain scaling factor does not actually pass through a value of 1.0. Even if a hysteresis buffer was applied, the system would likely result in erratic oscillations in the controls around this critical range. A sigmoid function was possible, but the sigmoid was more difficult to shape asymmetrically around the value of 1.0. In the case shown above, the gain scaling factor only ranges 0.5 – 1.5, instead of 0.5 – 2.0. A linear function – saturated on the low end in this example in order to prevent either zero or negative gain values – is a simple and viable solution.

The most accurate gain scaling function is an exponential shape, controlled by a function of range. This is an art, not a science, and it requires engineering input in order to identify a set of operating points that the designer wanted to correlate to specific scaling factors. The desired operating points chosen are shown below in Table 10.

Table 10. Choosing Desired k_{n_R} Gain Scaling Factors as a Function of Range

Range (ft)	Desired Scaling Factor
9,000	0.5
6,000	0.75
2,000	1.0

500	1.5
0	2.0

The equation chosen to fit a curve along these points is:

$$k' = e^{\left(1-\sqrt[3]{\frac{r_{bdt}}{2000}}\right)} \tag{37}$$

Where $k_{n_R}{}' = k \cdot k_{n_R}$, and r_{bdt} is the range (in feet) from the fighter to the bandit.

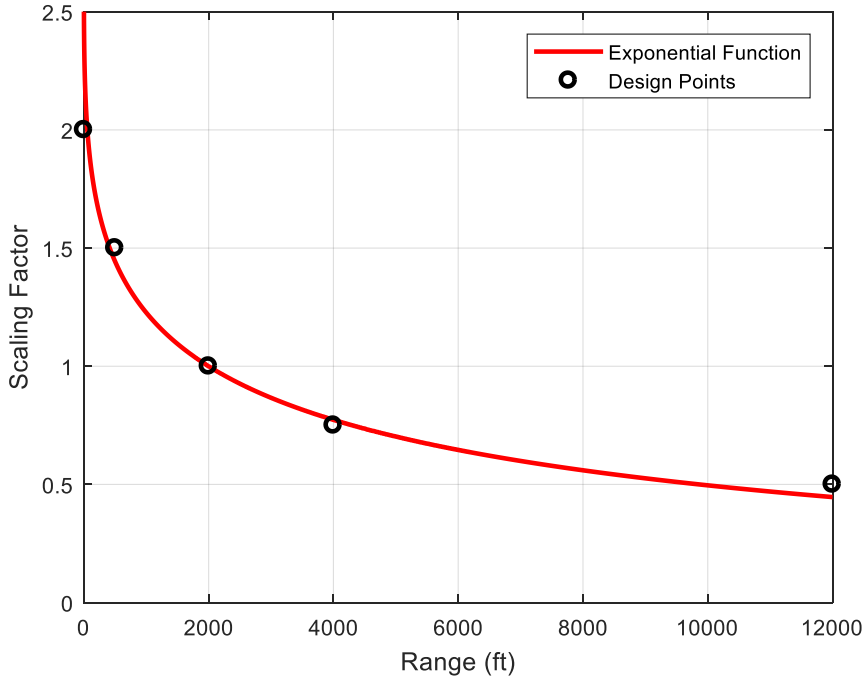

Figure 41. Exponential n_R Gain Scaling Function

These numbers work well for a bandit with these specific performance conditions and a turn radius of approximately 1,000 ft. But the more generic form of Eq. (37) is as follows:

$$k' = e^{\left(1-\sqrt[3]{\frac{r_{bdt}}{2 \cdot R_{bdt\,min}}}\right)} \tag{38}$$

This equation accounts for the bandit's dynamically changing maximum performance turn circle.

This gain scheduling is only part of the solution, however. Going back to the E-M diagram, it is also important to understand the additional penalty that is incurred when the fighter is below corner airspeed. Therefore, the fighter should balance the aggressiveness of the maneuver inside vs. outside the bandit's maximum performance turn circle, with a resistance to bleed energy unnecessarily below corner airspeed. The solution was not a switching function, but rather an additional scaling factor that is applied to the k_{nr} term when the fighter is below corner airspeed.

$$k_{n_R}{}' = \begin{cases} k_{n_R} \cdot e^{\left(1-\sqrt[3]{\frac{r_{bdt}}{2 \cdot R_{bdt\,min}}}\right)} & ; v_{ftr} \geq v_{corner} \\ k_{n_R} \cdot e^{\left(1-\sqrt[3]{\frac{r_{bdt}}{2 \cdot R_{bdt\,min}}}\right)} \cdot \left(\frac{v_{ftr}}{v_{corner}}\right) & ; v_{ftr} < v_{corner} \end{cases} \quad (39)$$

Assuming a corner airspeed of 500 ft/sec, and a k_{nr} of 0.1667, the total gain scheduling function looks like Figure 42 below.

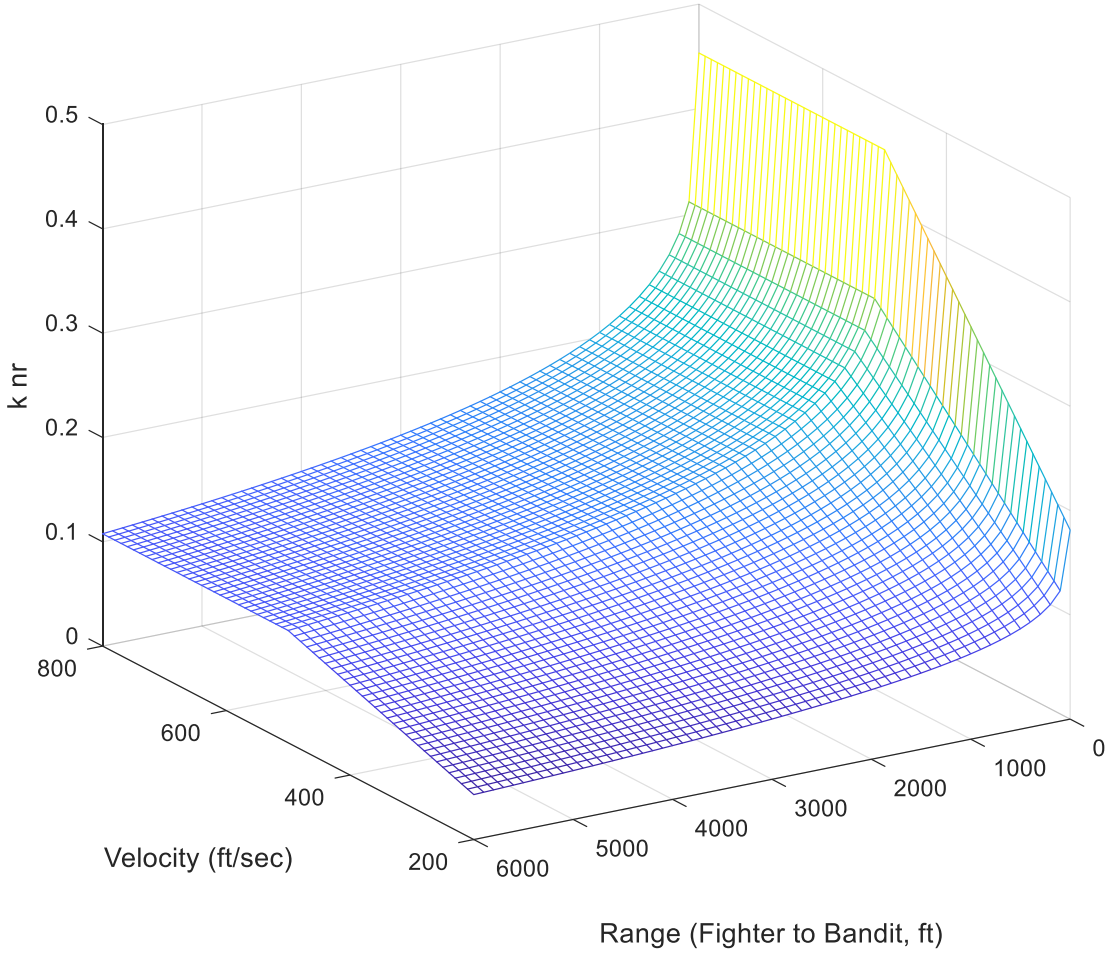

Figure 42. k_{nR}' Gain Scheduling

This is a near-complete picture of how the radial acceleration should be scheduled as a function of ATA_{ap} and range between the fighter and bandit. The objective is to get the fighter to null out the ATA_{ap}. An updated guidance block diagram is shown below.

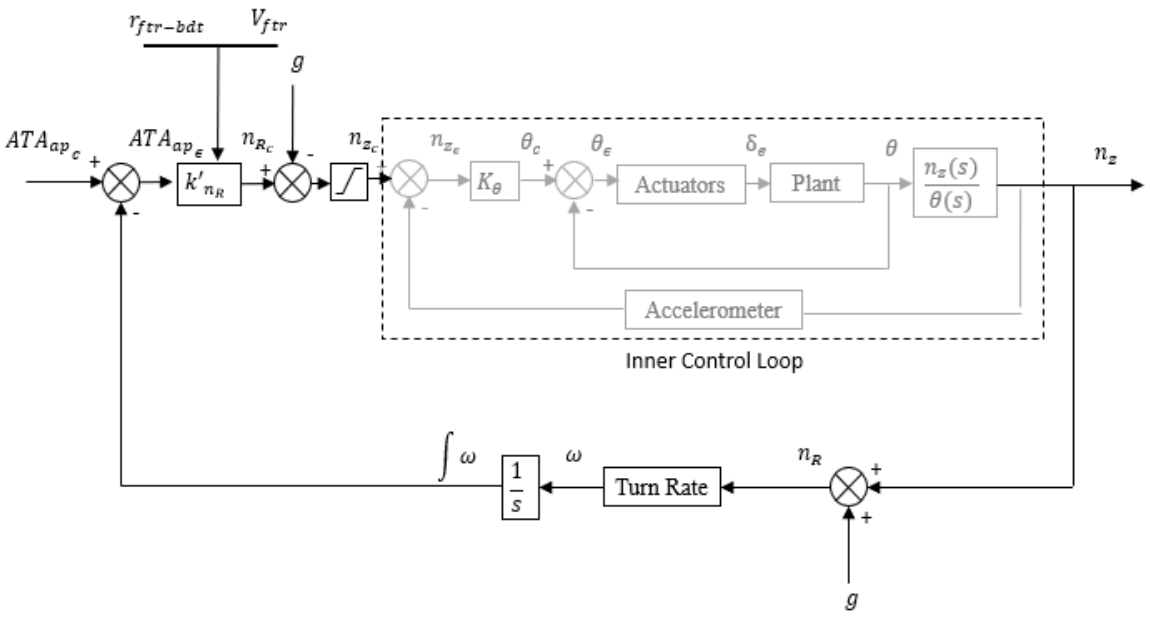

Figure 43. Acceleration Guidance Block Diagram

But as explained previously, the flight control systems of the fighter do not execute based on radial acceleration; the flight control surfaces deflect in order to generate pitch and longitudinal acceleration in the body and/or wind frame of reference. In order for the fighter to execute a radial acceleration, a roll command must be executed in order to align the fighter's radial frame of reference properly with respect to the commanded radial acceleration.

The angular relationship between the fighter and aimpoint is important. See Figure 44 below. Both aircraft are shown from behind, and the aimpoint is directly behind the bandit, as is the case in the abeam scenario with a non-maneuvering bandit. Unlike the abeam scenario in Figure 37 however, Figure 44 shows the aircraft at different altitudes in order to better illustrate the generalized form of this angular relationship.

The process that follows may seem cumbersome at first. But in simplest terms, it is a mathematical way to determine what magnitude the fighter needs to roll, and in what direction,

in order to align the fighter aircraft to the desired angle and affect radial acceleration in the proper direction.

In any state, the fighter has a value that defines its current roll angle, φ. But in order to generate the desired roll angle command (φ_{cmd}), the commanded radial acceleration must first be corrected for gravity.

$$\underline{n}_{z_B\,cmd} = \underline{n}_{z_R\,cmd} + \underline{g} \tag{40}$$

And of course, the magnitude of the gravity correction is a function of the fighter's pitch angle (θ_{ftr}).

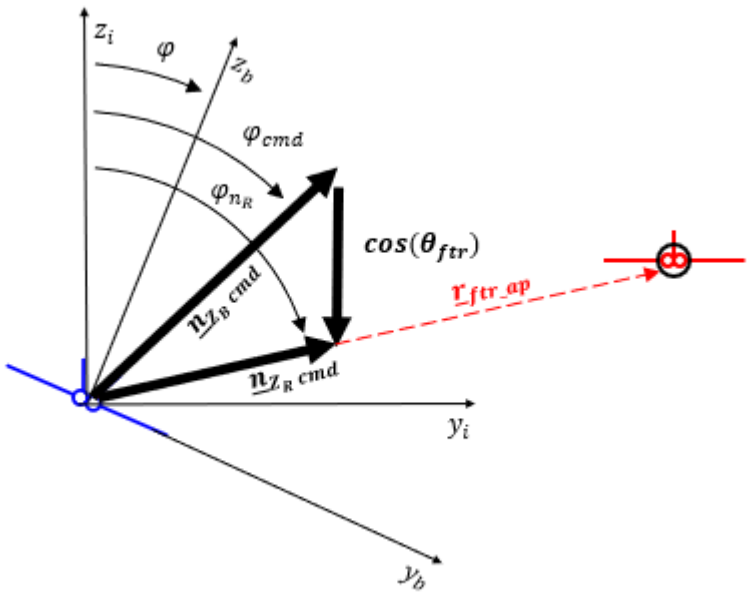

Figure 44. Angular Relationship Between N_{Z_B} and N_{Z_R}

Note that the entirety of the $\underline{n}_{z_B\ cmd}$ and $\underline{n}_{z_R\ cmd}$ vectors are in line with the *y*-*z* frame in the fighter aircraft's body frame of reference. This is derived from the very definition of the radial frame of reference in Section 6.1, where the vector $\underline{n}_{z_R}$ is orthogonal to the aircraft's velocity vector (leveraging the simplifying assumption that α is negligible at high speeds).

But the direction of $\underline{n}_{z_B\ cmd}$ vectors is not the whole story either, because the magnitude of the $\underline{n}_{z_B\ cmd}$ vector is saturated by the aircraft design limits. In the case shown above, even if $\left|\underline{n}_{z_R\ cmd}\right|$ is saturated by gain scheduling, the magnitude $\left|\underline{n}_{z_B\ cmd}\right|$ could possibly exceed aircraft design limits after correcting for gravity. Therefore, $\underline{n}_{z_R\ cmd}$ needs an additional check (and possible adjustment) while calculating the roll and acceleration guidance commands. Figure 45 below shows the problem in more detail. The maximum magnitude of $\underline{n}_{z_B\ cmd}$ is shown as a circle around the fighter.

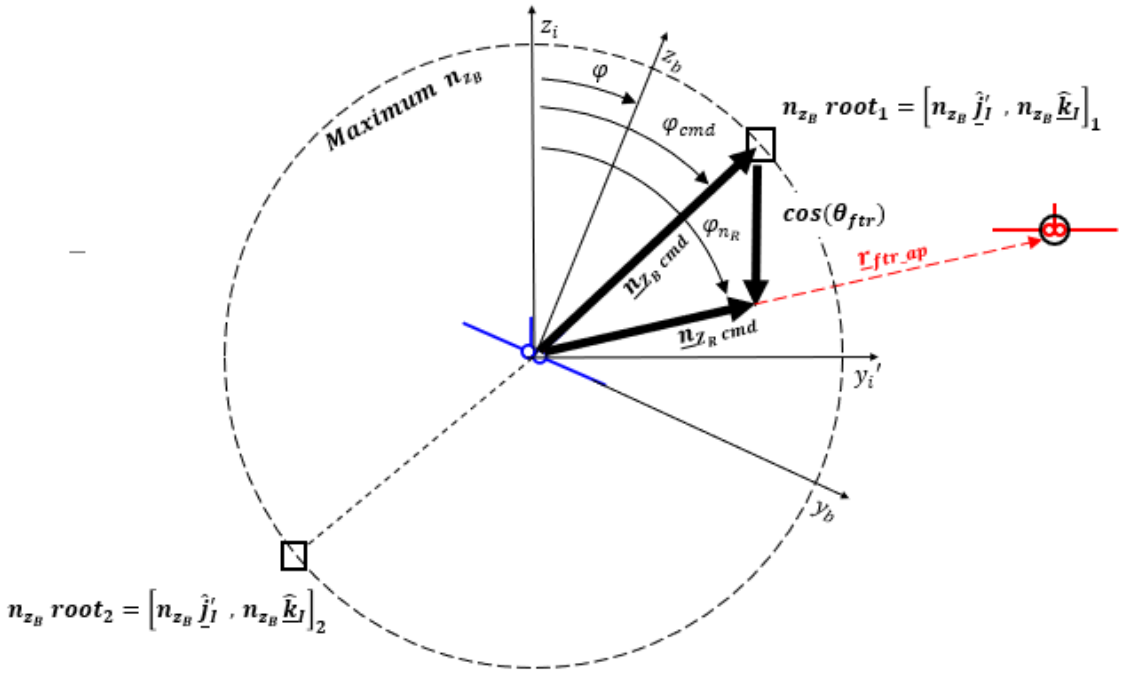

Figure 45. Calculating φ_{n_R}

The angle φ_{n_R} is the angle of the $\underline{n}_{z_R\,cmd}$ vector off the inertial *z*-axis.

$$\varphi_{n_R} = \measuredangle\left(\left[\hat{\underline{I}}\right]^T\begin{bmatrix}0\\0\\1\end{bmatrix}, \left[\hat{\underline{I}}\right]^T\underline{n}_{z_R\,cmd}\right) \tag{41}$$

But in order to calculate φ_{cmd}, the angle off the inertial *z*-axis must be known, as in Figure 44. This is a busy figure, but here are some takeaways: First, the bearing of the resultant $\underline{n}_{z_B\,cmd}$ vector (the angle relative to true North) is inconsequential to calculating the roll angle command. The only thing that matters here is the angle of depression off the inertial *z*-axis. The fighter could be heading North, East, or any direction for that matter. For this reason, and for the purposes of calculating the roll angle command, the inertial *y*-axis and respective $\hat{\underline{j}}_I$ component vectors in Figure 44 are represented with an apostrophe ($\hat{\underline{j}}_I{}'$), which simply represents the *relative* bearing from the fighter to the bandit. Because the magnitude of the fighter's maximum load factor is known, the roll command angle at the maximum load factor can be determined from φ_{n_R} and $\underline{n}_{z_B\,max}$.

Examine the singular case where $\underline{n}_{z_B\,cmd}$ is set equal to $\underline{n}_{z_B\,max}$. In this condition, the following equation holds true:

$$\left|n_{z_R\,max}\right| =$$

$$\left|\underline{n}_{z_B\,max}\right| \cdot \{1 + \left|\sin\left(\varphi_{n_R}\right)\right| \cdot (1 - \sin\left(\operatorname{acos}\left(\frac{1}{\left|\underline{n}_{z_B\,max}\right|}\right)\right)\} - \cos\left(\varphi_{n_R}\right) \cdot \left|\cos\left(\theta_{ftr}\right)\right| \tag{45}$$

Since the orientation of the $\underline{n}_{z_R\,cmd}$ vector is known, the entirety of the vector $\underline{n}_{z_R\,cmd}$ is derived. Using the correction for gravity from Eq. (40), the vector and magnitude of the maximum load factor command is determined.

Because the endstate is a desired roll command, the final concern at this point is the angle about the *x*-axis of the body frame. Therefore, the difference between φ and φ_{cmd} is calculated trigonometrically within the *y*-*z* plane of the body frame.

$$\varphi - \varphi_{cmd} = \Delta\varphi_{cmd} = \measuredangle\left(\left[\underline{\hat{B}}\right]^T\begin{bmatrix}0\\0\\-1\end{bmatrix}, \left[\underline{\hat{B}}\right]^T\underline{n}_{z_{B\,cmd}}\right) \tag{46}$$

Just to recap the process up to this point: the desired radial acceleration vector ($\underline{n}_{z_{R\,cmd}}$) was specified as a function of ATA_{ap}, $|r_{ftr\text{-}bdt}|$, and V_{ftr}. The magnitude $\left|\underline{n}_{z_{R\,cmd}}\right|$ was then corrected for gravity and truncated, in order to derive a command for longitudinal acceleration in the body frame ($\underline{n}_{z_{B\,cmd}}$) that is within fighter aircraft design limits. Finally, the roll angle command (φ_{cmd}) was derived from the $\underline{n}_{z_{B\,cmd}}$ vector.

The shaping function for scheduling the roll command was chosen as a function of range from the fighter to the aimpoint. The objective was to keep the gain constant (and high, based on a fighter aircraft's capability for high roll rates), but to reduce the gain as the fighter settled closer to rendezvousing at the aimpoint. At ranges greater than 1500 feet, the gain was constant at k_φ= 8. Inside of 1500 feet, this term was multiplied by the exponentially decreasing ratio.

$$k_\varphi{}' = \begin{cases} k_\varphi \cdot \left(\frac{r_{ap}}{1500}\right)^2 & ;\, r_{cz} \le 1500\,ft \\ k_\varphi & ;\, r_{cz} > 1500\,ft \end{cases} \tag{47}$$

From Eq. (47) above, the block diagram in Figure 39 is updated to reflect the roll-command guidance in Figure 46 below.

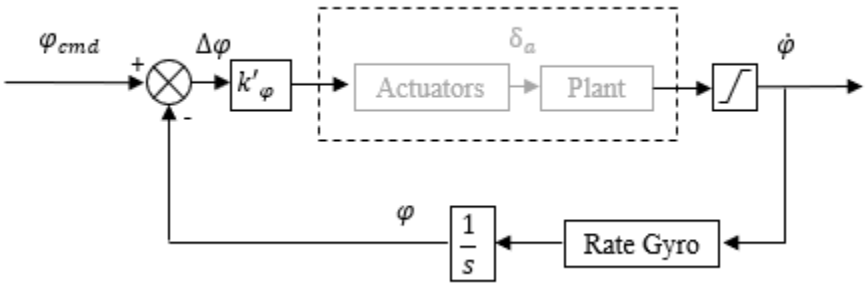

Figure 46. Updated Roll Guidance Block Diagram

There is one more factor to consider before these roll and acceleration commands are coupled in an effective guidance scheme. The fighter aircraft should not execute the full magnitude of roll and acceleration commands simultaneously. They should be done in sequence. This can be managed by scaling k_{n_R} (once again!) as a function of $\Delta\varphi_{cmd}$. When $\Delta\varphi_{cmd}$ is large, the fighter needs to prioritize an unloaded roll to the desired orientation. As $\Delta\varphi_{cmd}$ decreases, the fighter can then increase the longitudinal acceleration command. Previously in Eq. (38), k' was used as a function of range. Now, k'' is used as a function of $\Delta\varphi_{cmd}$.

$$k'' = min(1, \frac{6^\circ}{\Delta\varphi_{cmd}}) \tag{48}$$

$$k_{n_R}{}'' = k'' \cdot k_{n_R}{}' \tag{49}$$

where $\Delta\varphi_{cmd}$ is in degrees. The resultant curve is shown below in Figure 47.

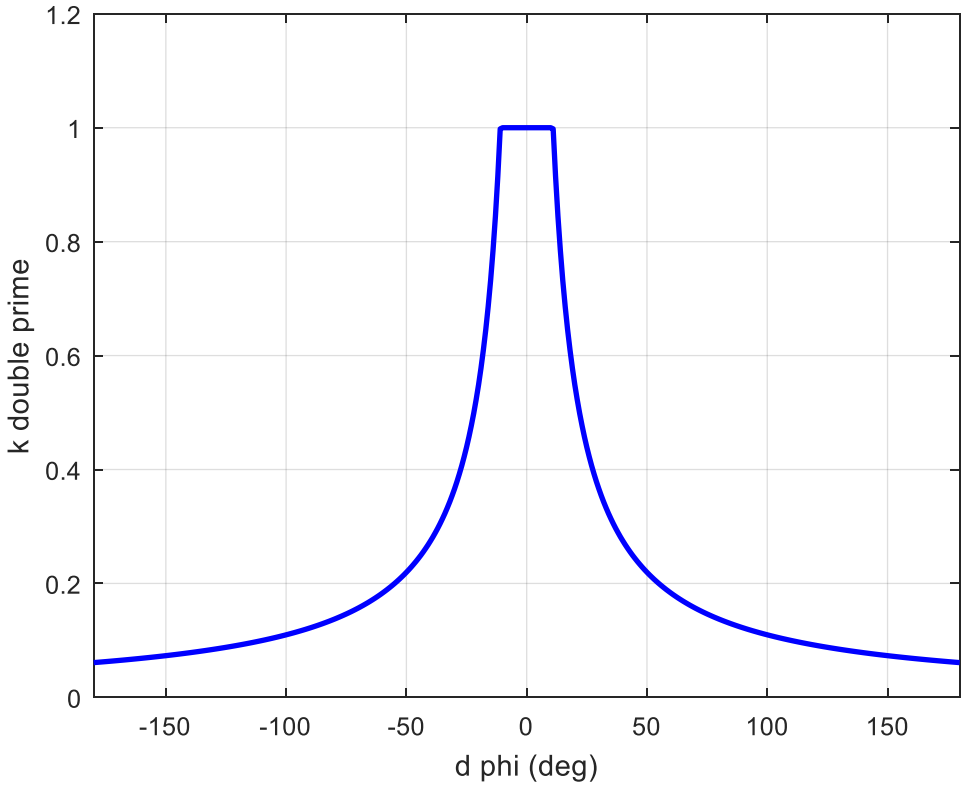

Figure 47. K''$_{nr}$ Gain Scheduling

This final scaling factor creates the effect of sequential actions (roll-THEN-pull) instead of simultaneous actions (roll-AND-pull). It also epitomizes how coupled the roll and acceleration guidance commands are. The guidance block diagrams are updated once more, and joined, in Figure 48.

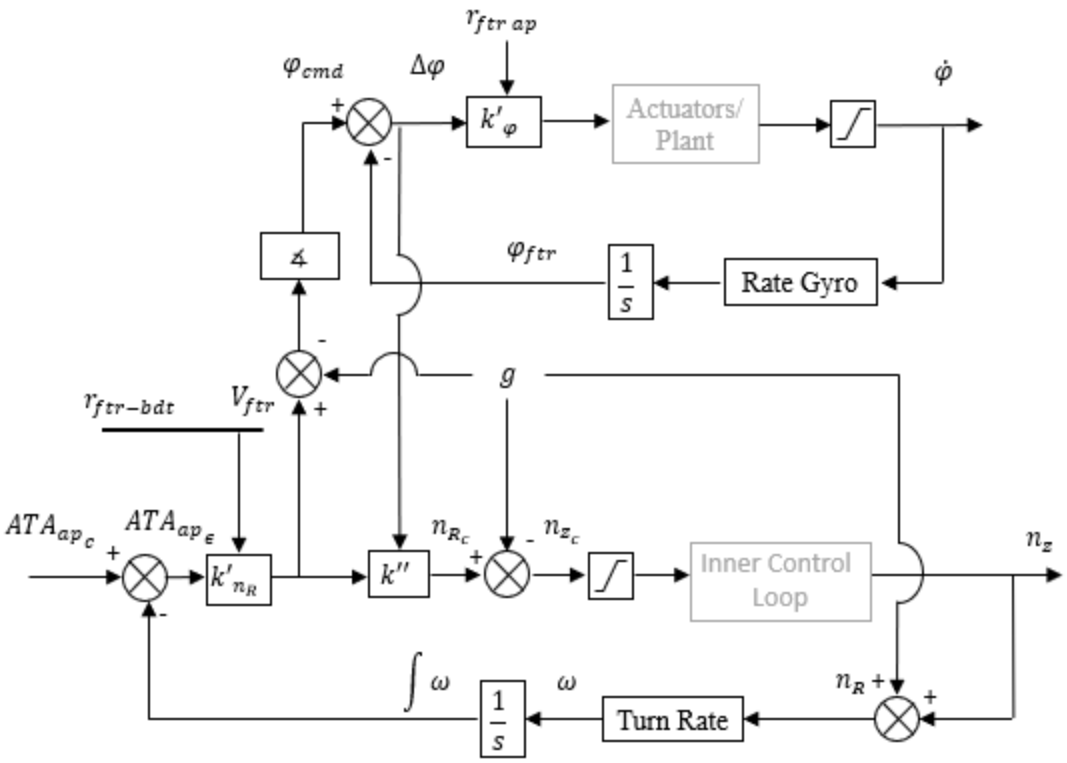

Figure 48. Roll and Acceleration Guidance Block Diagram

There is one more important state to consider, which is the relative velocity between the fighter and the bandit. Energy advantage is beneficial in the short term, but at some point, airspeed needs to be controlled in order to prevent the fighter to overshoot the close-edge of the control zone. Recall from the example all the way back in Figure 18, the worst-case scenario for the fighter would be to overshoot the bandit's aircraft entirely, trading an offensive position for a defensive one.

As a baseline assumption, the fighter should maintain maximum allowable thrust throughout most of the engagement, in order to maintain as much kinetic energy as possible. Therefore, while the guidance command to reduce the fighter's velocity should be such that the velocities of these two aircraft are equal, the execution of this control scheme should be limited to *only when the*

fighter is established at the desired aimpoint and the angular problem is solved. This emphasized caveat is shown below, with selected design points for gain scheduling factor, $k_{\Delta v}$:

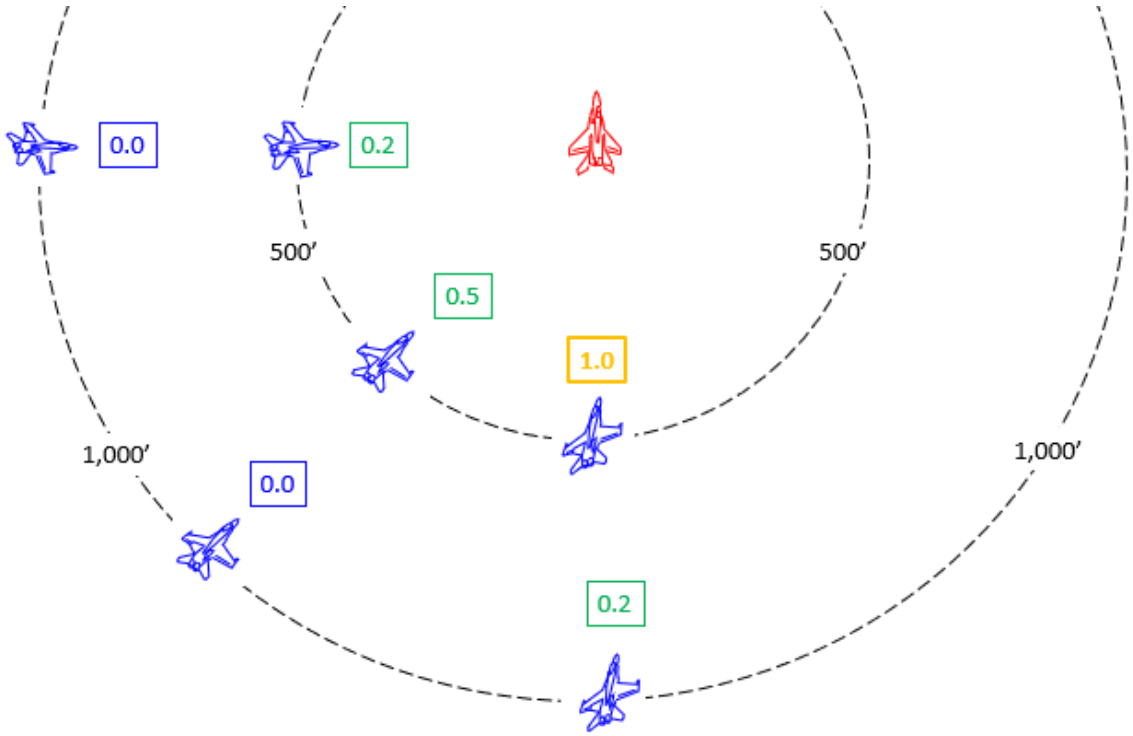

Figure 49. Desired $k_{\Delta v}$ Gain Scaling Factors

These desired values are subjective design points chosen by the author, based on engineering judgement. Note that the highest gain should occur when the fighter is close to the bandit with low ATA. The gain scaling factor decreases as range and ATA increase. Just as before, this relationship can be a number of possibilities, including linear, exponential, etc. For this example, the author chose the following gain scaling function:

$$k_{\Delta v}{}' = \begin{cases} k_{\Delta v} \cdot \left[\left(\left(\frac{|r_{ftr-ap}|}{500} \right)^3 \right) \left(\frac{|ATA|}{45°} + 1 \right) \right]^{-1} & ; ATA_{cz} \leq 60° \\ 0 & ; ATA_{cz} > 60° \end{cases} \quad (50)$$

This function obviously has two independent variables: the fighter's range to the bandit in feet ($r_{ftr-bdt}$) and the antenna train angle to the bandit in degrees (ATA_{bdt}). The relationship between these two is shown graphically in Figure 50 below.

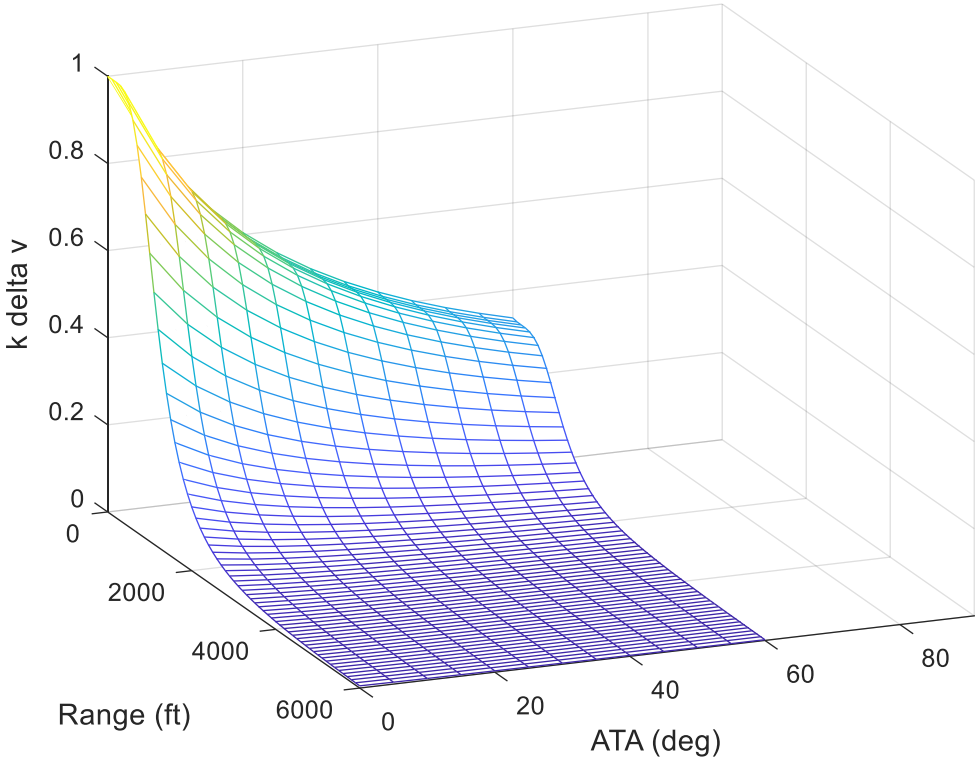

Figure 50. $k_{\Delta V}$ Scheduling

3. Managing Pursuit Curves Through an Adjustable Aimpoint

Both scenarios demonstrated in the previous section (5.2.2) used a constant value for k_{ap}. The aimpoint was coincident with the near-side of the bandit's control zone. This essentially forced the fighter into lag pursuit and in-plane with the bandit's turn circle, regardless of the positional and angular relationship between the fighter and the bandit, or the difference in airspeed between

the two. This is not optimal, because BFM should include a mix of lag pursuit, pure pursuit, and even lead pursuit sometimes. It should also include vertical or out-of-plane maneuvering when required. The very nature of BFM requires an autonomous platform to smoothly transition between these pursuit curves.

In order to smoothly change from one pursuit curve to another, the aimpoint must be adjusted. From Section 3.3.4, the control zone is located at 1-2 turn radii behind the bandit and along the turn circle [11]. That definition does not change. Nor do the roll, acceleration, and velocity commands change. These guidance commands remain the same as in the previous section. The concept of a moveable aimpoint is another novel concept that differs from all the other attempts at autonomous BFM found in the literature survey. So how is the aimpoint adjusted?

The best method is to adjust k_{ap} as a function of relative offensive/defensive advantage for the fighter. When the fighter is more offensive, lag pursuit is prioritized in order to manage the range, angles and closure problem. If the fighter is neutral, then pure pursuit is prioritized. When the fighter is defensive, then lead pursuit is used to create a range, angles, and closure problem, by moving the aimpoint in front of the bandit. See Figure 51.

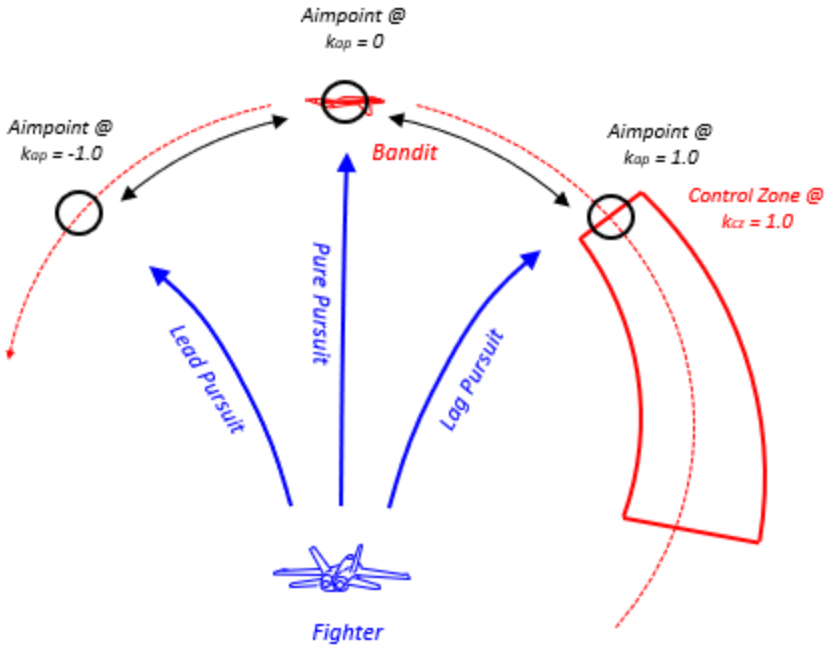

Figure 51. Lead, Pure, and Lag Pursuit with Adjustable Aimpoint

This method of adjusting k_{ap} requires a parameter to specifically define offensive vs. defensive BFM. In Section 3.3.1, advantage was defined as two types: energy advantage or angular advantage. These can be quantified via fuzzy methods, just like the scaling functions for roll, acceleration, and velocity commands. With respect to angular advantage, the two angles that matter are *TA* and ATA_{bdt}. The equation used to define angular advantage (S_A) is similar to McGrew's method in reference [67] and Eq. (11). The value here is bounded between -0.5 and 0.5.

$$S_A = \frac{180° - |ATA_{bdt}| - |TA|}{360°} \tag{52}$$

Energy advantage is defined by the relationship of specific energy (E_s) between the fighter and the bandit. This is an exponential sigmoid function in order to bound the top and bottom value of the energy advantage value (S_E). This number is also bounded between approximately -0.5 and 0.5.

$$S_E = e^{\left(-\frac{E_{s\,bdt}}{E_{s\,ftr}}\right)} - (0.15 + e^{(-1)}) \tag{53}$$

The total advantage factor for the fighter (S) is the sum of the angular advantage factor and the energy advantage factor. This aimpoint scaling factor (k_{ap}) is set equal to S. Thus, the total value of k_{ap} is bounded between -1.0 and 1.0.

$$S = S_A + S_E \tag{54}$$

$$k_{ap} = S \tag{55}$$

At the extreme of fighter advantage (maximum angular advantage and energy advantage), k_{ap} is set to 1.0, and the aimpoint is coincident with the near-side of the bandit's control zone. When the fighter and bandit are completely neutral, k_{ap} is set to zero, and the aimpoint is coincident with the bandit's aircraft, forcing pure pursuit. At the extreme of fighter disadvantage (maximum angular disadvantage and energy disadvantage), k_{ap} is set to -1.0, and the aimpoint is in front of the bandit, forcing lead pursuit.

The aimpoint is also adjusted higher or lower in inertial space in order to facilitate vertical maneuvering. When the fighter wants to maneuver upwards, the aimpoint is adjusted higher in inertial space. Conversely, when the fighter wants to maneuver downwards, the aimpoint is moved

lower in inertial space. Since the aimpoint is defined by a position in inertial space ($\underline{r}_{i\ ap}$), the $\hat{k}$ component can simply be increased or decreased, as required.

Section 3.3.8 discussed how the fighter can capitalize on vertical maneuvering, particularly if the fighter has a broader envelope of maneuverability on the VEM diagram. But it only makes sense for the fighter to make an extreme out-of-plane maneuver if the bandit cannot immediately threaten the fighter, e.g. in a high-aspect or neutral scenario. The following equation governs the movement of the aimpoint guidance up or down in inertial space. The term $r_{i\ ap_{corr}}$ is the additive applied to the $\hat{k}$ component of the aimpoint in inertial space.

$$r_{ap_{corr}} = ((V_{ftr} - V_{min\ vert\ ftr}) - (V_{bdt} - V_{min\ vert\ bdt})) \cdot (|ATA_{bdt}| + |TA_{bdt}| + 1) \quad (56)$$

$$\underline{r}'_{ap} = [\underline{\hat{I}}]^T\ \underline{r}_{ap} + [\underline{\hat{I}}]^T \begin{bmatrix} 0 \\ 0 \\ r_{ap_{corr}} \end{bmatrix} \quad (57)$$

7. ANALYSIS OF RESULTS

The results of the proposed guidance system are very promising. Not only do they yield an offensive position for the fighter, they efficiently mimic the actions and reactions of an experienced fighter pilot. This section examines results in detail from each of the ten scenarios listed previously.

1. Abeam Scenario

In the abeam scenario, the fighter begins 2,000 ft to the bandit's side, at 90° ATA and 90° TA. The bandit is non-maneuvering. The fighter is expected to execute a hard turn towards the bandit's control zone, followed by a reversal as the fighter approaches the bandit's flight path.

In each of the figures in this section, the blue lines represent the fighter data, and the red lines represent the bandit data. The black x's represent the dimensions of the bandit's control zone, along an arclength between 1-2 times the minimum turn radii.

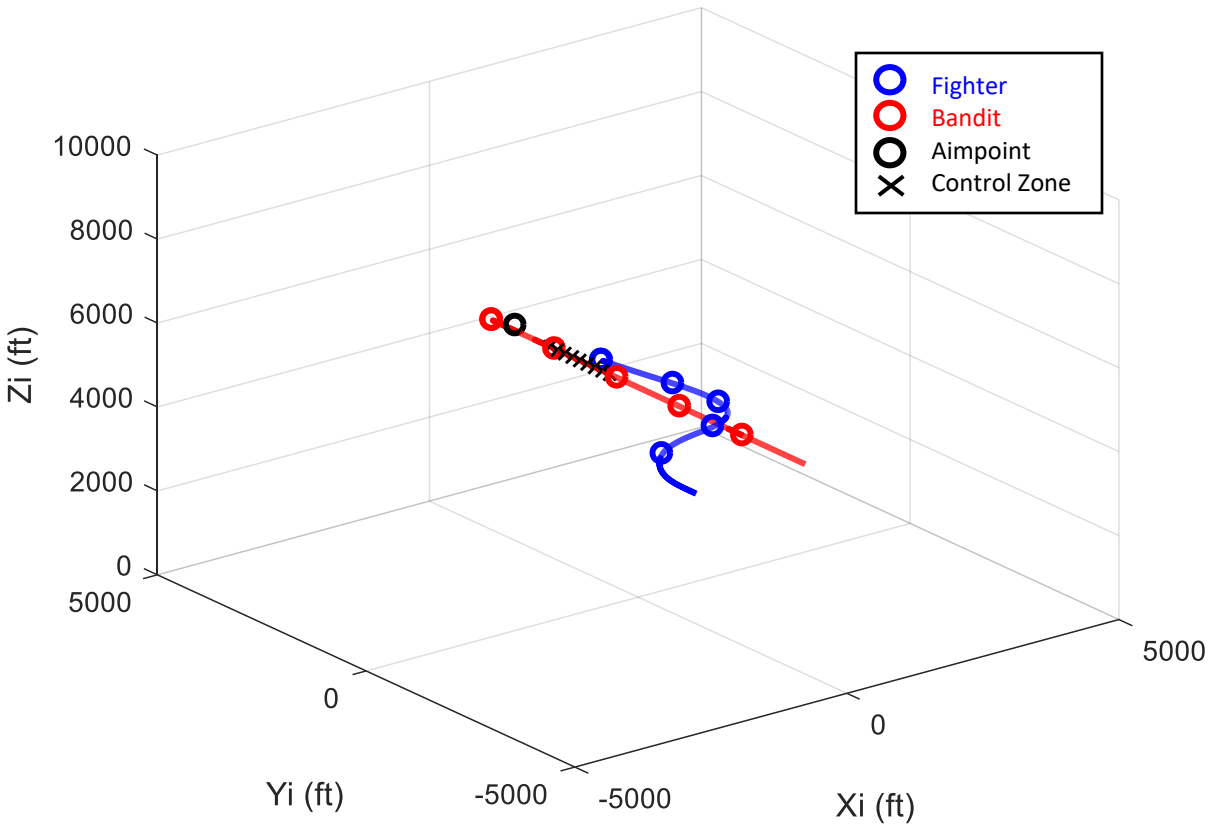

Figure 52. Abeam Scenario: Trace Plot

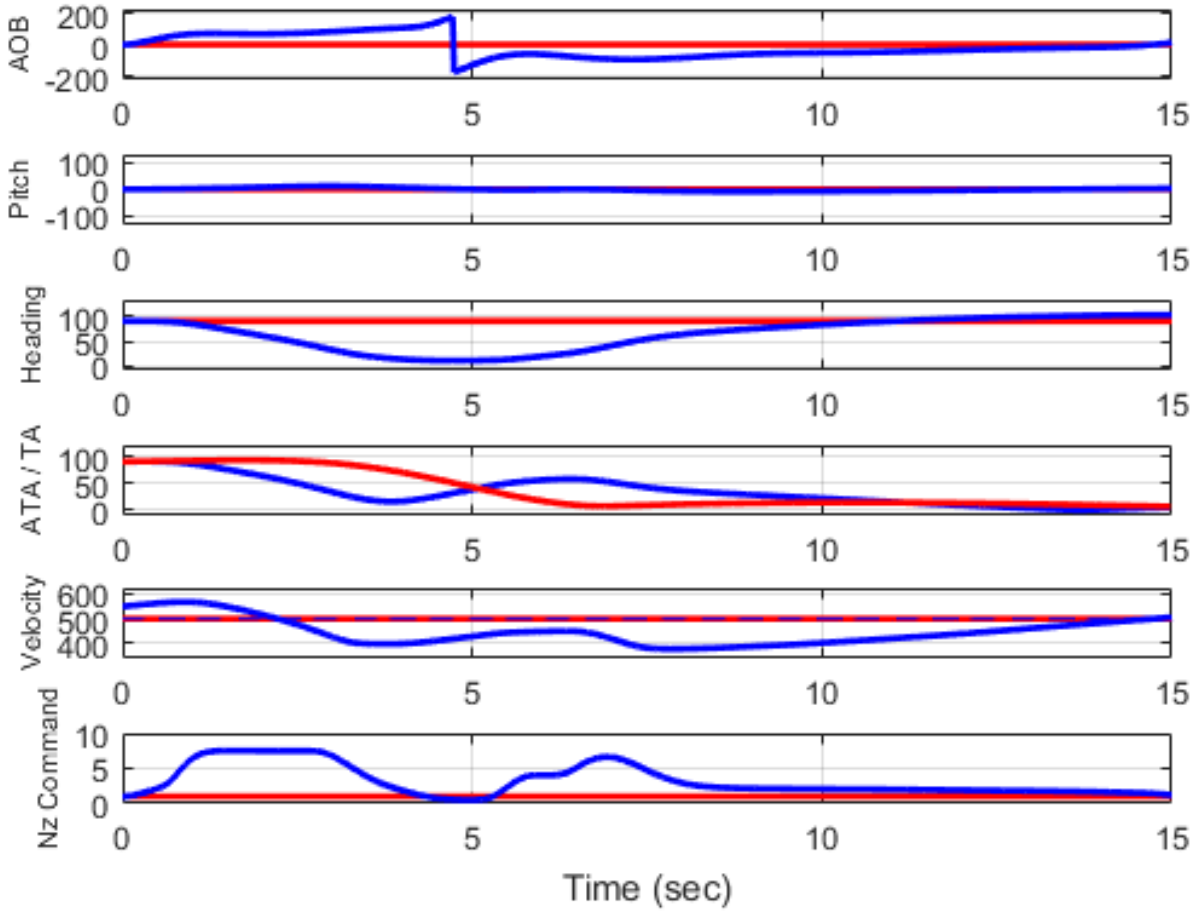

Figure 53. Abeam Scenario: Data Plot

Note that at the start, the fighter and bandit are in a neutral position, with the fighter at a +50 ft/s airspeed advantage over the bandit. The fighter's aimpoint is behind and above the bandit, as expected from equations (55) and (56). The fighter executes a roll to the right to just over 70° AOB. By t=1.25 seconds, the fighter is established in a 7.4 g turn towards an aimpoint just above the bandit's control zone.

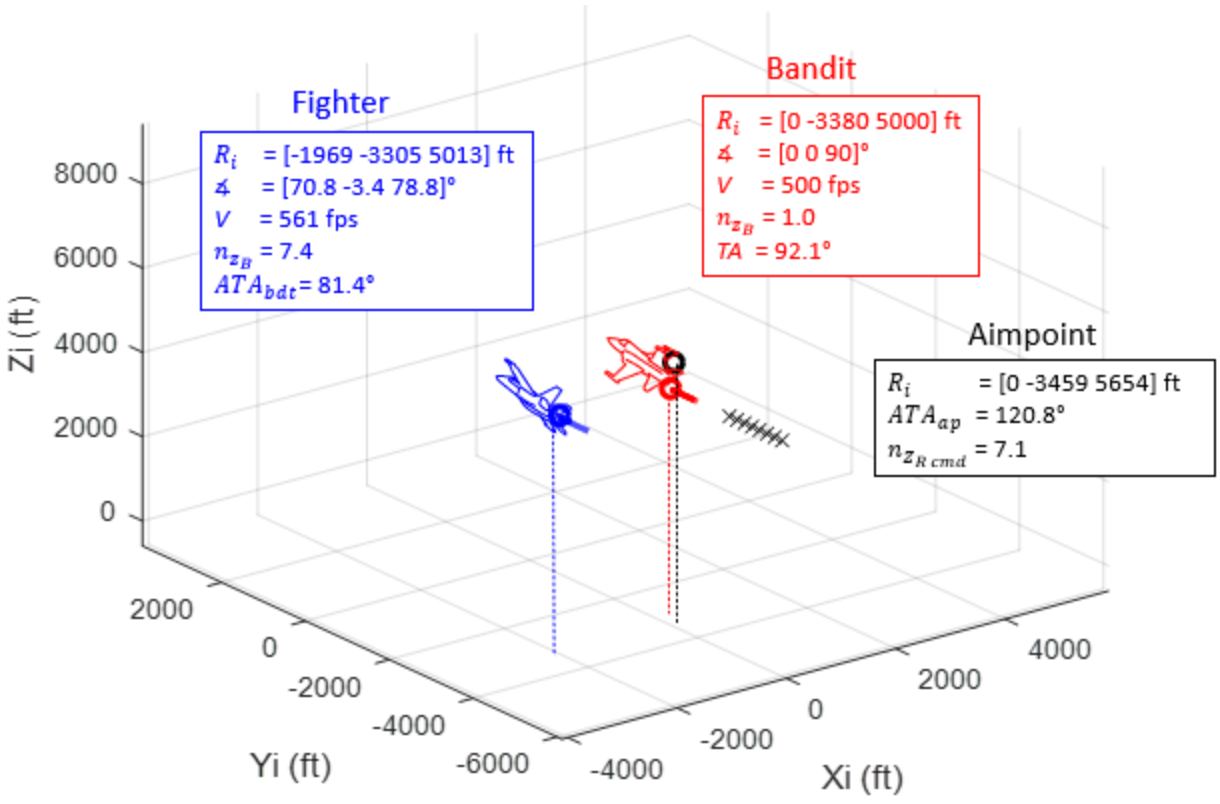

Figure 54. Abeam Scenario: Trace Plot (3D View), t=1.25 sec

Between *t*=1.25 and 3 seconds, the fighter's airspeed decreased commensurate with the maximum longitudinal acceleration. This is expected. And while airspeed loss is often not desirable, in this case the loss of airspeed serves to purposes. First, energy and maneuverability are always a tradeoff. The fighter is, in a sense, 'trading' airspeed for a more offensive positional and angular relationship with the bandit and the bandit's control zone. The second advantage is that the decreased airspeed, combined with the fighter's maneuvering, stops the downrange travel relative to the bandit. This action gives the fighter a more offensive position behind the bandit. By t=3 seconds, the *ATA* decreased to 34.5°, and the ATA_{ap} decreased to 38.0°.

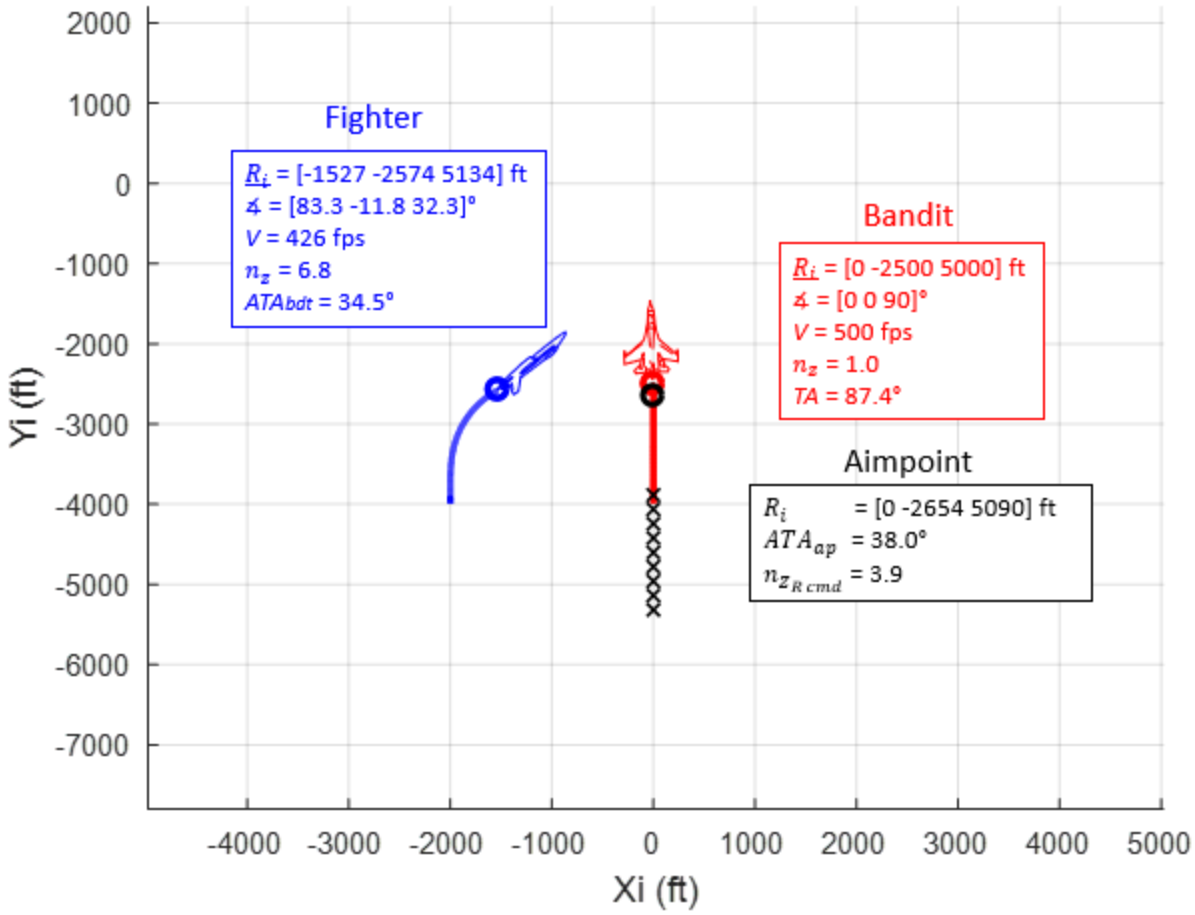

Figure 55. Abeam Scenario: Fighter Initial Turn (Top View)

At *t*=6 seconds, the fighter continues the right roll in order to start aligning fuselages with the bandit. The roll rate continues in the positive (*right-hand*) direction until the fighter is once again oriented to execute a *left-hand* reversal towards the bandit's control zone. This is known as a barrel roll attack [11], [18]. The fighter overshoots through the bandit's control zone momentarily, but the reversal is a necessary maneuver in order to establish and maintain an offensive advantage. Another highlight is that while the fighter is rolling during the reversal, the load factor is very low. This allows the fighter to regain some the airspeed lost during the initial

maneuver. Between *t*=4 to 6 seconds, the fighter's airspeed increases by +48 ft/s. (See data plots in Figure 51.)

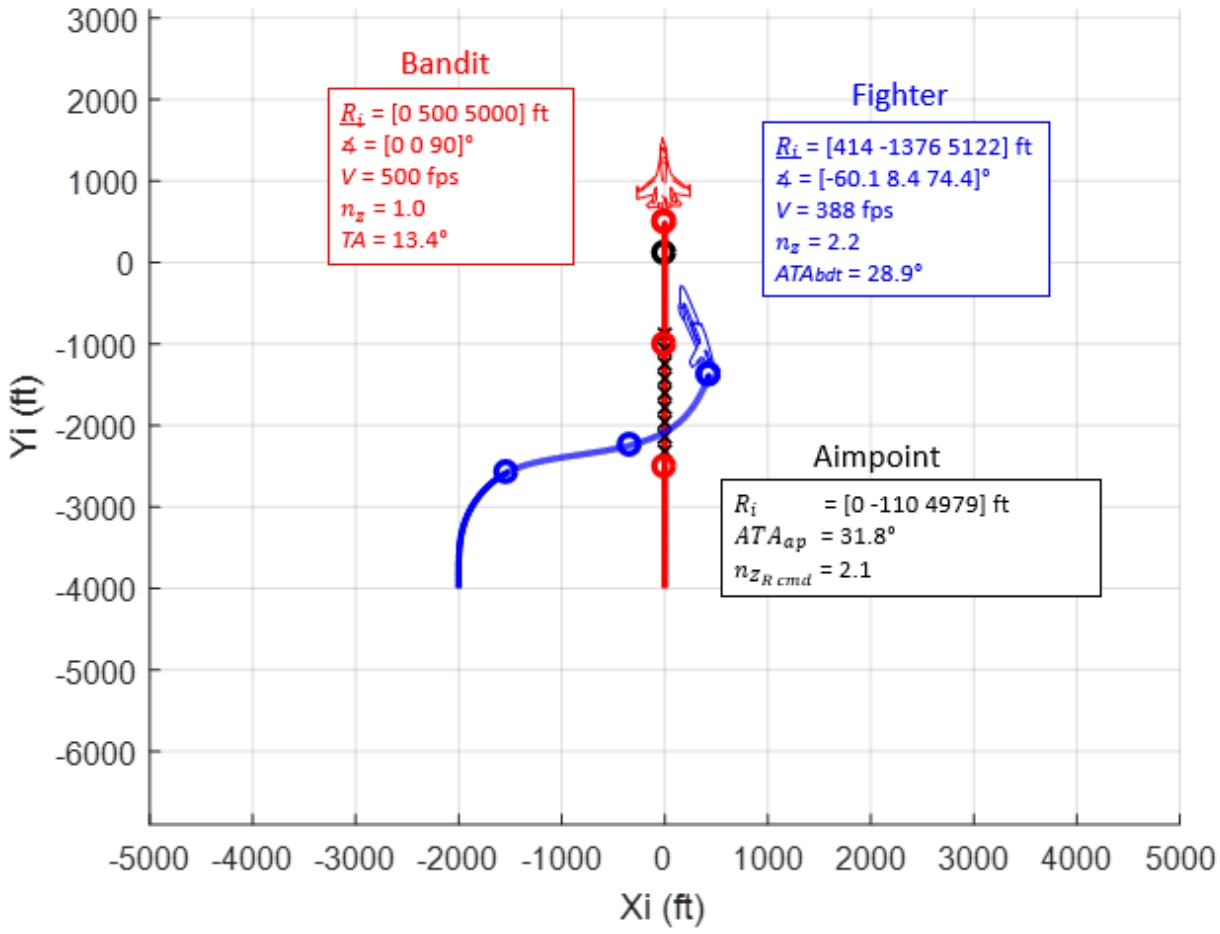

Figure 56. Abeam Scenario: Fighter Reverses (Top View)

At *t*=15 seconds, the fighter has clearly established an offensive position. The fighter is 2300 ft behind the bandit and co-altitude. The fighter's airspeed is 505 ft/s compared to the bandit's constant 500 ft/s. ATA and TA are both less than 10°. In no uncertain terms, this example represents a classic and flawless barrel roll attack from an abeam position.

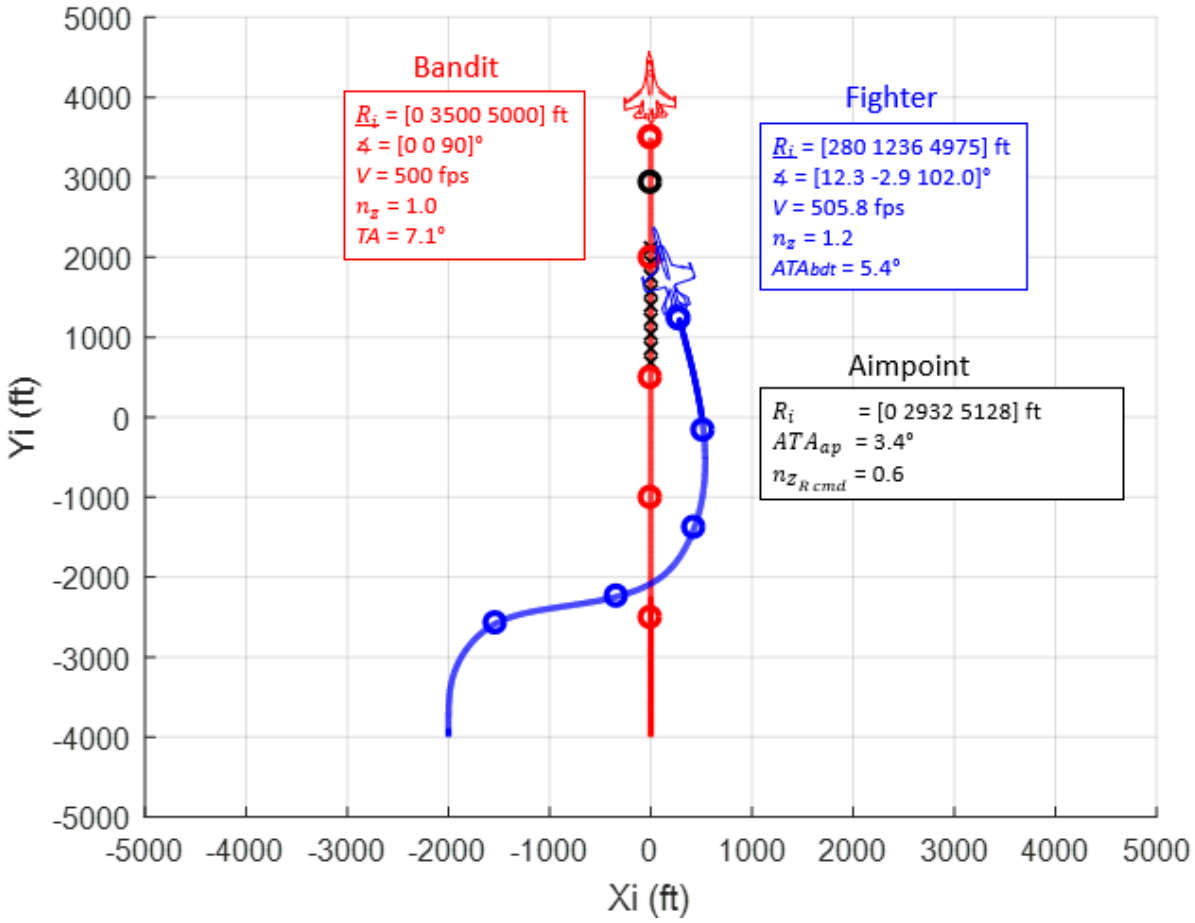

Figure 57. Abeam Scenario: Fighter Offensive (Top View)

2. 3,000 ft Perch Scenario

In the 3,000 ft perch scenario, the fighter is offensive at 40° TA behind the bandit. This places the fighter within the confines of the control zone at the start of the engagement. However, the fighter must manage a +200 ft/s airspeed advantage from the beginning.

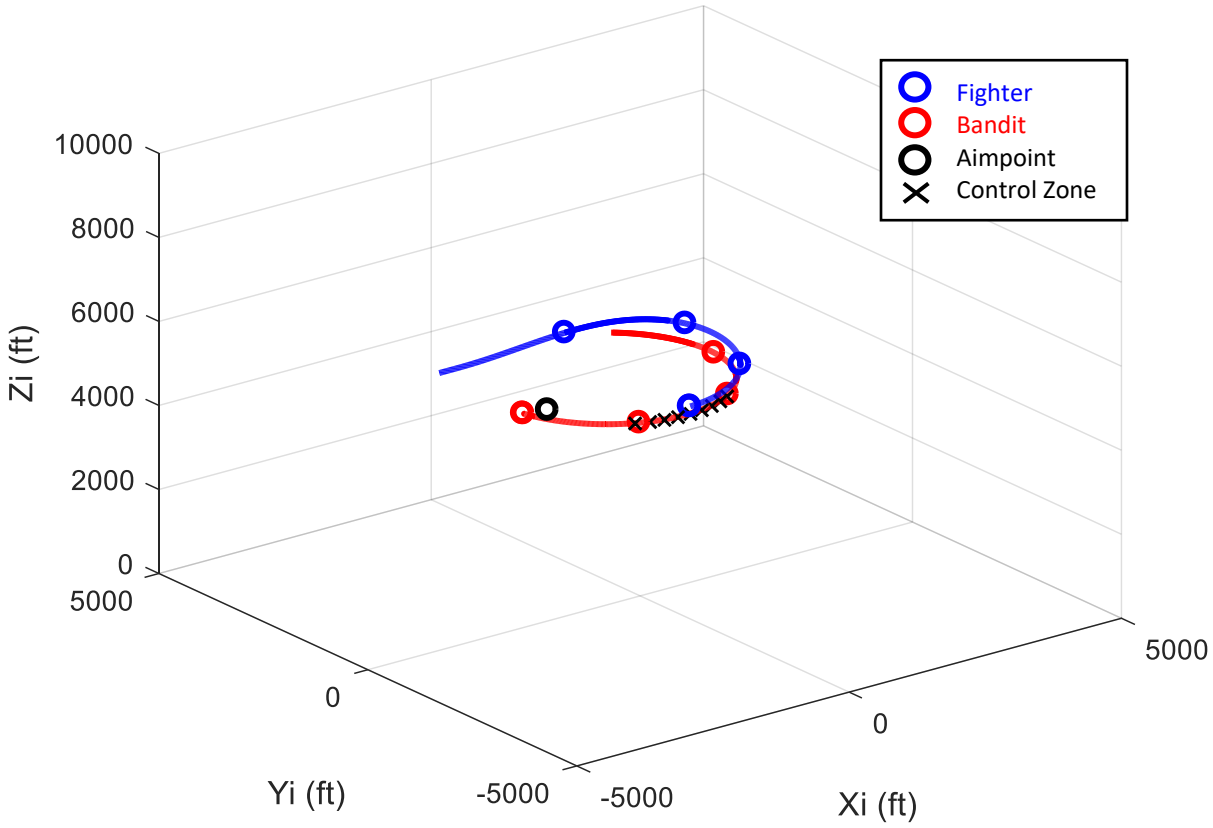

Figure 58. 3,000 ft Perch Scenario: Trace plot

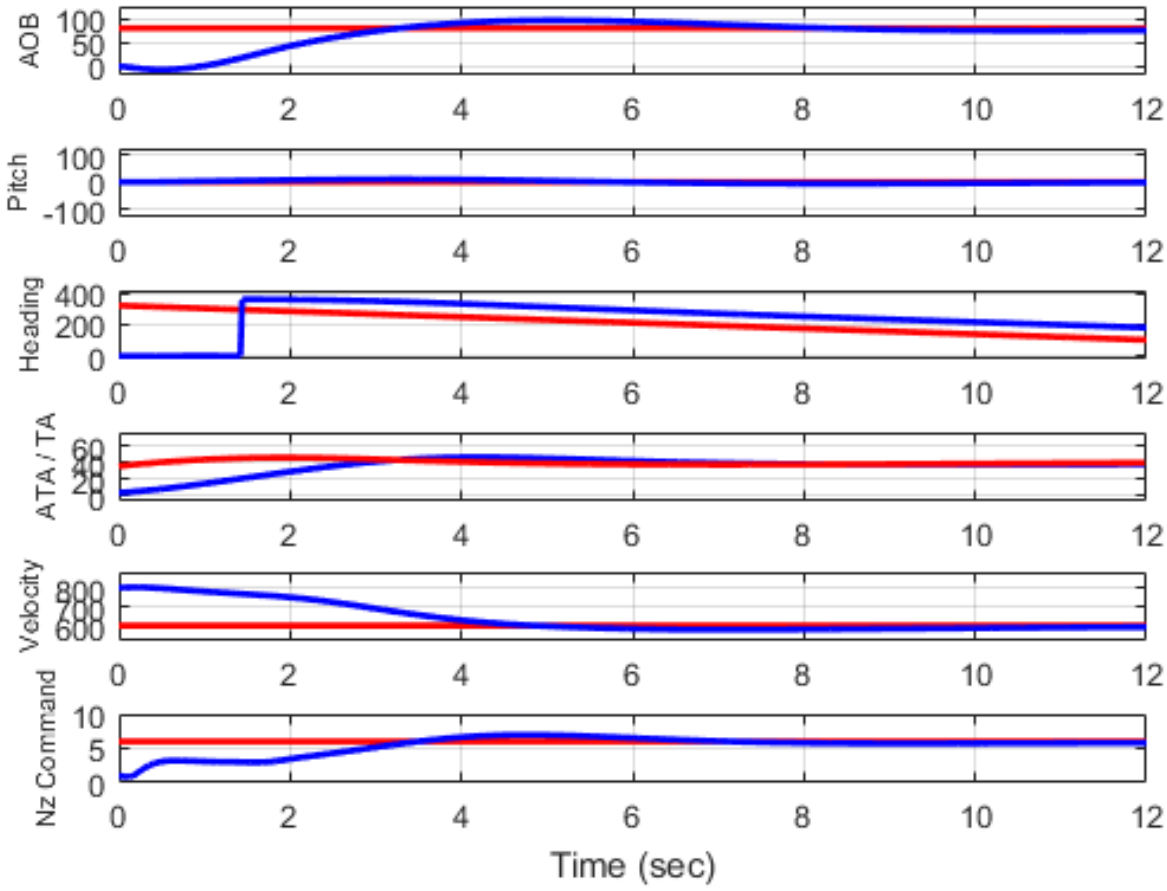

Figure 59. 3,000 ft Perch Scenario: Data Plot

At the start of this scenario, the fighter initiates a moderate 3 g pull upwards, while maintaining an offensive position in the bandit's control zone. This is more of a pause than a deliberate delay tactic. At t=1 sec, the fighter begins to roll right in order to align the fighter fuselage on the bandit's turn circle.

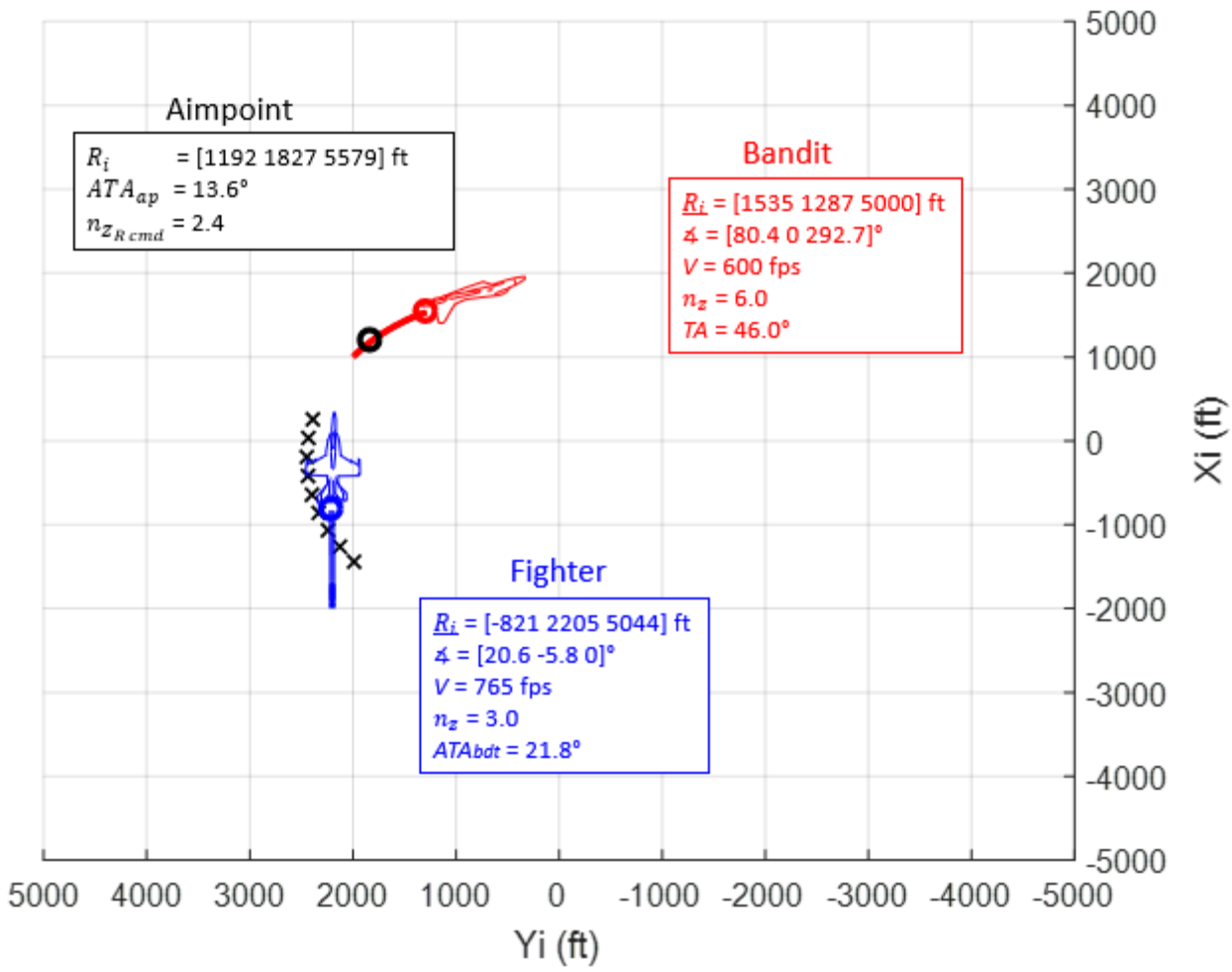

Figure 60. 3,000 ft Perch Scenario: Fighter Maneuvers to Lag (Top View)

The most interesting aspect of this example is how well the fighter is able to manage the excess airspeed from the very beginning. Using Eq. (50) in the gain scheduling guidance scheme, the fighter immediately commands a decrease in velocity. This commanded airspeed decrease, along with the negative P_s that comes with the fighter's maneuvering, enables the fighter to maintain an extremely offensive position within the bandit's control zone for the entire set. As long as the fighter has a higher airspeed than the bandit and has good fuselage alignment in accordance with Eq. (50), the fighter's command signal is to decrease airspeed.

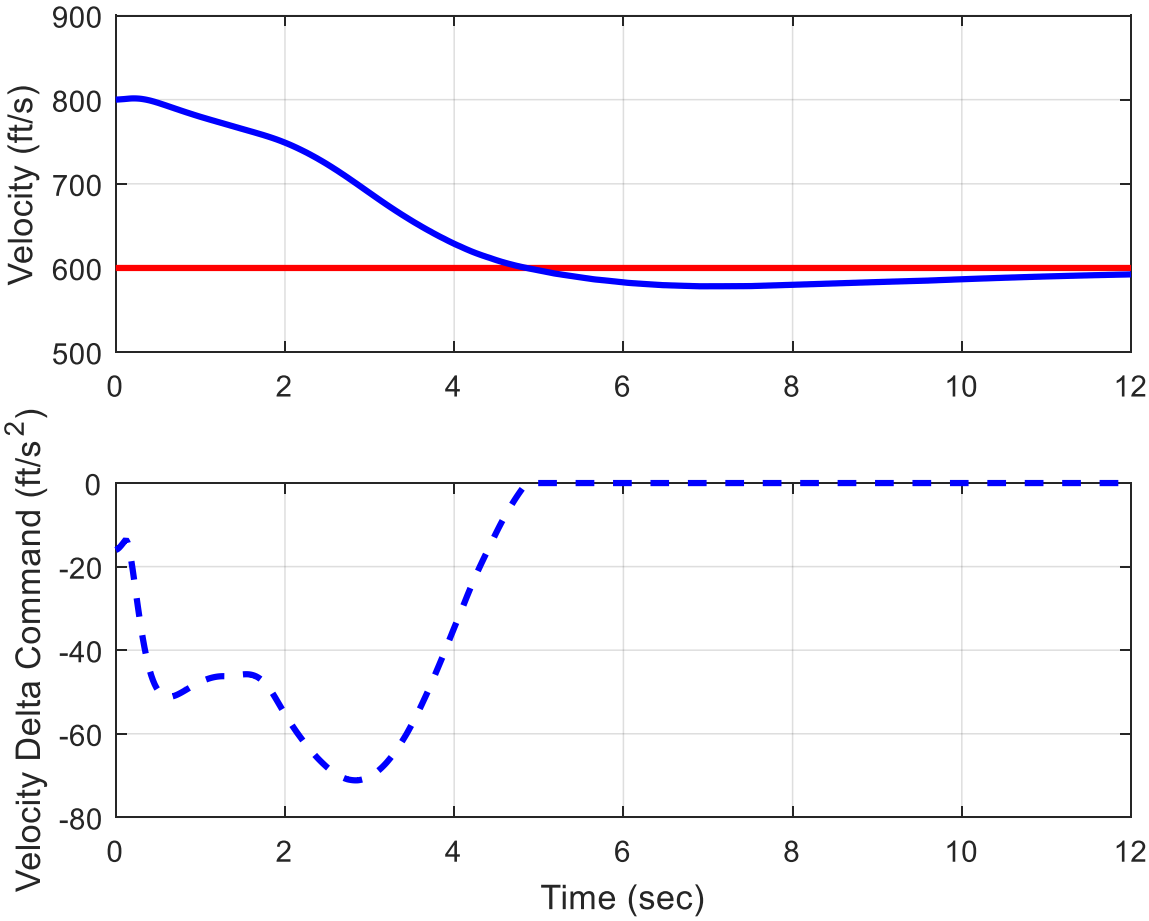

Figure 61. 3,000 ft Perch Scenario: Fighter Velocity and Velocity Command Signals

Overall, the 3,000 ft perch scenario is another successful example of the proposed guidance scheme.

3. 6,000 ft Perch Scenario

The 6,000 ft perch scenario is similar to the 3,000 ft perch scenario, except the fighter begins outside the bandit's turn circle and control zone. Instead of starting with a momentary pause, the

fighter is expected to make a deliberate move towards lag pursuit before executing a hard turn towards the control zone.

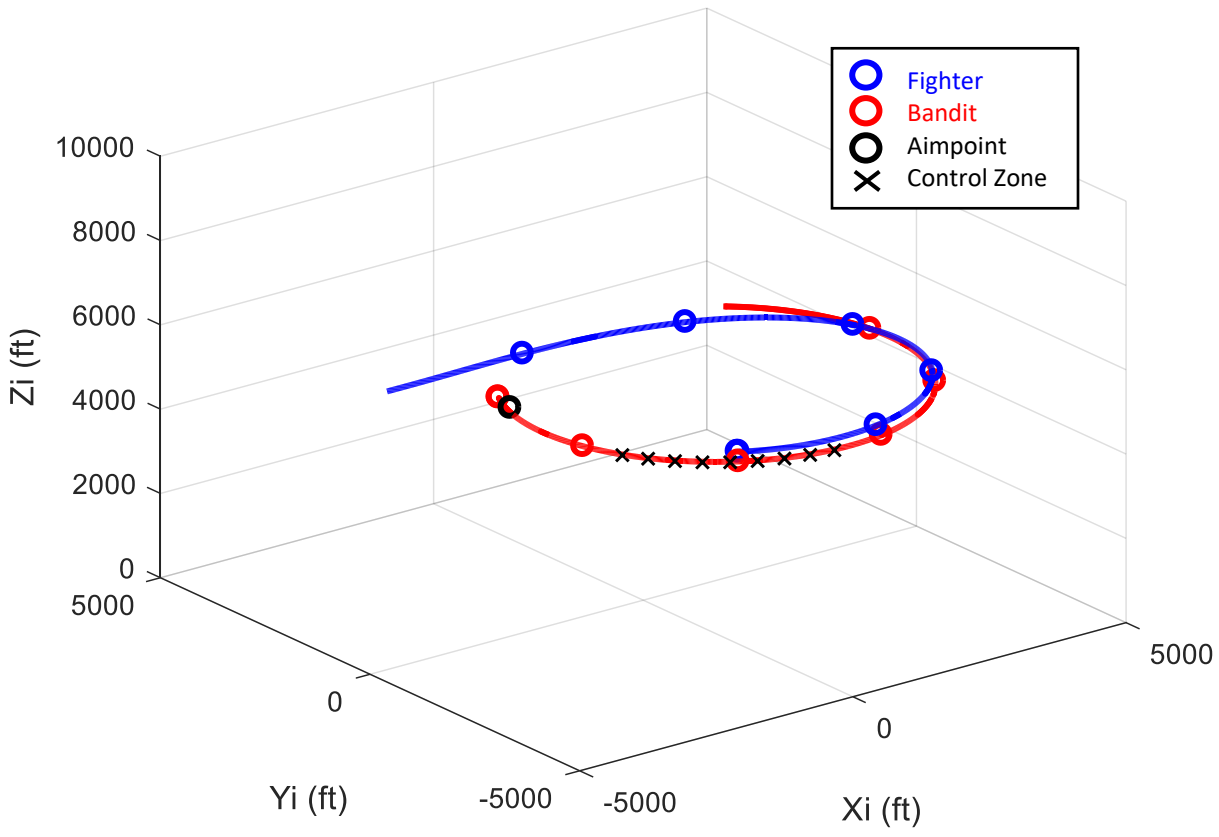

Figure 62. 6,000 ft Perch Scenario: Trace Plot

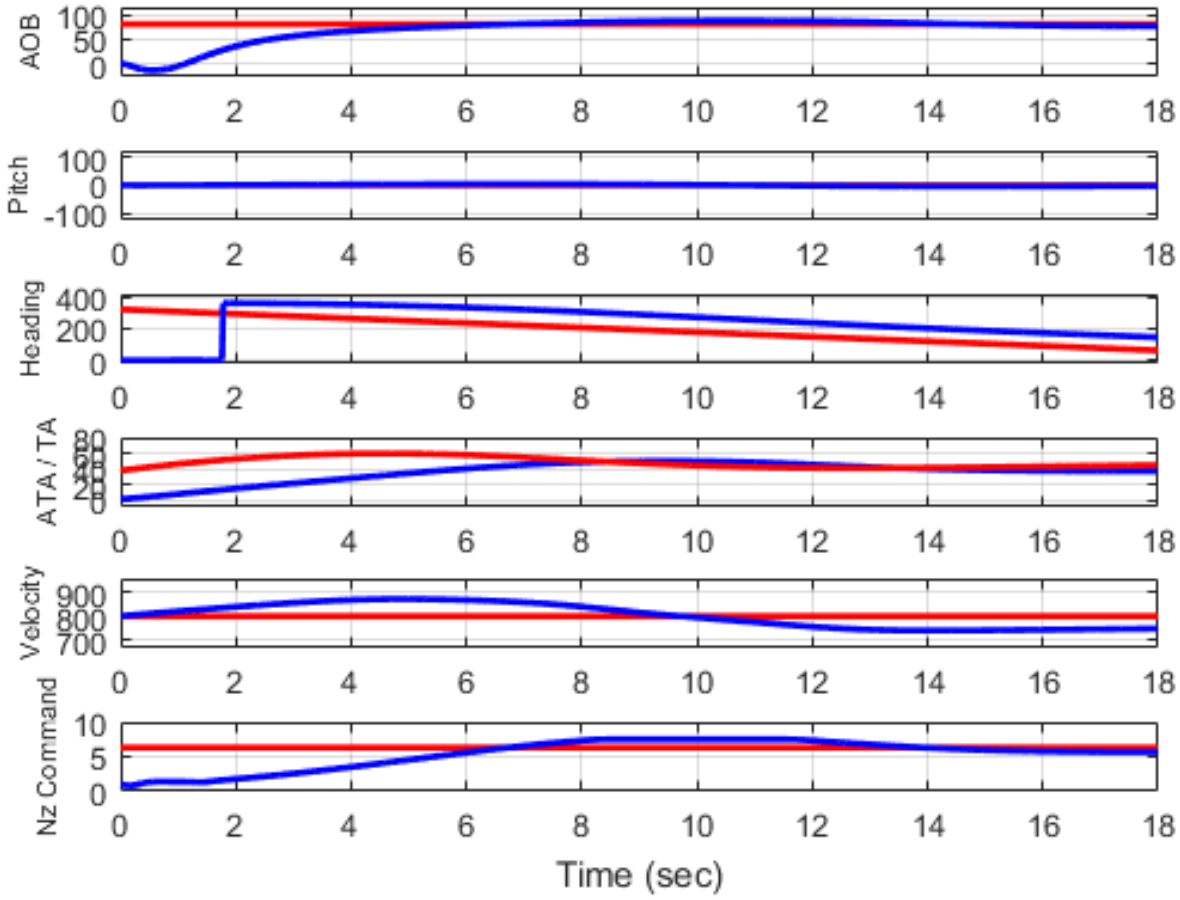

Figure 63. 6.000 ft Perch Scenario: Data Plot

The fighter's initial maneuver is a small but deliberate turn to left. This establishes the fighter in lag pursuit in order to maintain an offensive advantage [11], [19]. Between *t*=0 and *t*=1 second, the fighter rolls to 14° left AOB. The aimpoint remains behind and slightly above the bandit.

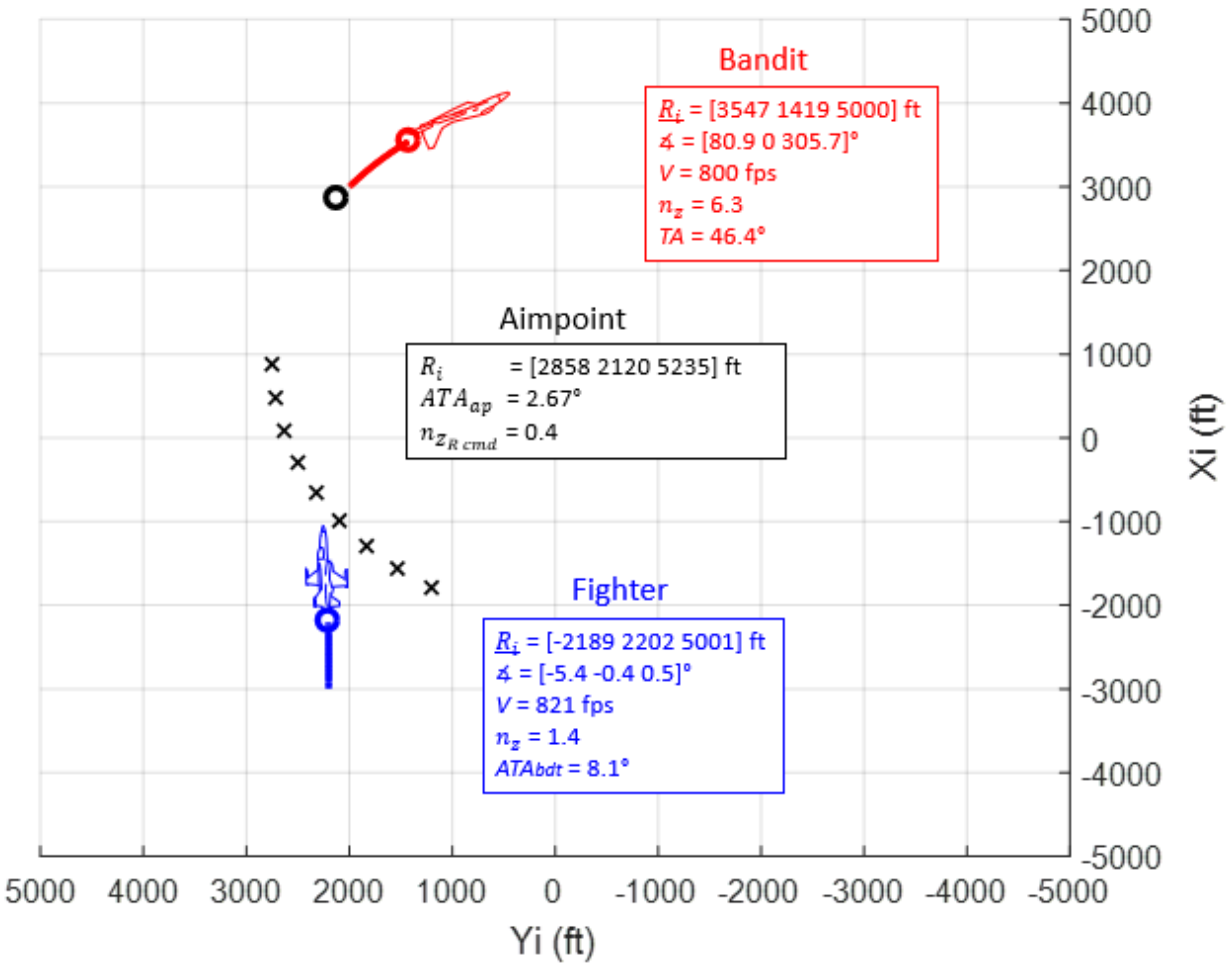

Figure 64. 6,000 ft Perch Scenario: Fighter Maneuvers to Lag (Top View)

At *t*=2 sec, the fighter begins to roll right, towards the bandit. As the fighter enters the bandit's turn circle and ATA begins to increase, the commanded radial acceleration increases as well. The fighter increases the right AOB and the load factor until established in 2-circle, right-hand flow, with the fighter on the inside portion of the bandit's control zone. By *t*=9 sec, the fighter is at the load factor limit of 7.5 g's.

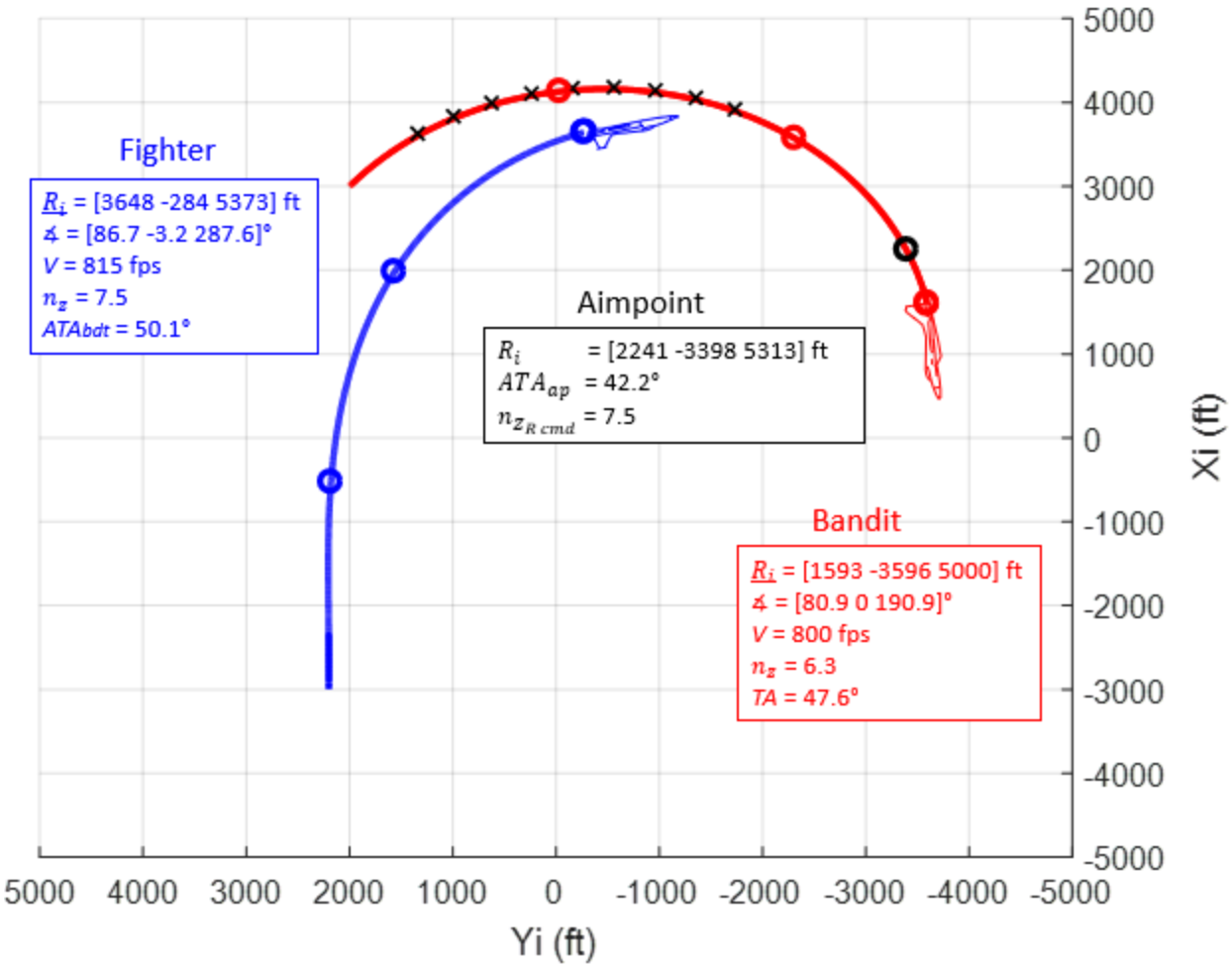

Figure 65. 6,000 ft Perch Scenario: Fighter Initial Turn (Top View)

At the end of this scenario simulation, the fighter maintains a consistent position in the heart of the bandit's control zone. This scenario exemplifies a classic perch setup for the fighter [9].

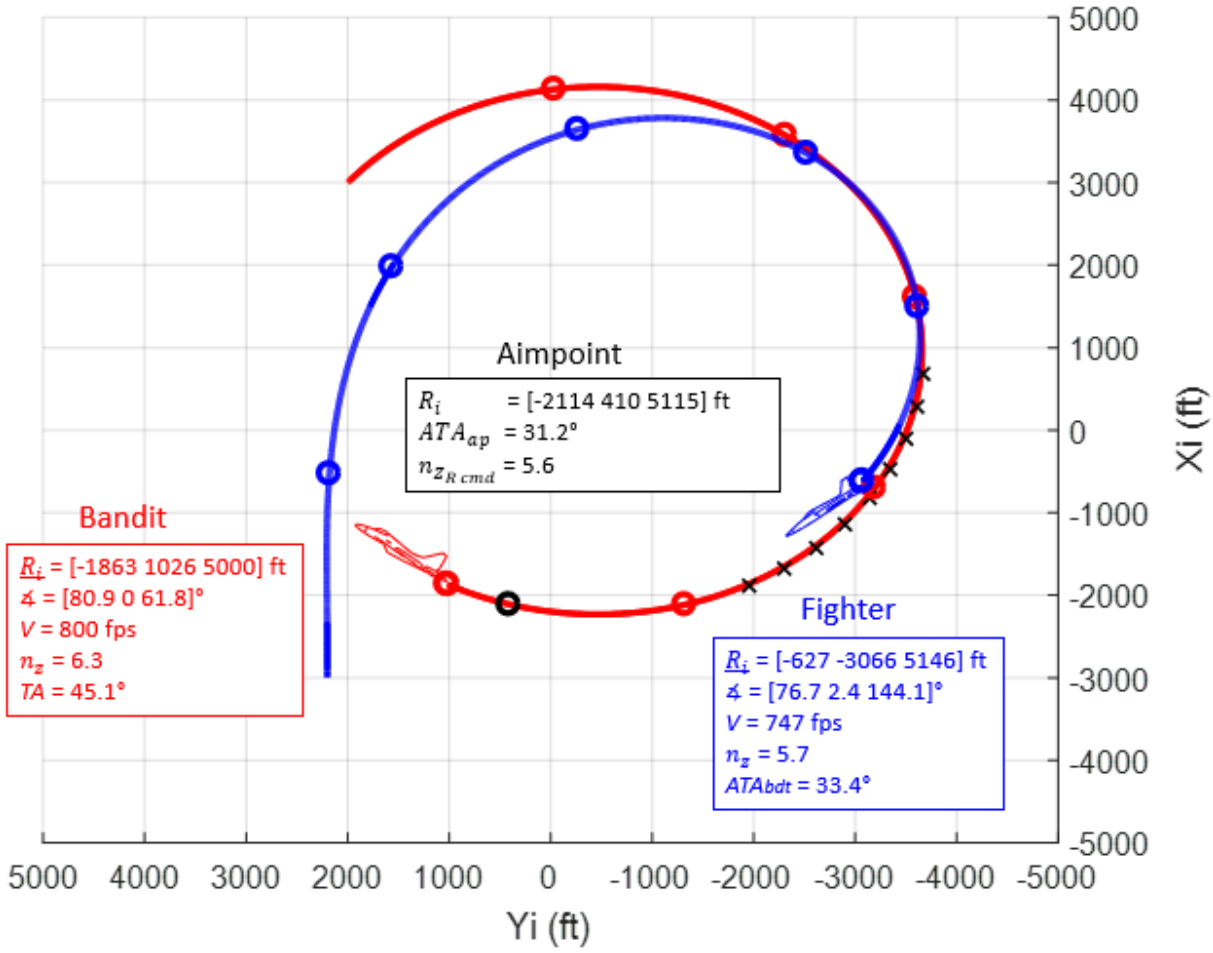

Figure 66. 6,000 ft Perch Scenario: Fighter Established in Control Zone (Top View)

4. 9,000 ft Perch Scenario

The 9,000 ft perch scenario, the fighter begins sufficiently far away from the bandit that the bandit has time to negate a significant portion of the fighter's offensive advantage. The separation is not sufficient for the bandit to completely neutralize the fight, but it does create an angular problem for the fighter to solve.

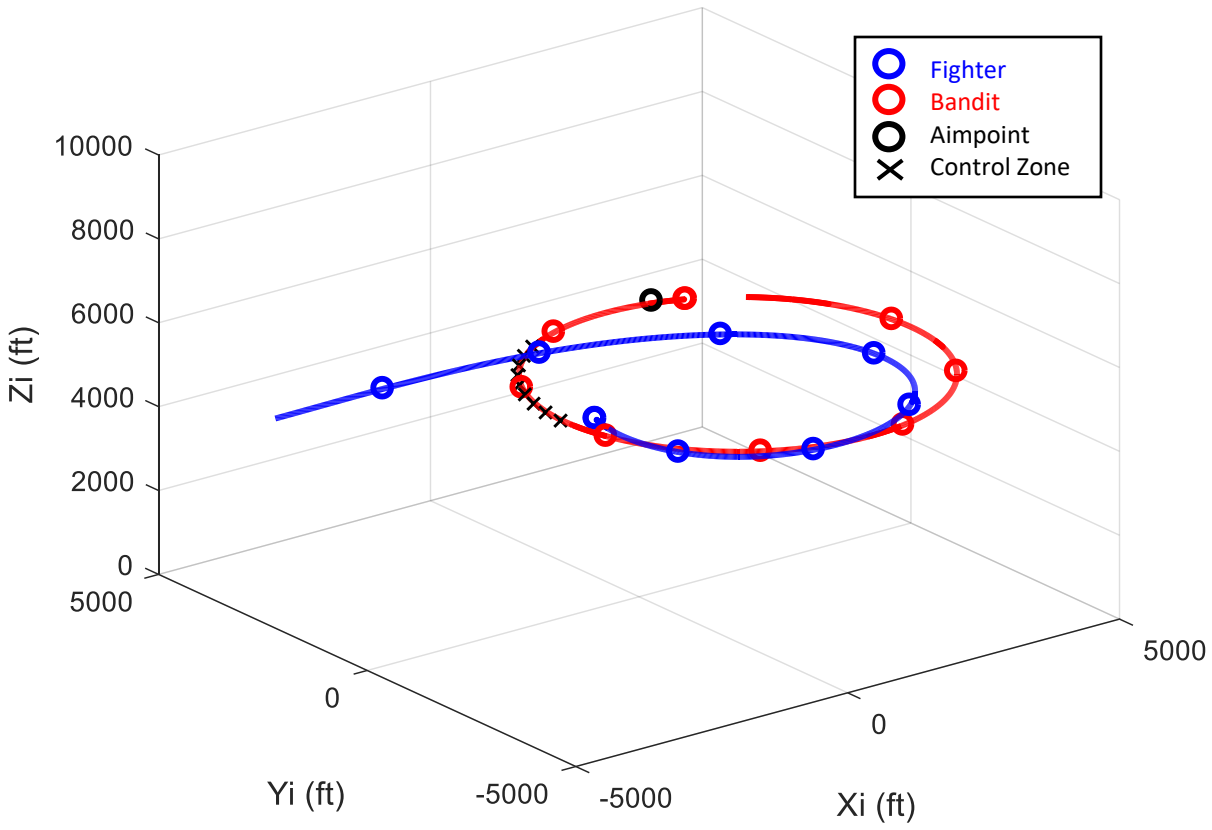

Figure 67. 9,000 ft Perch Scenario: Trace Plot

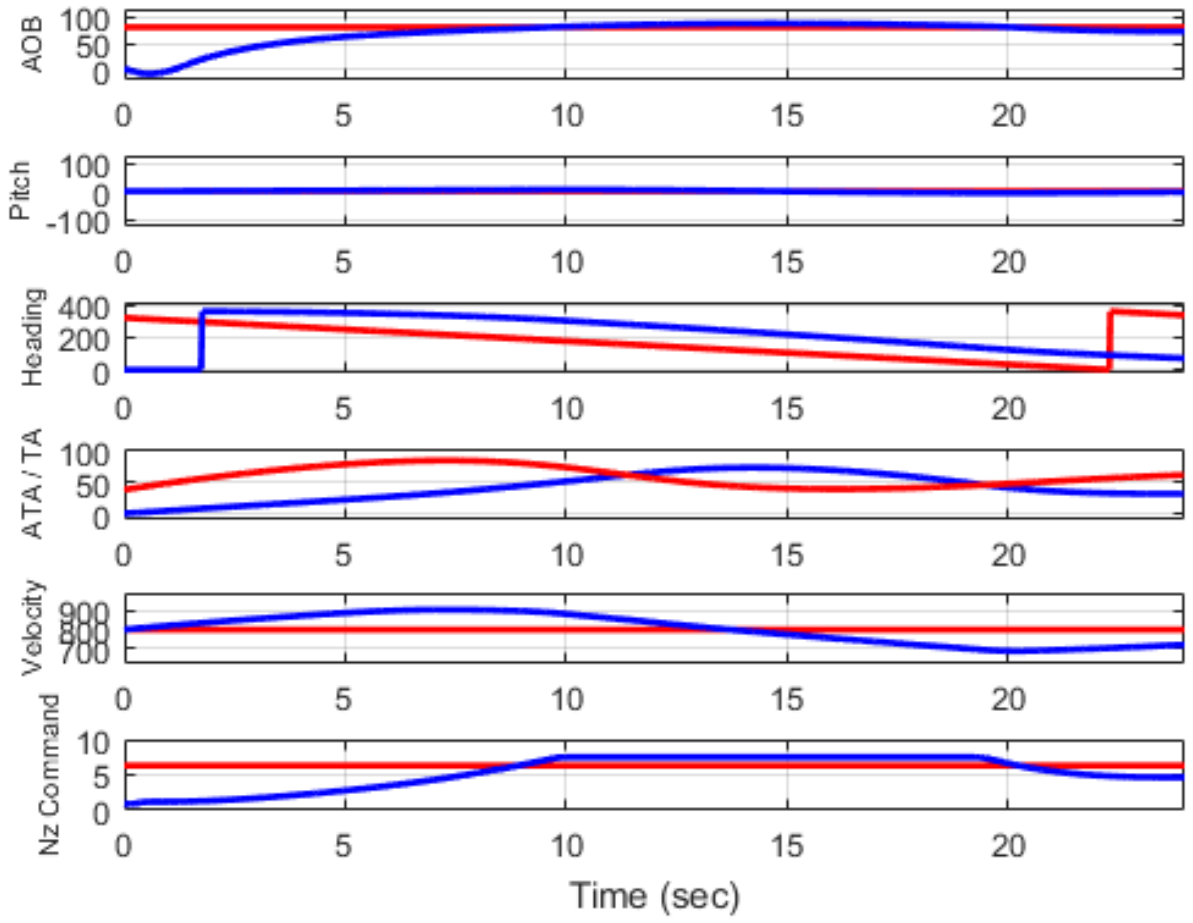

Figure 68. 9,000 ft Perch Scenario: Data Plot

Just as in the previous scenario, the fighter first action is a slight maneuver left towards lag pursuit. This left roll lasts only for about a second before the fighter rolls back to the right. However, the fighter has to travel farther to get inside the bandit's turn circle, and it takes approximately two seconds longer for the fighter to be established in a maximum performance turn compared to the 6,000 ft perch scenario.

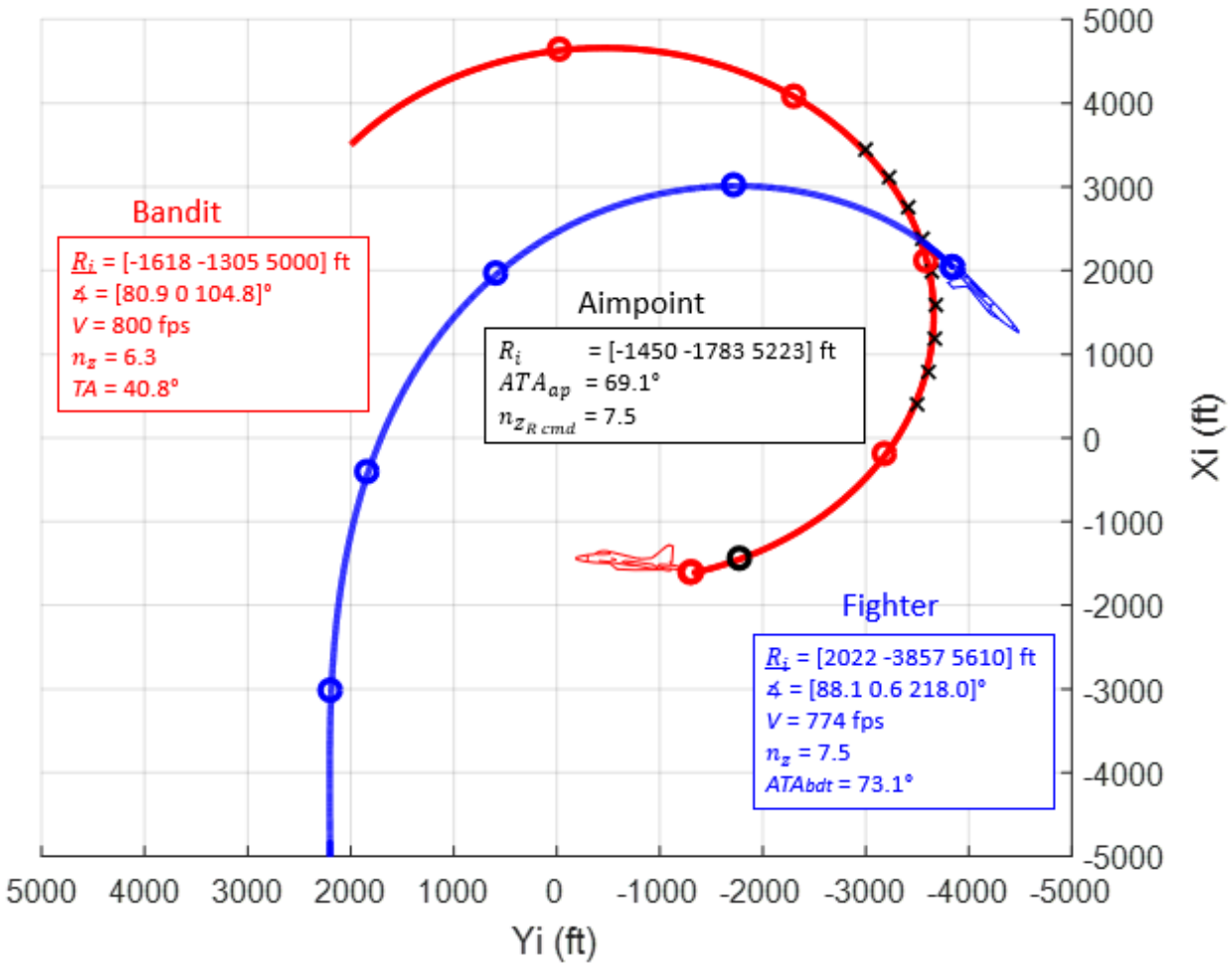

Figure 69. 9,000 ft Perch Scenario: Fighter Overshoots Control Zone (Top View)

Another difference between the 9,000 ft perch scenario and the 6,000 ft perch scenario is that the fighter overshoots the bandit's turn circle with a much higher ATA than before. In the figure above, the fighter is actually within the confines of the bandit's control zone, but the fighter's heading is such that the fighter overshoots to well outside of the bandit's turn circle. The fighter must maneuver to the protected space inside the bandit's turn circle as quickly as possible, without suffering too much energy loss in the process [19]. As the ATA_{ap} decreases below 45°, the fighter decreases the commanded load factor accordingly. This action balances the energy

and maneuverability as the fighter re-enters the bandit's turn circle with an offensive advantage at *t*=23 seconds.

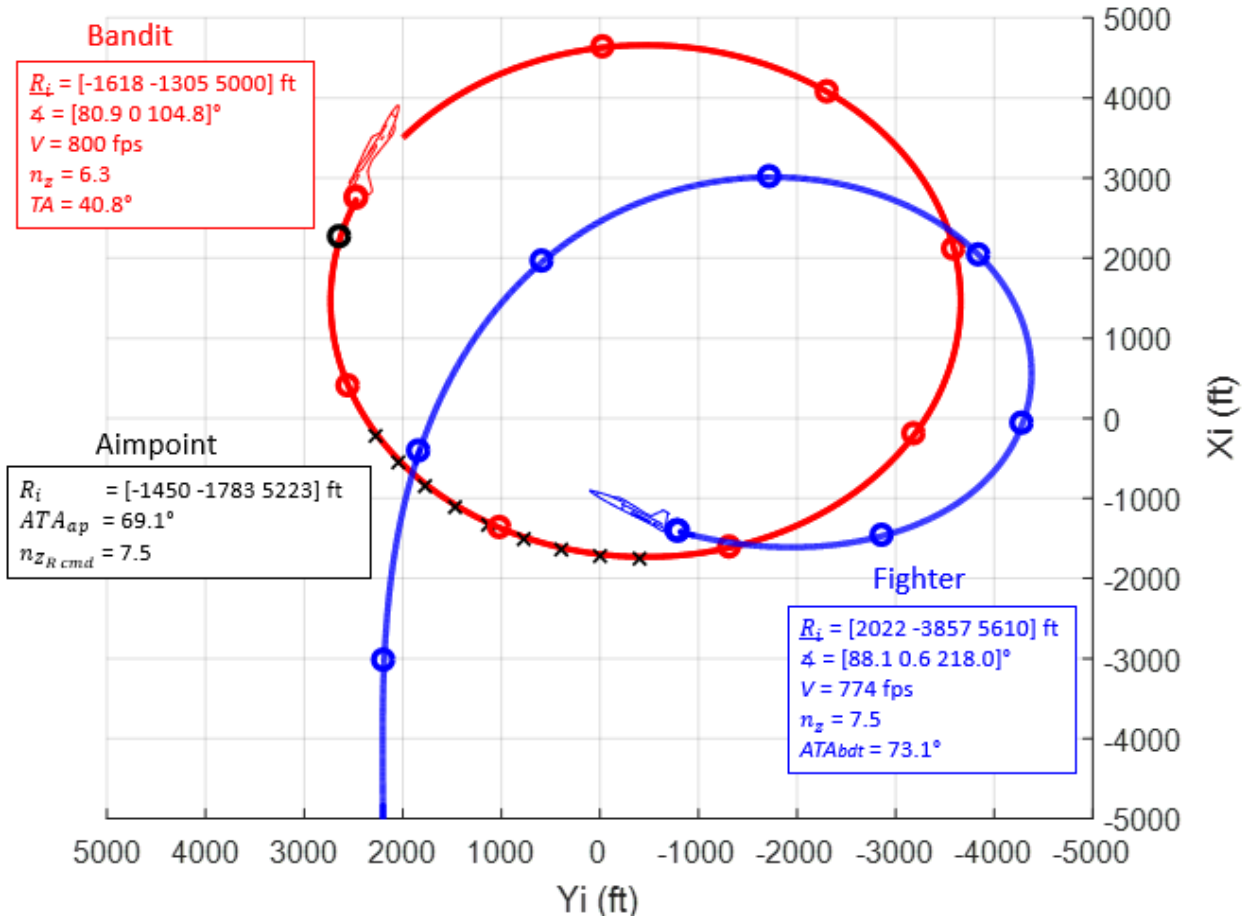

Figure 70. 9,000 ft Perch Scenario: Fighter's Second Turn Circle Entry (Top View)

Through each of these perch scenario simulations, the fighter executed superbly.

5. In-Close Overshoot Scenario

The in-close overshoot scenario begins with the fighter at high ATA and low TA. These conditions result in an impending overshoot of the bandit's flight path. The fighter must

simultaneously manage airspeed and geometry. In this scenario, the bandit executes a pre-planned reversal in order to complicate the fighter's situation.

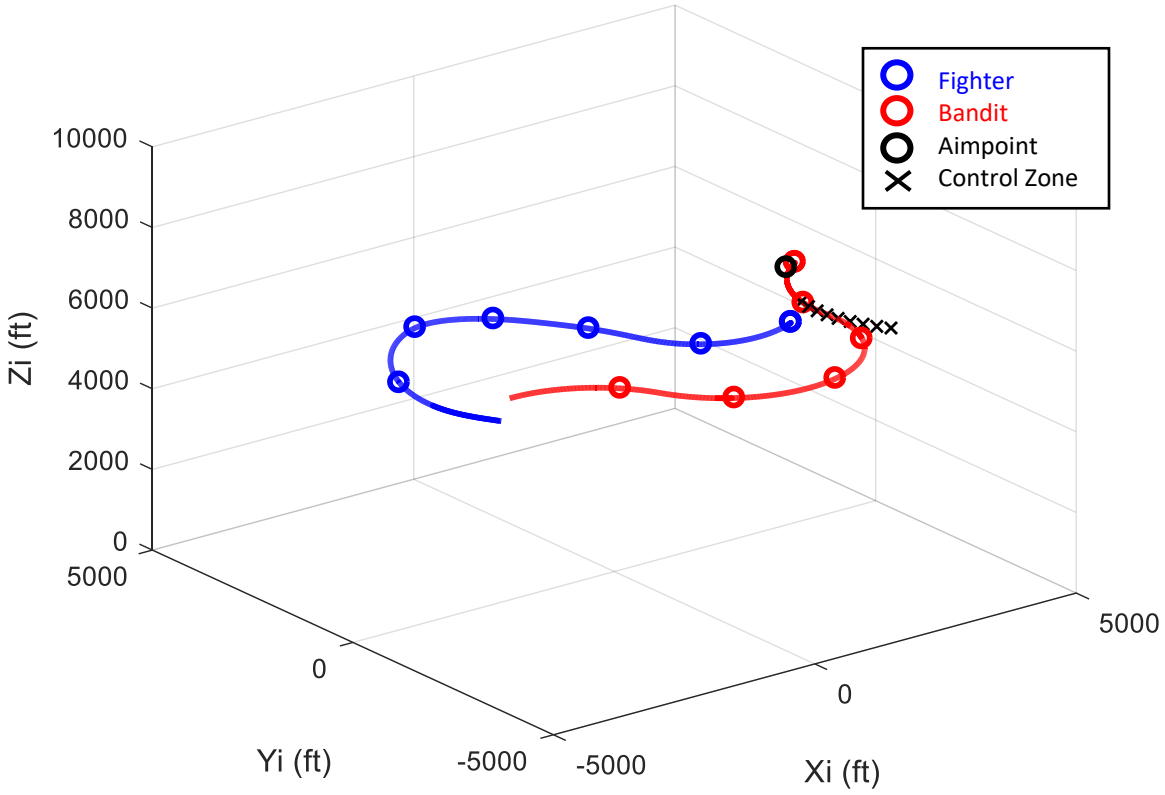

Figure 71. In-Close Overshoot Scenario: Trace Plot

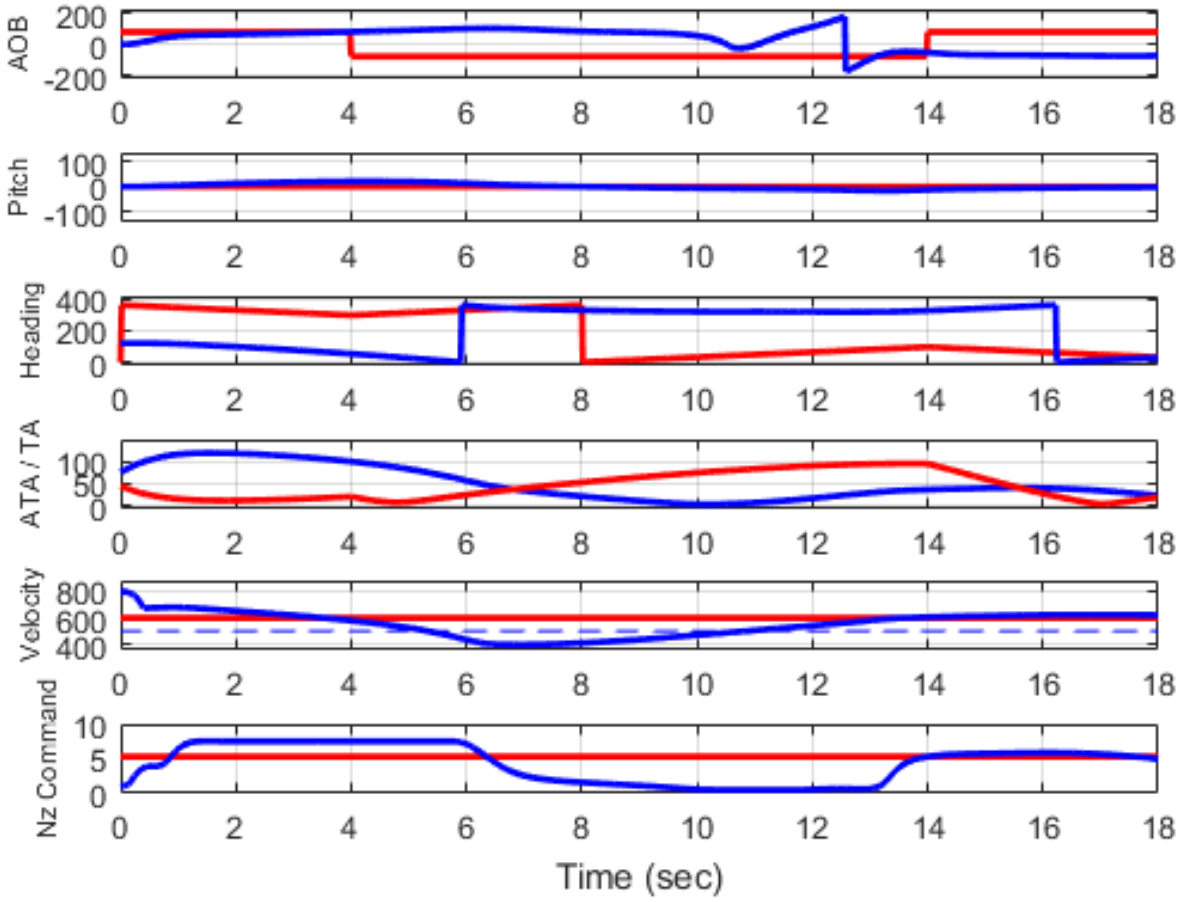

In order to manage both angles and closure, the fighter initiates a maneuver known as a “high yo-yo” [11], [18], [19]. The fighter pulls nose-high, trading airspeed for altitude, while commanding a reduction in airspeed and decreasing turn radius. Since this is a one-circle fight (defined in Section 3.3.5), minimizing turn radius is an important factor. In the first six seconds, the fighter decreases airspeed from 800 ft/s to just over 400 ft/s.

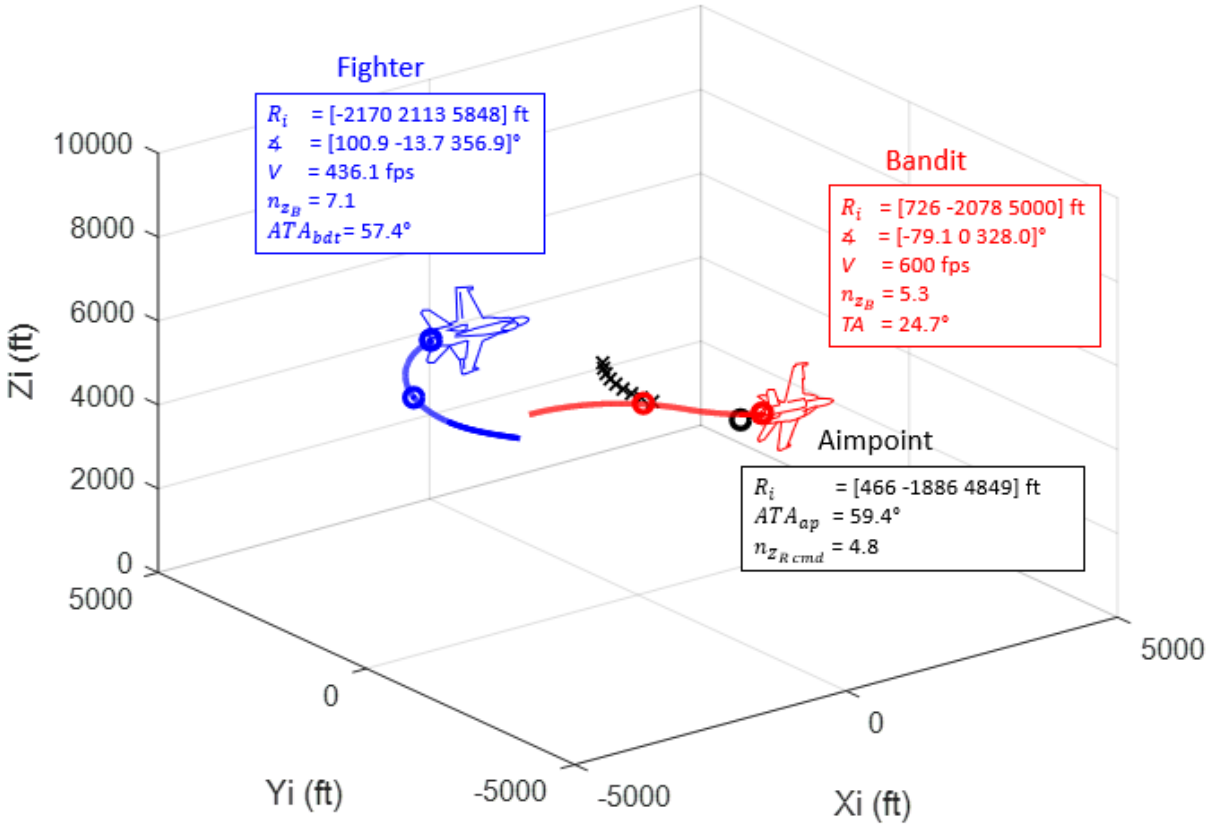

Figure 72. In-Close Overshoot Scenario: Fighter High Yo-Yo (3D View)

The bandit reverses the turn at *t*=4 seconds, and again at *t*=14 seconds. These reversals force the fighter and bandit into 1-circle flow. The fighter's reversals are out-of-phase with the bandit's because the fighter is continually maneuvering towards lag pursuit. The more offensive the fighter is, the more out of phase the fighter is with the bandit. In this case, the fighter's initial high yo-yo maneuver is done so well, that the fighter is almost 180° out of phase with the bandit. The fighter is significantly offensive and on the verge of the bandit's control zone by *t*=18 seconds.

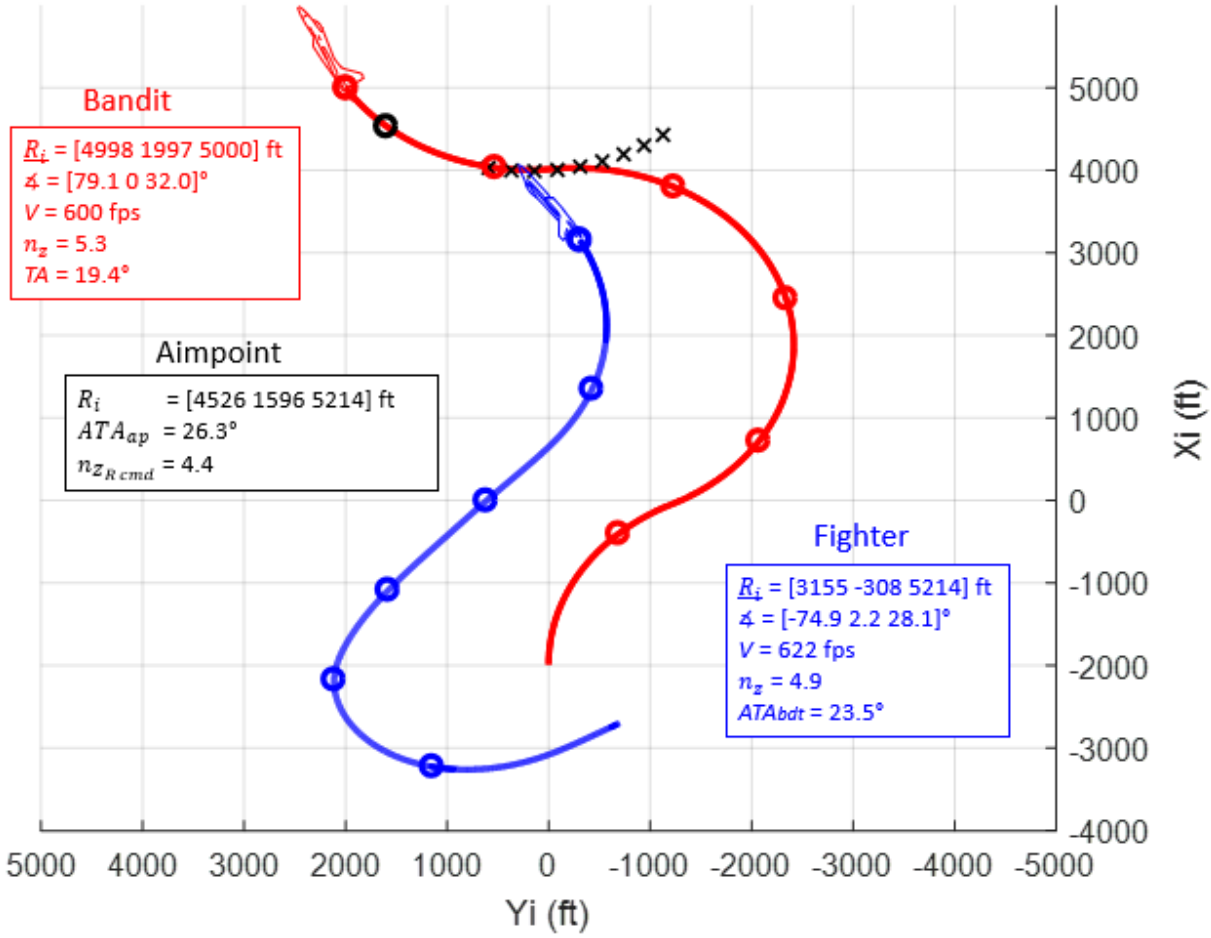

Figure 73. In-Close Overshoot Scenario: Fighter Reverses Offensive (Top View)

.

In addition to the successful maneuvers in the perch scenarios, this in-close scenario demonstrates the ability of the fighter to trade energy for altitude and continued offensive advantage.

6. Rolling Scissors Scenario

The rolling scissors is unique because it combines a series of vertical and horizontal overshoots. The fighter and bandit begin with a neutral start, even though they are at different altitudes. The fighter starts at the "bottom" of the rolling scissors maneuver at an airspeed of 690

ft/s. The bandit starts at the "top" of the rolling scissors maneuver at an airspeed of 450 ft/s. From this neutral start, the fighter initiates a nose-maneuver that trades airspeed for altitude, minimizes downrange travel, and sets up the first vertical overshoot.

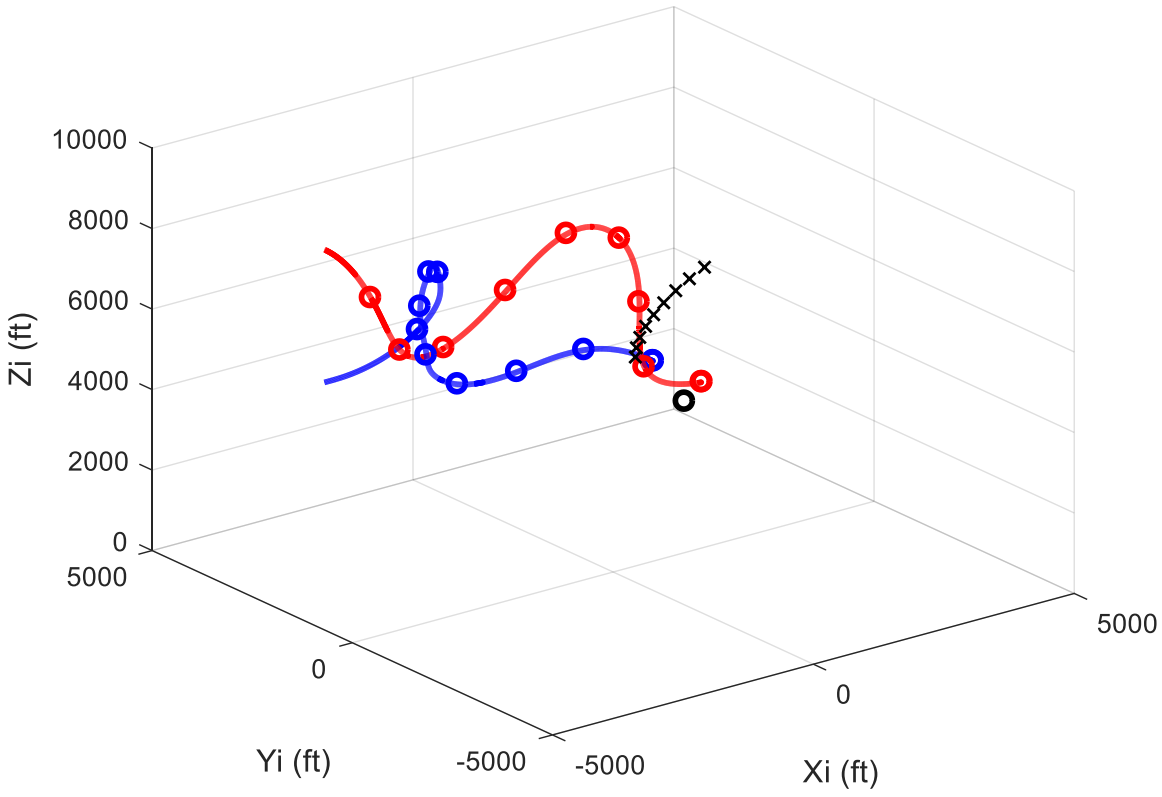

Figure 74. Rolling Scissors Scenario: Trace Plot

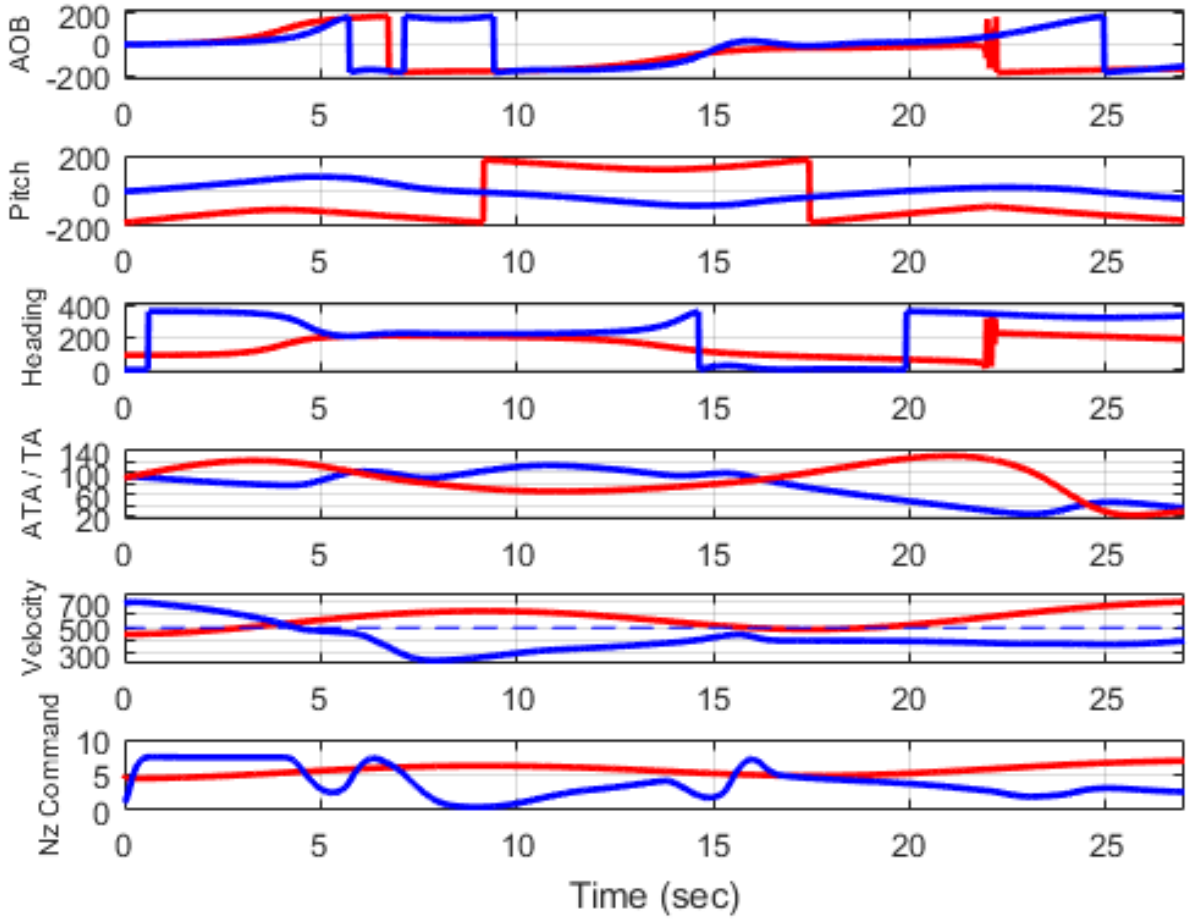

Figure 75. Rolling Scissors Scenario: Data Plot

The fighter's initial nose-high maneuver is done almost entirely with an increase in pitch, which forces the vertical overshoot. (The overshoot occurs as the bandit descends below the fighter's altitude. The bandit is nose low, and the fighter is nose high in this case.) This is in accordance with current BFM tactics [11]. Note that the fighter does not begin to roll significantly until approximately t=4 sec. By t=6 seconds, the fighter starts a rolling pull over

the top of the rolling scissors, and the bandit is extreme nose low on the backside of the rolling scissors.

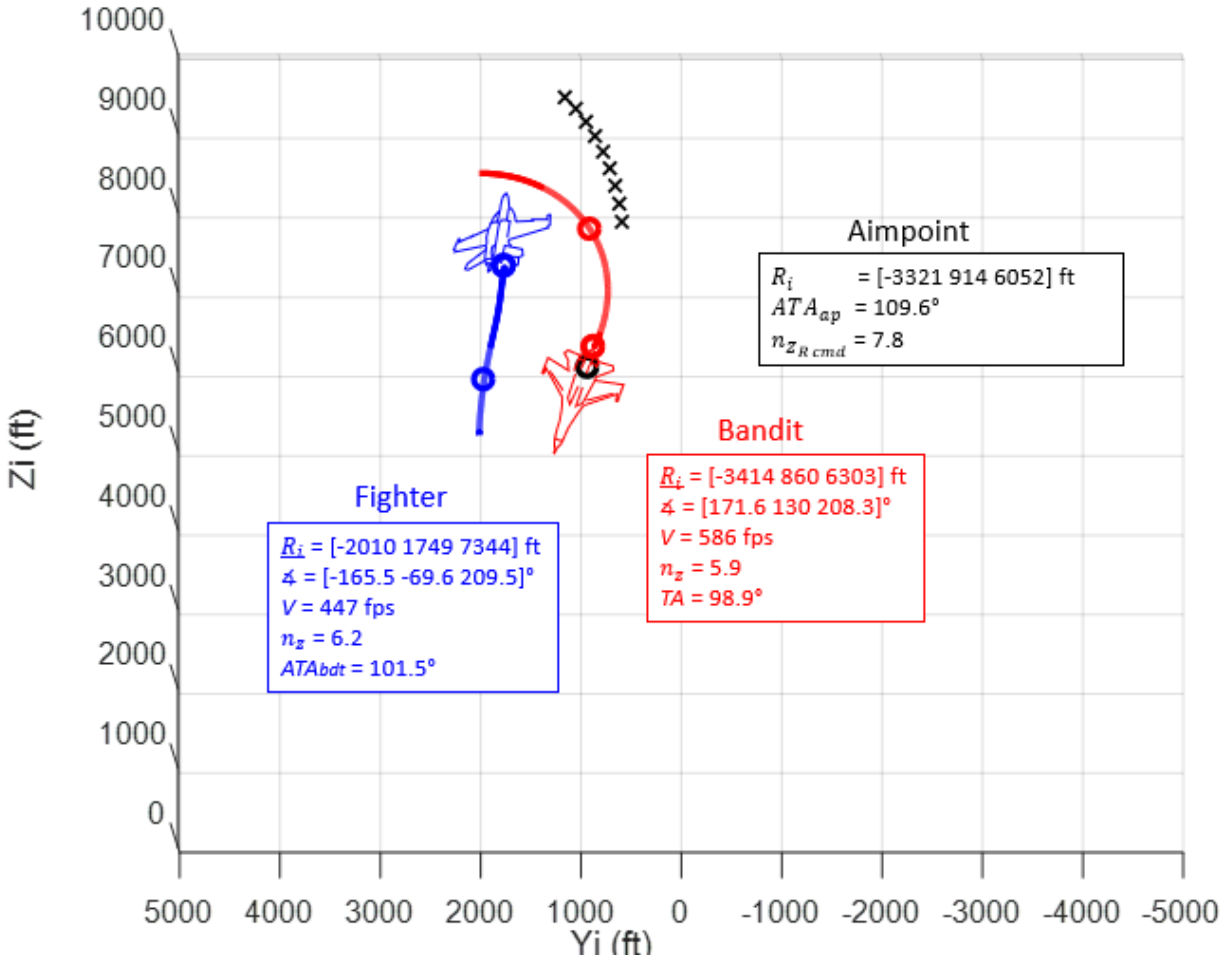

Figure 76. Rolling Scissors Scenario: Initial Pull Nose-High (Back View)

As the engagement continues to develop, it takes only one and a half iterations before the fighter has turned the neutral start into an offensive advantage. But there is even more to the story. The fighter is not only successful but also efficient. The most remarkable points to highlight from this engagement are when the fighter is either extreme nose high or extreme nose low. At *t*=5 seconds, the fighter is at +81° pitch. At *t*=15 seconds, the fighter is at -81° pitch. In

both cases, the fighter decreases the load factor to 2.5 g's and 1.7 g's, respectively. This is important because the fighter rolls much more efficiently at reduced load factors, made easier by the extreme vertical pitch angles. The fighter quickly rolls and repositions the lift vector. Additionally, by unloading and "cleaning the wings" to reduce drag, the fighter accelerates even quicker when extreme nose low. Note that between t=14 seconds and t=16 seconds, the fighter accelerates from 380 ft/s to 440 ft/s. (See Figure 75). The specific power actually peaks at P_s = +245 ft/s at t=15 sec.

The result is a highly successful rolling scissors by the fighter. The maneuvers shown are in accordance with current tactical recommendations [10], [11].

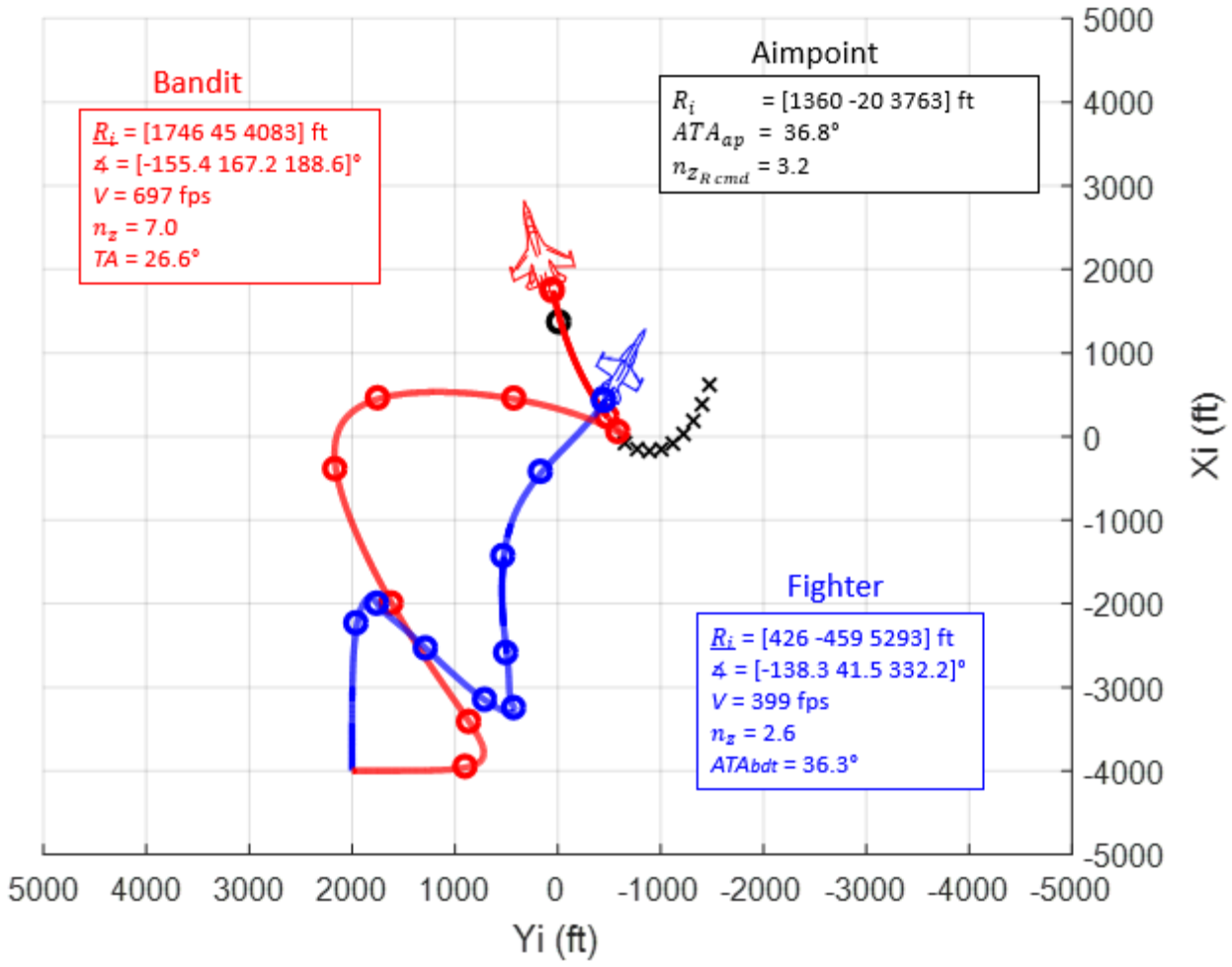

Figure 77. Rolling Scissors Scenario: Fighter Offensive (Top View)

7. 6,000 ft Perch Defensive Scenario

The defensive scenario is tougher to mimic because the attacker – the bandit in this case – is constrained with a pre-planned maneuver. However, the scenario still validates the fighter's ability to execute aggressive vertical maneuvers in order to transition from defensive to neutral or offensive BFM. The fighter "redefines" the fight to an out-of-plane flow, in accordance with references [10], [11], [18], and [19].

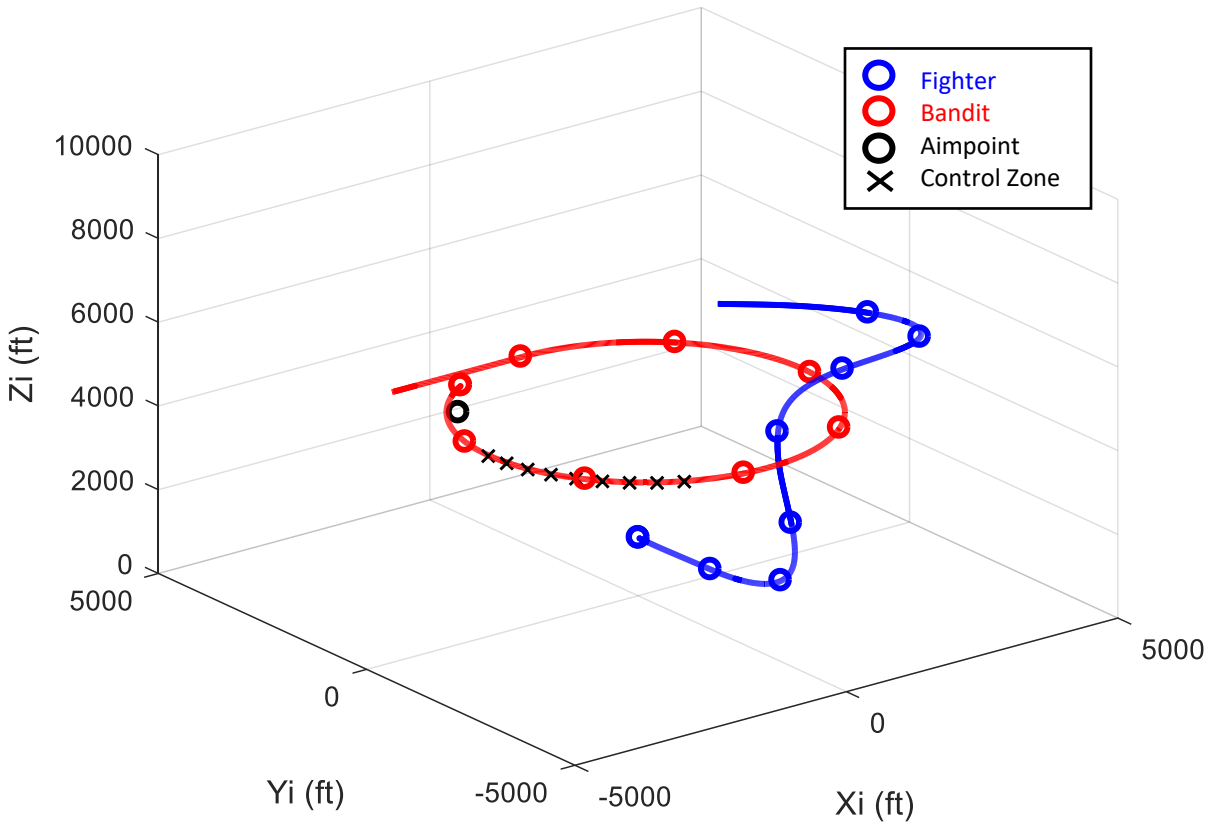

Figure 78. Defensive Perch Scenario: Trace Plot

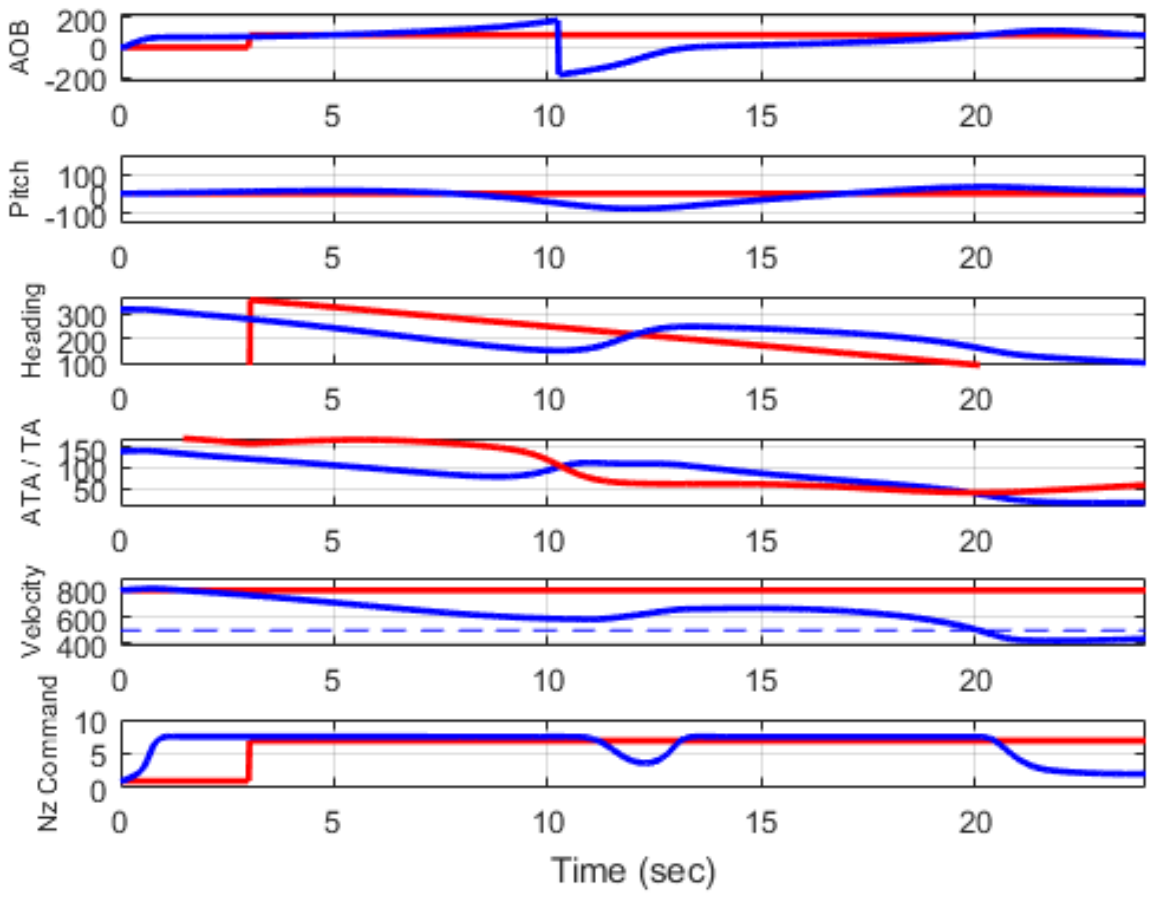

Figure 79. Defensive Perch Scenario: Data Plot

The begins with a maximum performance pull towards the bandit. From Eq. (55), the aimpoint is well in front of the bandit, forcing lead pursuit, because the fighter is at a significant positional and angular disadvantage. Lead pursuit is used to create a problem of range, angles, and closure for the bandit.

The fighter's airspeed decreases rapidly along with the maximum performance turn, which further complicates the problem for the bandit. In this case, the fighter does pitch slightly nose high during the initial turn. This is not desirable, but not catastrophic either. The fighter's pitch stays below 6°, therefore the effect is minimal.

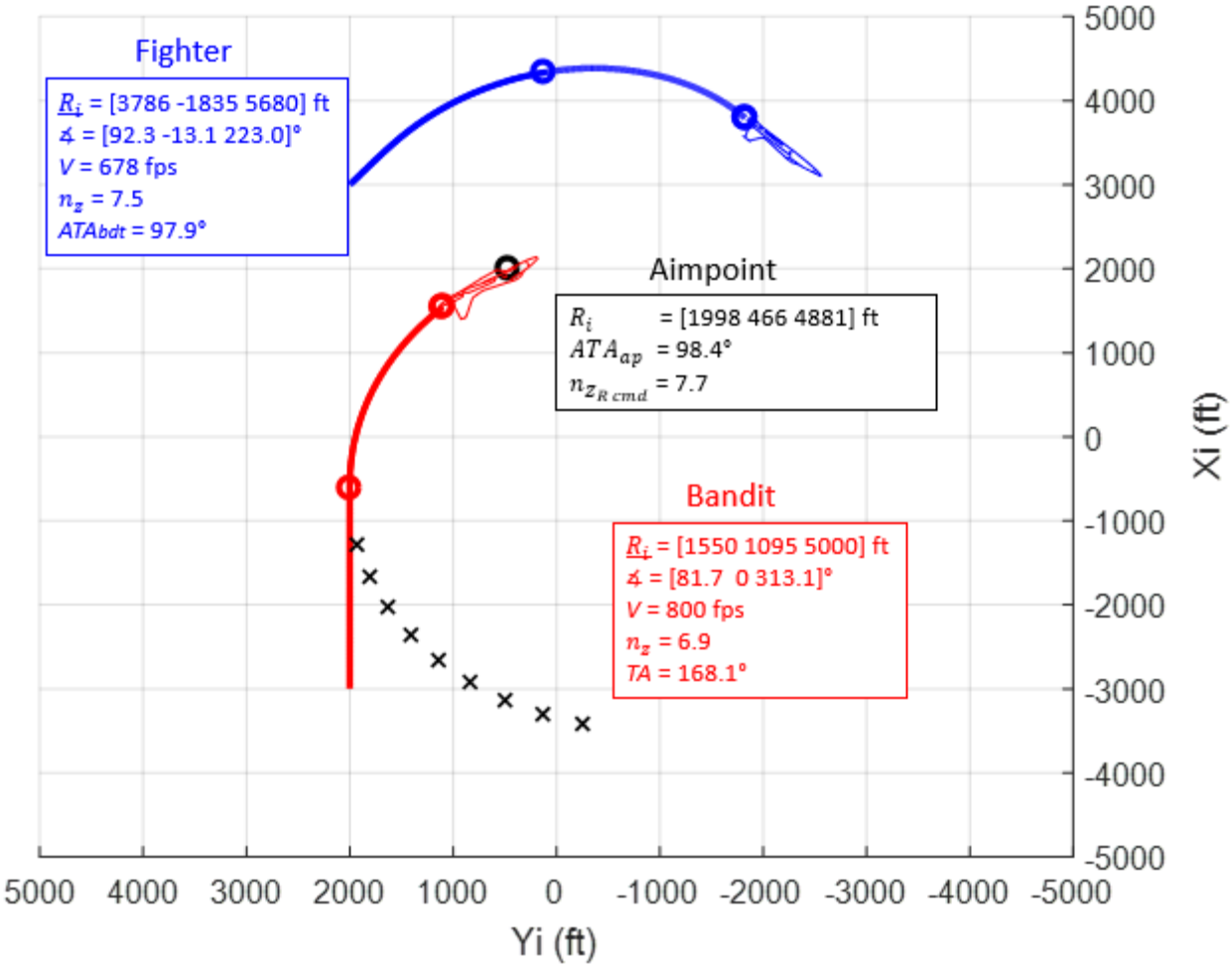

Figure 80. Defensive Perch Scenario: Fighter Initial Turn (Top View)

At *t*=10 sec, the fight drastically changes. The bandit overshoots the fighters flight path because of the range, angles, and closure problem the fighter created for the bandit leading up to this point. If the fighter had more airspeed available, one answer might be to execute a high yo-yo, just as in the in-close overshoot scenario. In this case however, the fighter is at a significant energy disadvantage to the bandit. Therefore, it makes sense that the aimpoint is significantly below the bandit.

The fighter's maneuver is known as a "redefinition". The fighter redefines the fight with an out-of-plane maneuver – extreme nose-low in this case. If the out-of-plane maneuver is left

uncountered by the bandit, the fighter has an opportunity to transition from defensive to offensive to BFM.

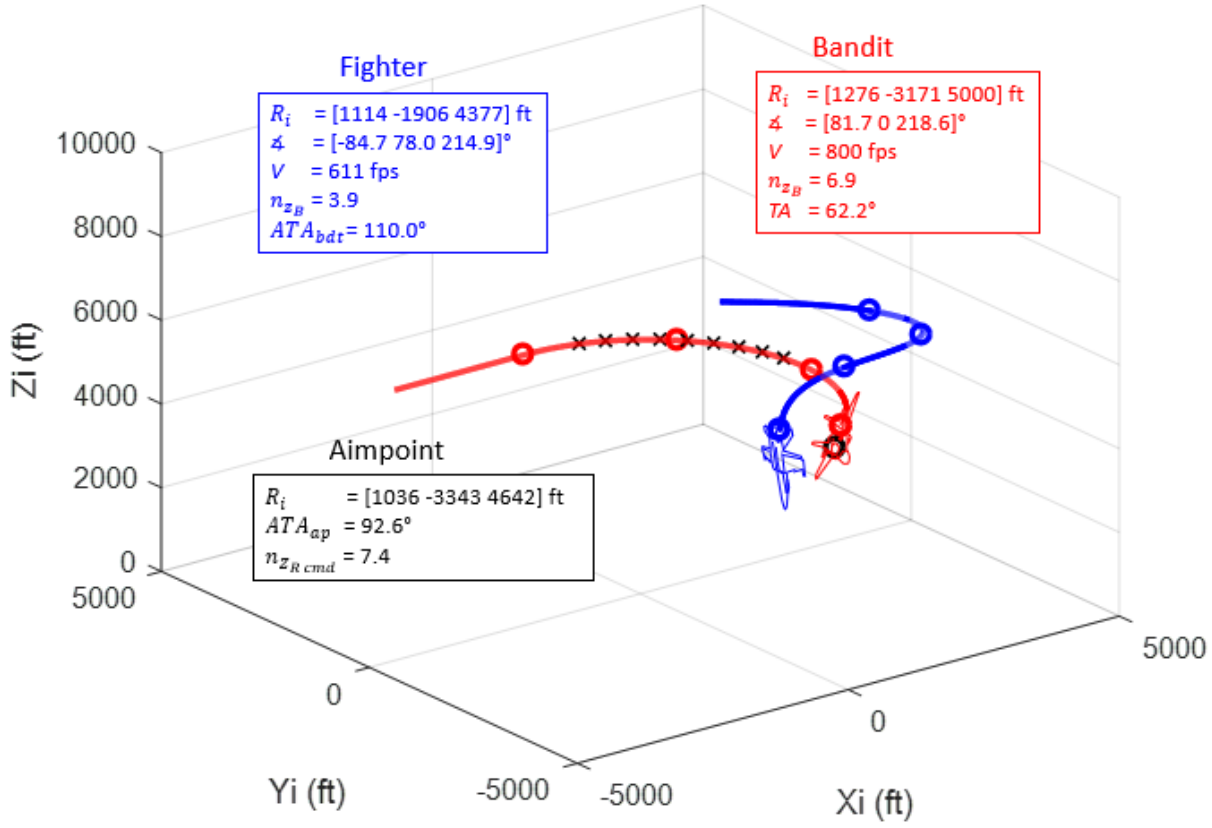

Figure 81. Defensive Perch Scenario: Fighter Redefines (3D View)

Because the bandit executes a pre-planned level turn and does not counter in this scenario, the fighter continues to reorient the aimpoint and gain energy across the bottom of the maneuver. Note that the fighter is still at a significant energy disadvantage at this point and still at a lower altitude than the bandit. However, the geometry is such that the fighter is significantly threatening the bandit with a net offensive position.

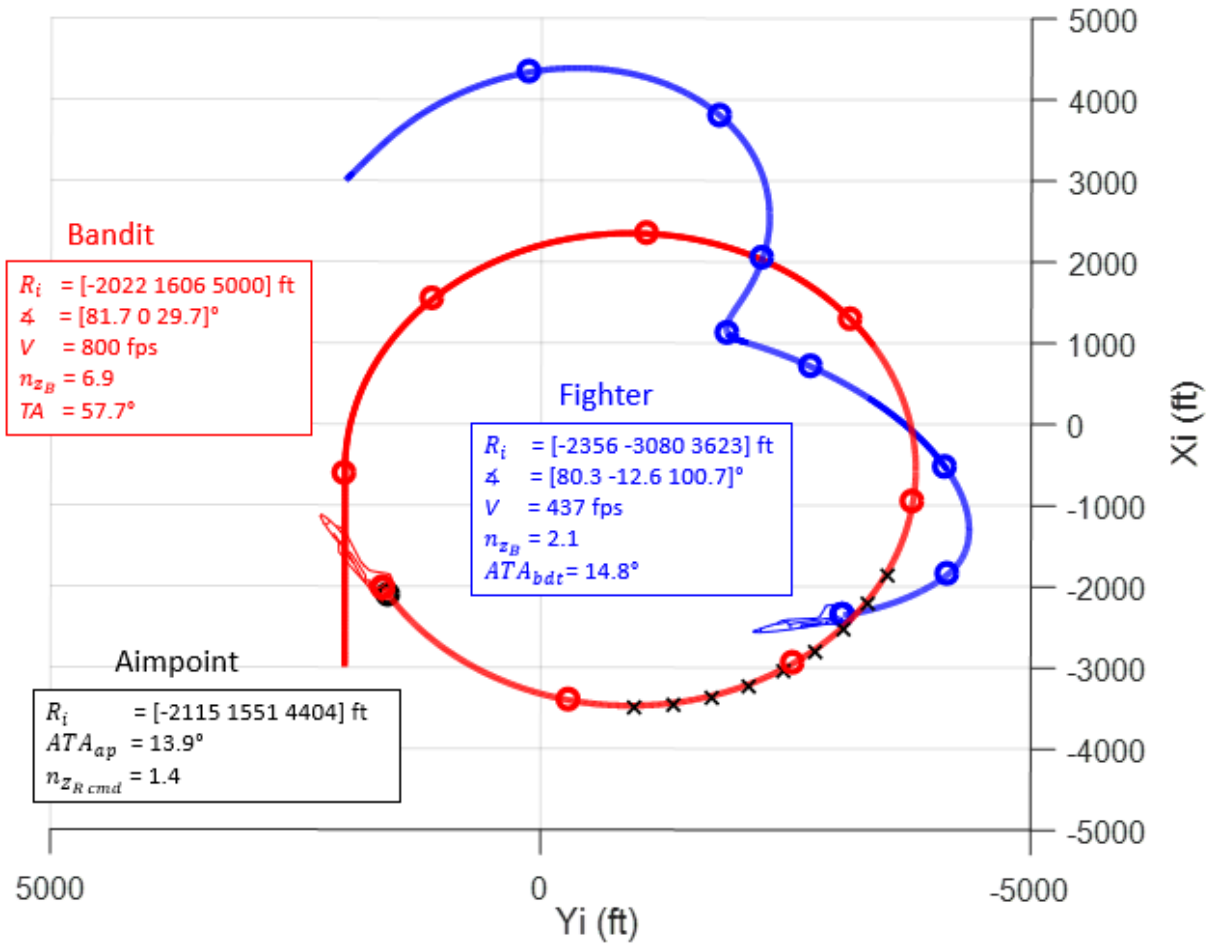

Figure 82. Defensive Perch Scenario: Fighter Transitions to Offensive BFM (Top View)

8. High Aspect (Energy Advantage) Scenario

The high aspect scenario(s) begin with a neutral, co-altitude merge. In this example, the fighter is at 800 ft/s, which is significantly above the fighter's initialized minimum vertical airspeed of 550 ft/s. The bandit begins at 600 ft/s, which is below the bandit's initialized minimum vertical airspeed of 650 ft/s. This example is indicative of two aircraft with different performance, energy, and maneuverability characteristics, e.g. a high thrust-to-weight F-16 vs. a high wing-loaded F-5.

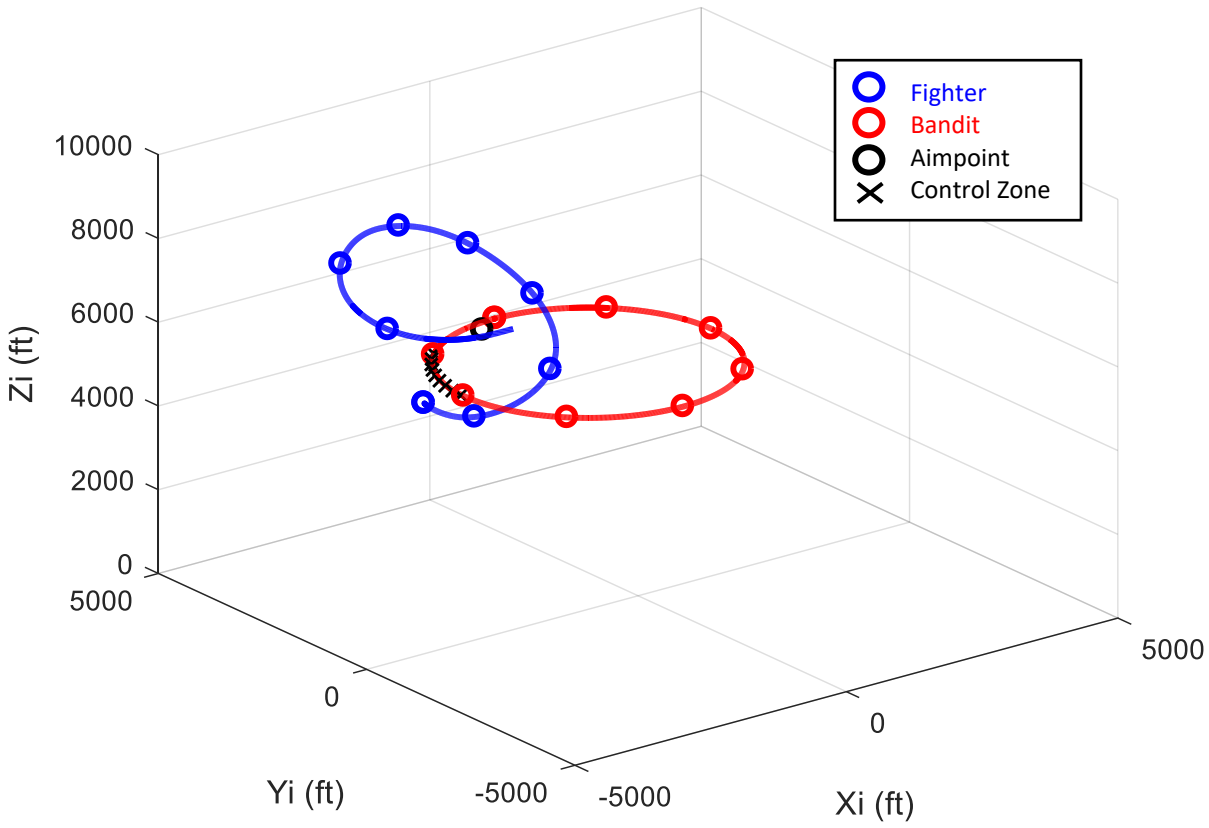

Figure 83. High Aspect (Fighter Energy Advantage) Scenario: Trace Plot

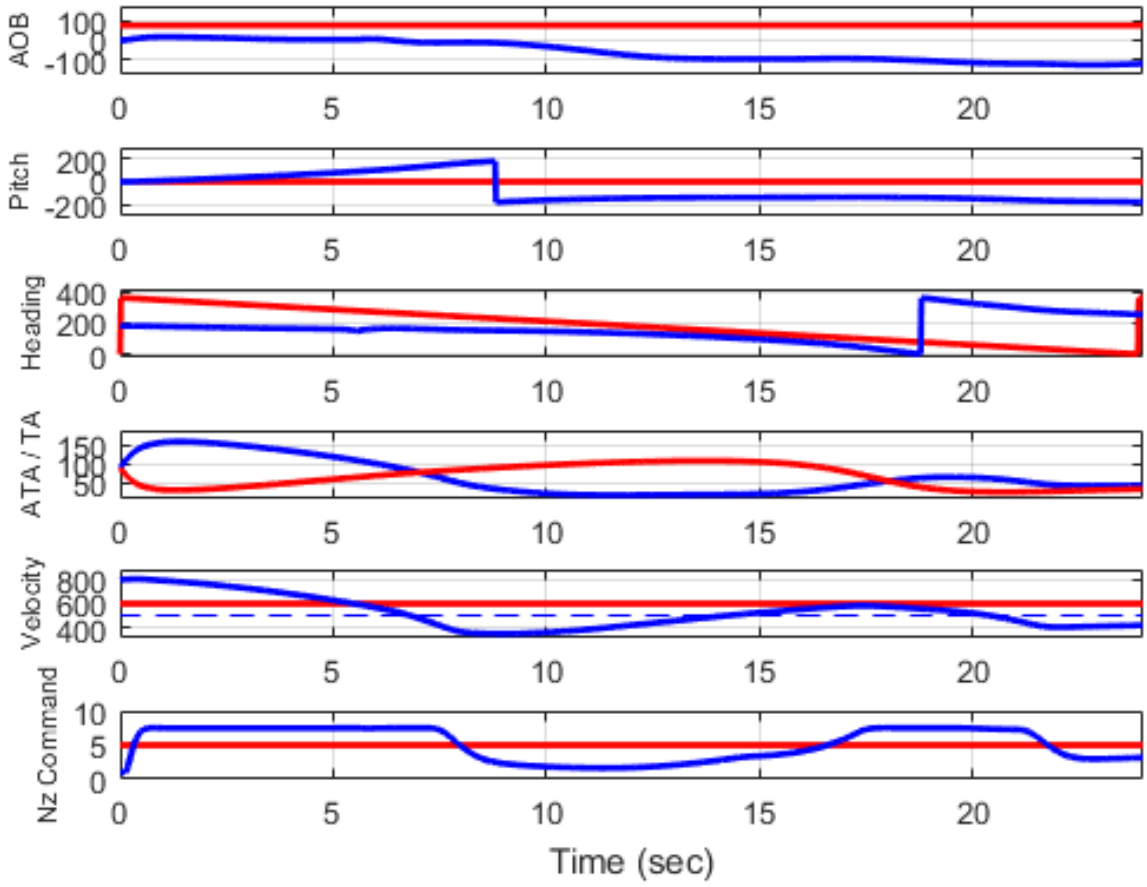

Figure 84. High Aspect (Fighter Energy Advantage) Scenario: Data Plot

From Eq. (56), the aimpoint is more than 1,200 ft above the bandit at the start. The fighter initiates a maximum performance pull nose-high. But as the fighter trades airspeed for altitude, the aimpoint drops to below the bandit's altitude, which drives the fighter to come down the backside of the vertical maneuver. The fighter uses just over 3,000 ft of altitude to complete the vertical maneuver.

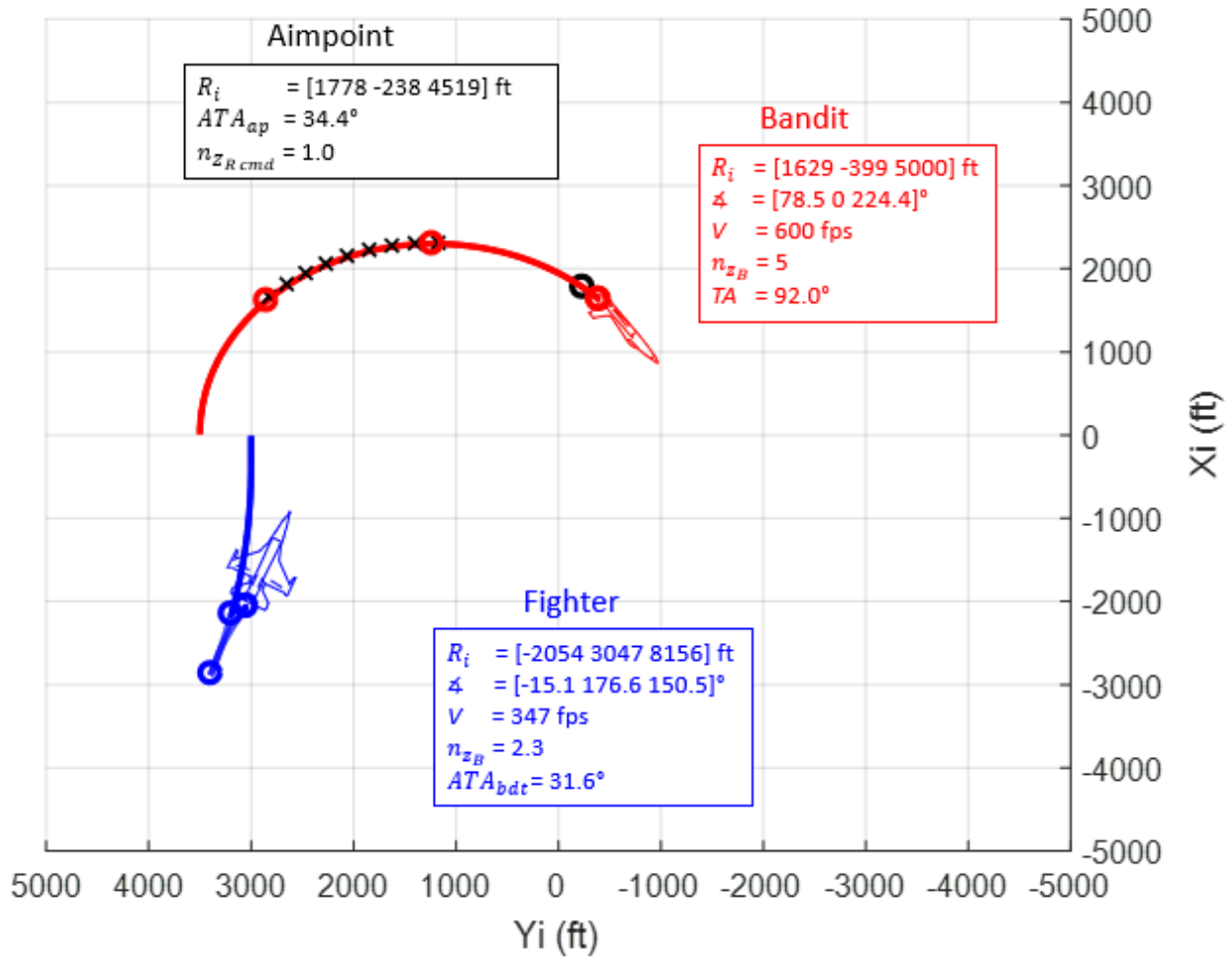

Figure 85. High Aspect (Fighter Energy Advantage) Scenario: Fighter Nose-High Maneuver (Top View)

Because the vertical maneuver is uncountered, the entire distance between the fighter and the bandit is protected area for the fighter. The fighter uses this room to maneuver to an offensive position. As the fighter comes down the backside of the vertical maneuver, the fighter rolls left in an attempt to align fuselages with the bandit. (The fighter rolls left while inverted over the top of the maneuver, even though the endstate is right-hand, two-circle flow.)

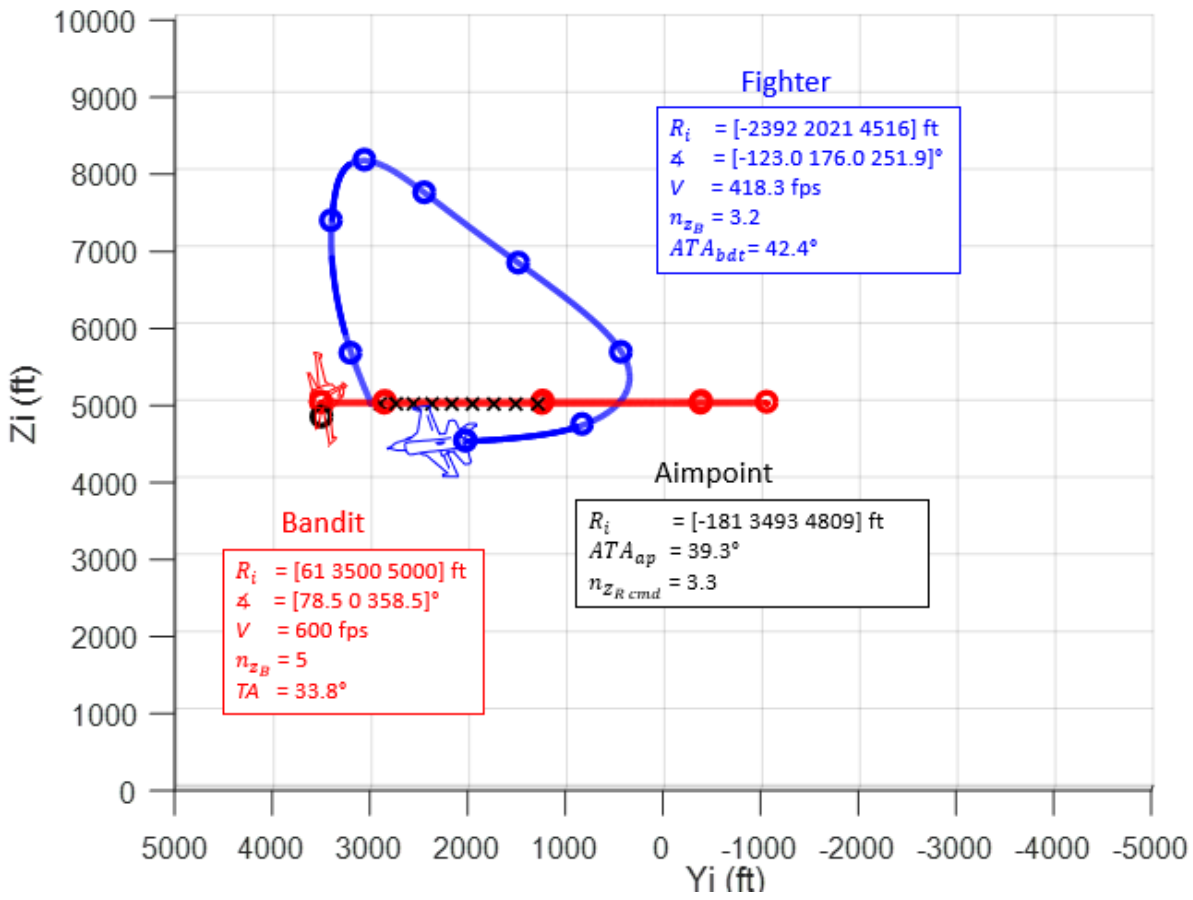

Figure 86. High Aspect (Fighter Energy Advantage) Scenario: Fighter Completes Offensive Transition

The fighter slightly overshoots the bandit's flightpath, but the aimpoint is converging toward the bandit's control zone. The offensive advantage clearly lies with the fighter before the bandit completes even one full turn circle.

9. High Aspect (Energy Disadvantage) Scenario

When the fighter had an energy advantage, the fighter executed an extreme nose-high maneuver. In this case, where the fighter has an energy disadvantage from a high aspect merge, the fighter does the opposite. The result is an extreme nose-low maneuver.

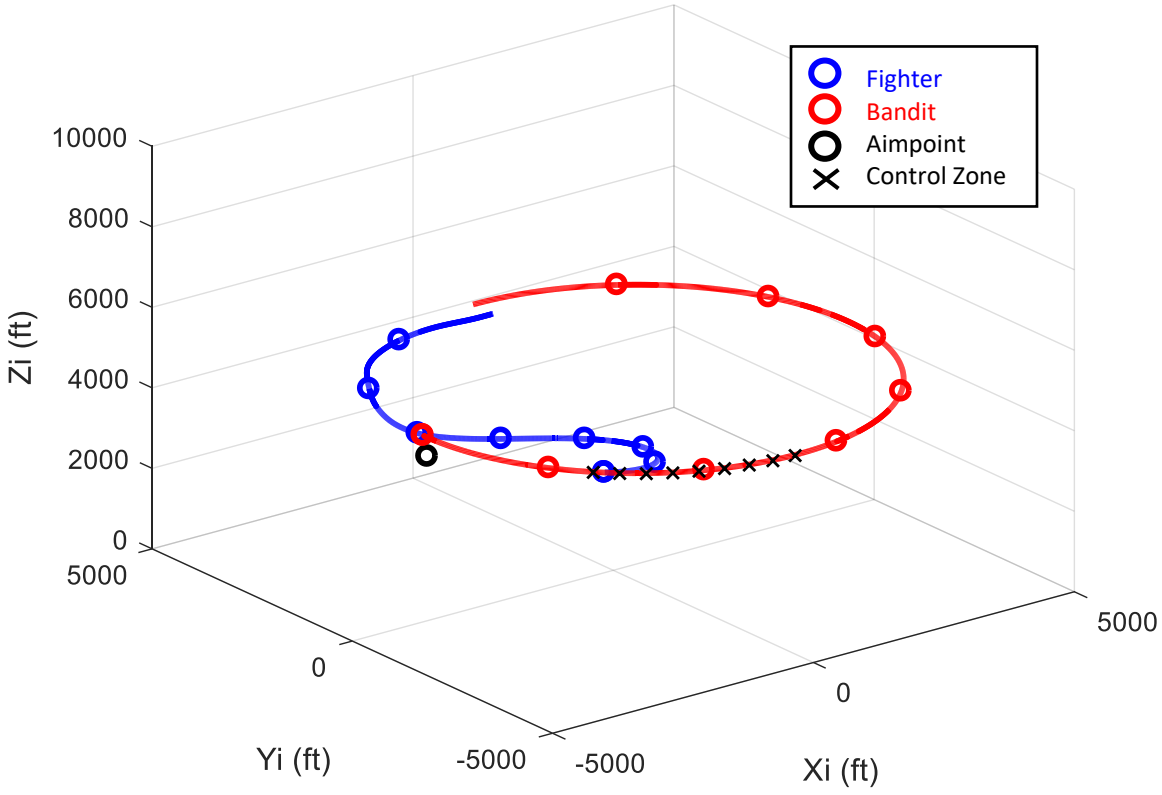

Figure 87. High Aspect (Fighter Energy Disadvantage) Scenario: Trace Plot

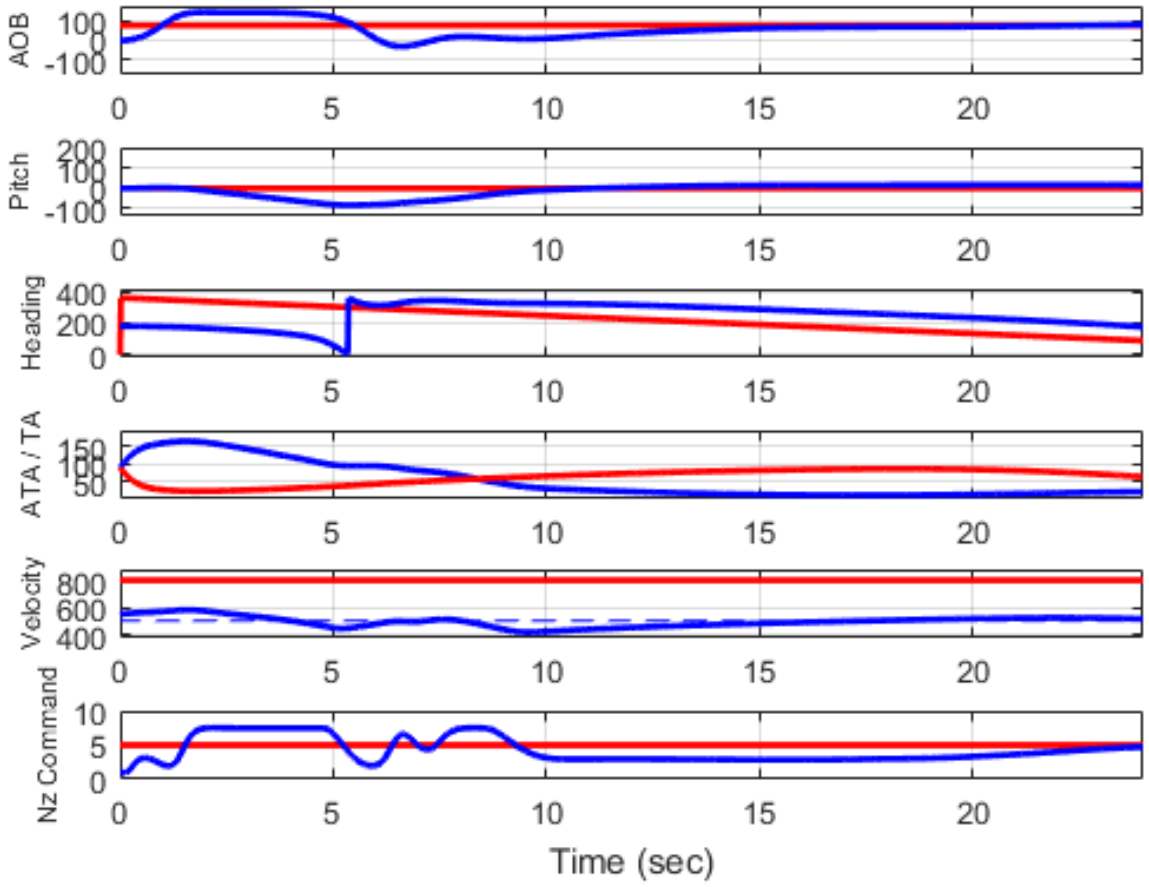

Figure 88. High Aspect (Fighter Energy Disadvantage) Scenario: Data Plot

The fighter's initial nose-low maneuver preserves most of the fighter's airspeed across the bottom. Energy management is even more precious when the fighter is at a disadvantage. Note that the fighter starts with approximately 3 seconds of maximum load factor, but then the load factor decreases as the fighter balances just below corner airspeed. At t=9 seconds, the fighter is extreme nose-low and still slightly defensive. The aimpoint is in front of and below the bandit, forcing lead pursuit by the fighter [11].

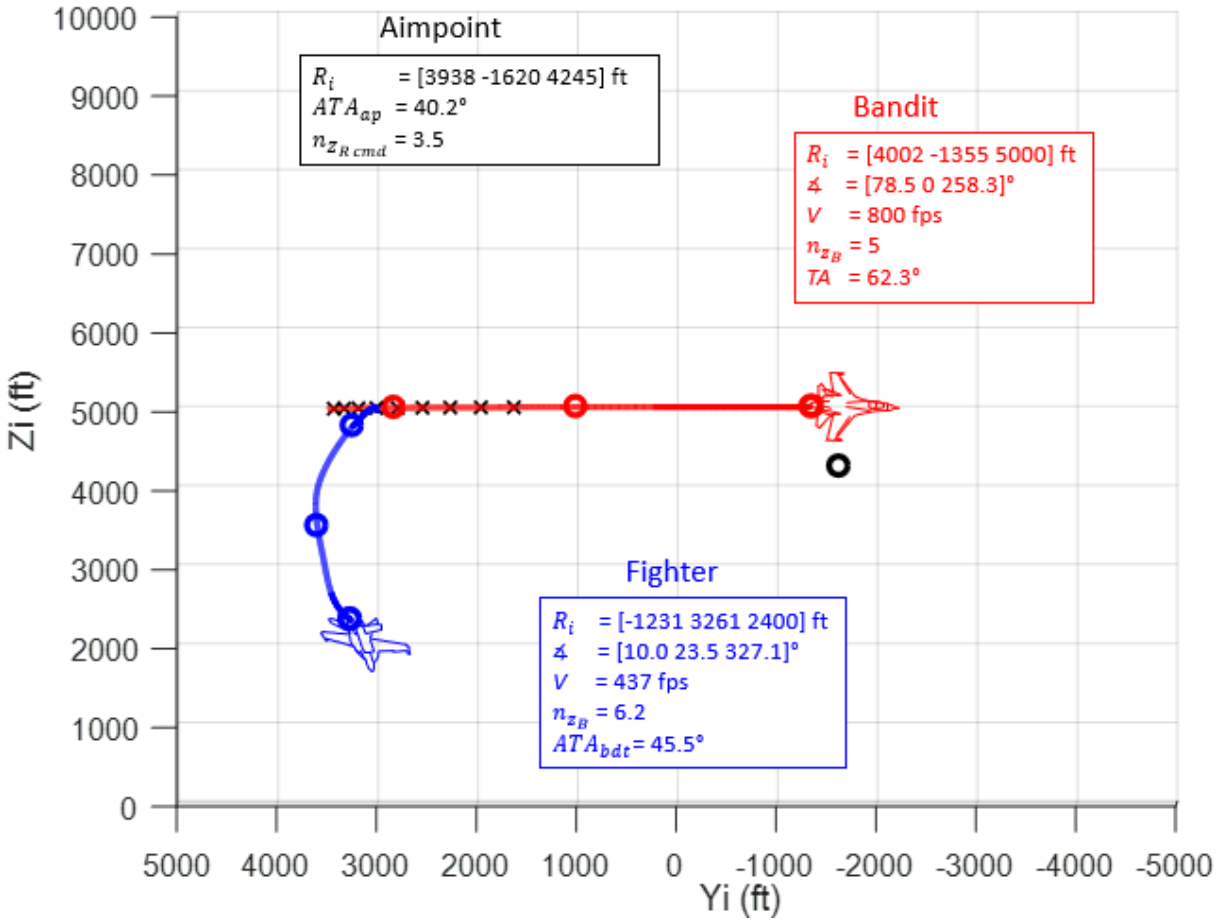

Figure 89. High Aspect (Fighter Energy Disadvantage) Scenario: Fighter Nose-Low (Side View)

As the fighter transitions across the bottom of the maneuver, the fighter is still at an energy disadvantage. But the fighter has gained a significant angular advantage. The aimpoint is essentially co-located with the bandit. The fighter's turn circle is smaller than the bandit's turn circle. Therefore, it makes sense that the fighter is cutting inside the bandit's turn circle via pure pursuit. Overall, this is yet another successful example.

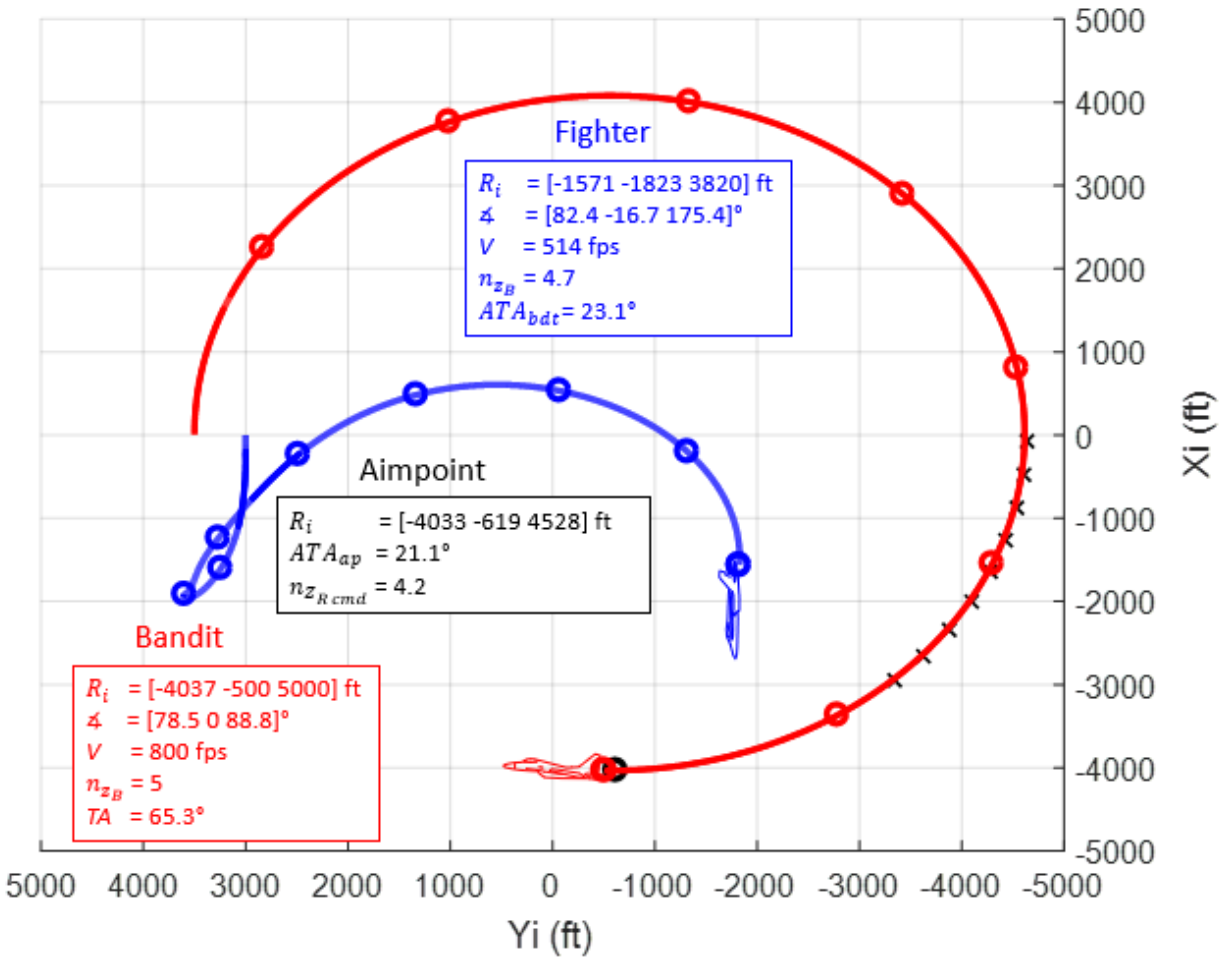

Figure 90. High Aspect (Fighter Energy Disadvantage) Scenario: Fighter Completes the Maneuver (Top View)

10. High Aspect (Bandit Pure Pursuit) Scenario

The final scenario is a high-aspect scenario from a neutral start; both aircraft are at 800 ft/s. The bandit is given the same guidance scheme as the fighter, with one exception: the bandit is forced to maintain pure pursuit. This would be akin to the very first instructions of an inexperienced fighter pilot, where the mantra is "place [the] lift vector on [the other aircraft] and pull" [11].

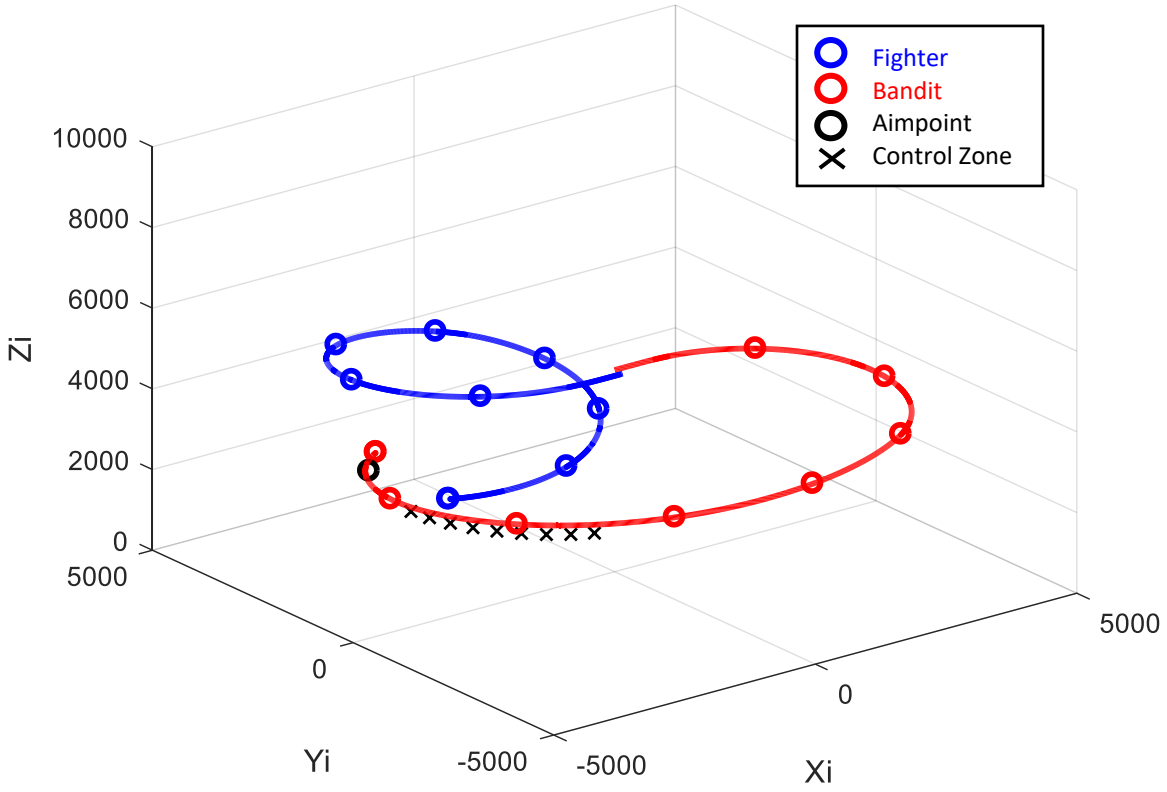

Figure 91. High Aspect (Bandit Pure Pursuit) Scenario: Trace Plot

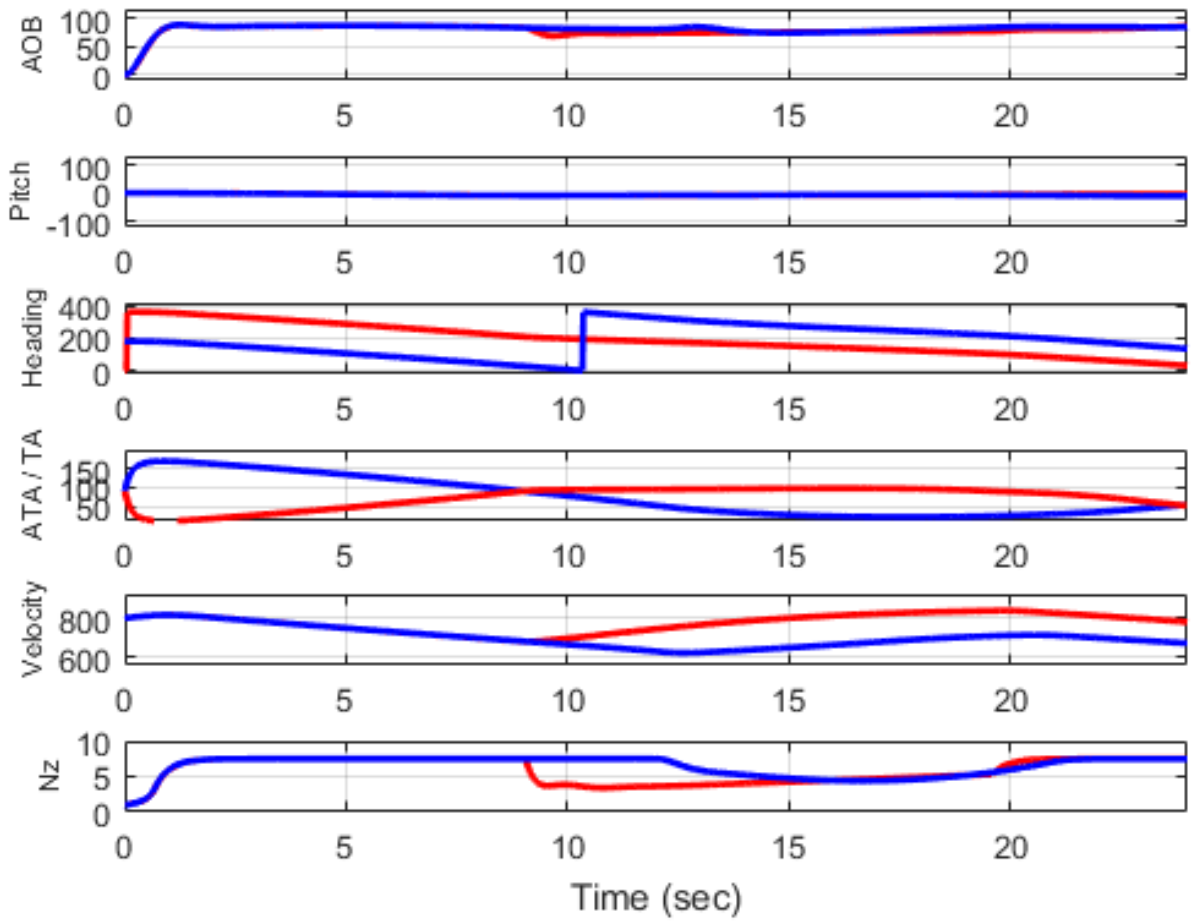

Figure 92. High Aspect (Bandit Pure Pursuit) Scenario: Data Plot

Once again, the fighter does extremely well in this scenario. By manipulating the aimpoint of the fighter's guidance scheme, the fighter is on the verge of a 6,000 ft perch scenario, albeit with greater target aspect from the bandit. At *t*=15 seconds, the fighter is pointing at the bandit and about to enter the bandit's turn circle with lag pursuit. The two aircraft are established in right-hand two-circle flow with a slight downward trend. By *t*=21 seconds, the fighter is fully established in the bandit's turn circle and maintains an offensive advantage.

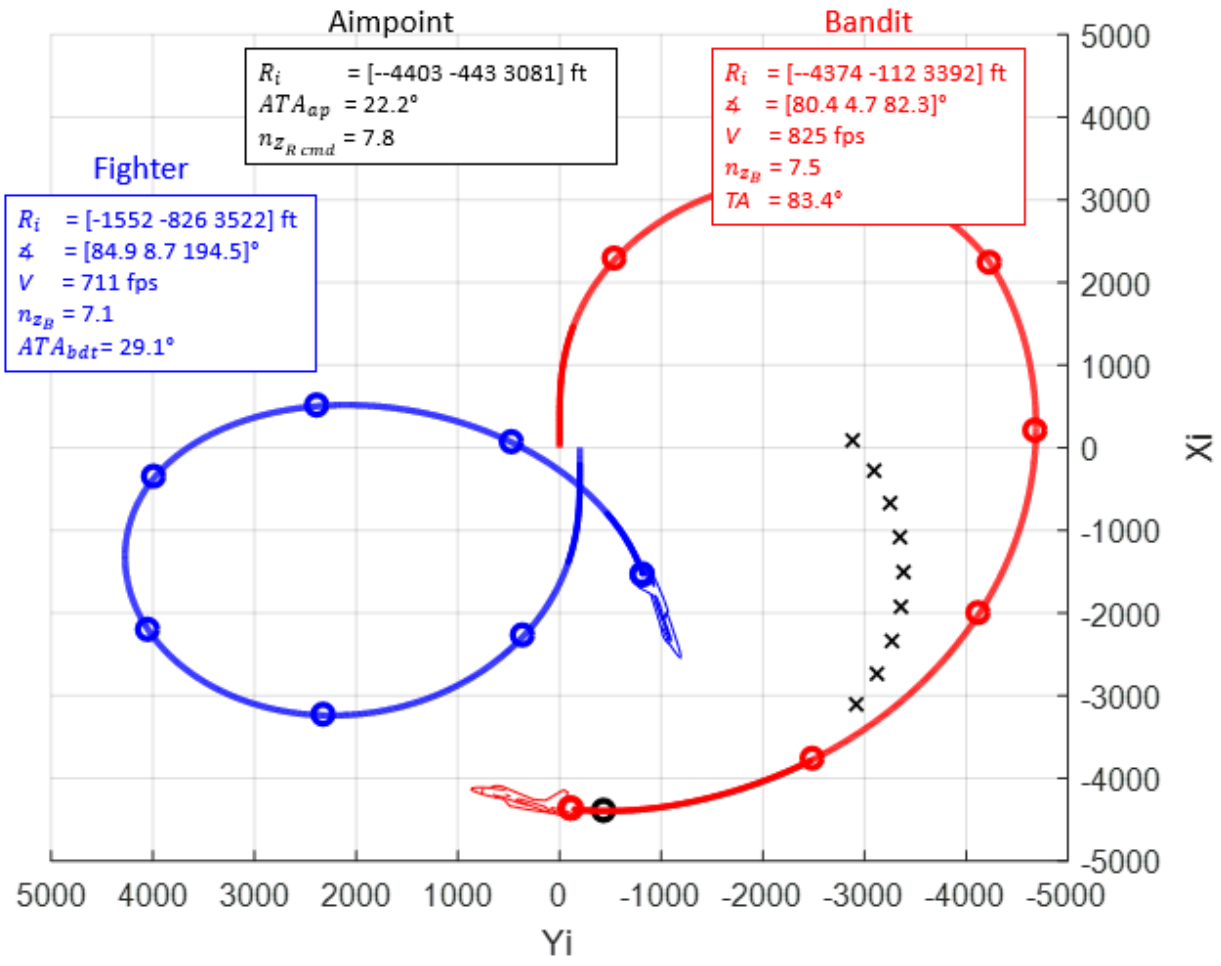

Figure 93. High Aspect (Bandit Pure Pursuit) Scenario: Fighter Re-Enters Bandit's Turn Circle with Offensive Advantage (Top View)

Because this last scenario is the only one with a truly reactive bandit, it is beneficial to examine the effects of noise added to the fighter's notional tracking solution. In the case below, the high aspect scenario is repeated, except noise is added to the bandit's position and velocity. The noise additive includes a standard deviation of +/- 100 ft in position and +/- 15 ft/s in velocity at every time stamp. The fighter's flight path is almost identical to Figure 93 above. The scattered plot of the bandit's flight path shows the "tracked" flightpath with noise added.

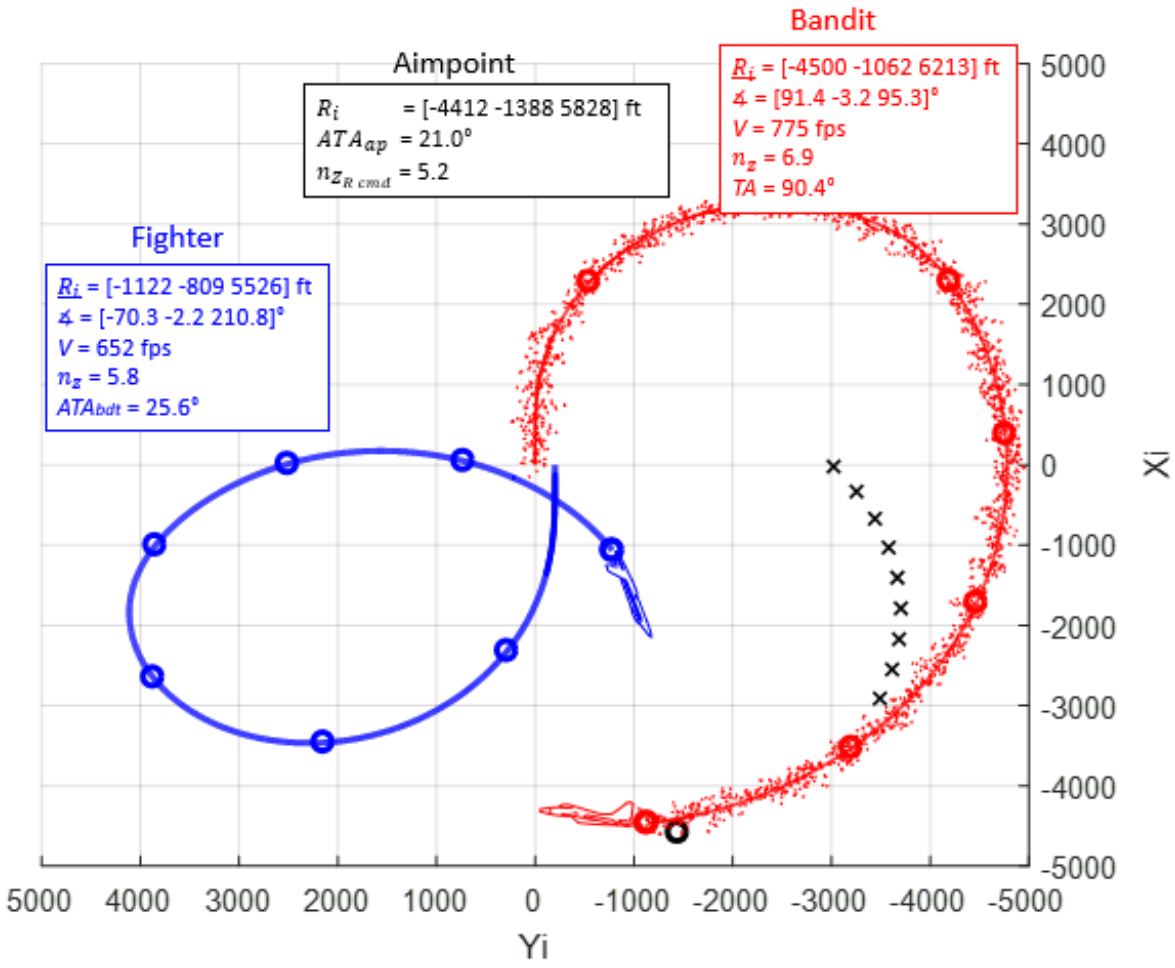

Figure 94. High Aspect Scenario: Noise Added to Fighter's Tracked Solution (Top View)

8. SUMMARY OF ORIGINAL CONTRIBUTIONS

From everything presented in this dissertation, there are four significant areas of original contribution toward the solution of autonomous BFM. The first original contribution is the incorporation of vertical energy-maneuverability and the use of the VEM diagram. This concept is briefly explained in section 3.3.8 and available in reference [13]. The concept of VEM is an original contribution by its own right, and understanding the relationship between energy and an aircraft's ability to maneuver vertically (or lack thereof) is important here.

The second contribution is the definition of a frame of reference for the bandit's control zone. This was done through a series of rotation matrices that account for gravity's effect on the bandit's acceleration, and a translation from the bandit to the control zone. By properly defining an aimpoint along the bandit's turn circle, the fighter can generate more suitable guidance commands for a BFM strategy.

The next contribution is the calculation of an adjustable aimpoint along the bandit's turn circle, as opposed to a fixed-distance aimpoint at 0° TA/0° ATA. The disadvantages of the latter "de facto standard" were laid out in Section 4 (Literature Survey). The advantages of calculating an aimpoint along the bandit's turn circle, on the other hand, gives the fighter a better chance of maintaining an offensive position behind the bandit, even as the bandit's energy and performance changes. Additionally, this concept allows the fighter to smoothly transition from offensive, to neutral and defensive BFM positions.

Finally, the implementation of a guidance method based on variable gains is a departure from the previously tried methods. Section 4 described the difference between what the author labeled as the "look-up" method and the "look-ahead" method. The former was not robust enough, and

the latter was too computationally expensive. The idea of combining roll, acceleration, and velocity inputs with gain scheduling is an entirely new approach to this problem.

9. CONCLUSION

Autonomous BFM is a subject that is not only new and demanding, it has direct applicability to design requirements of future UCAVs. It requires an understanding of century-old BFM principles, modern aircraft performance and flight dynamics, and complex guidance. Two methods of control that have already been proposed in other works include pre-planned maneuvers and approximate dynamic programming. Variable gain scheduling however, enables good autonomous fighter performance in this complex environment.

In no uncertain terms, the guidance scheme presented here is a success. This is a tremendous combination of identifying the control zone through rotation matrices, combined with variable gain scheduling as a guidance scheme and an adjustable aimpoint that moves between lead, lag, and pure pursuit and moves up and down in space based on the principles of vertical-energy maneuverability.

Appendix A

References

[1] J. A. Olson, A History of Air Warfare, Potomac Books, 2010.

[2] J. E. Neu, "Optimum Identification Criteria For Ait-To-Air Engagements," Air University, Maxwell AFB, AL, 1989.

[3] P. Higby, "Promise and Reality: Beyond Visual Range Air-To-Air Combat," Air War College, Air University, Maxwell Air Force Base, AL, 2005.

[4] Government Accountability Office, "GAO-09-520," GAO, Washington, DC, 2009.

[5] BBC News, "Russia 'shot down Georgia drone'," 21 April 2008. [Online]. Available: http://ww.news.bbc.co.uk/2/hi/europe/7358761.

[6] M. Davis, "Loyal Winmag to Take Australia's Airpower Into the Next Era," *Australia Strategic Policy Institute*, pp. https://www.aspistrategist.org.au/loyal-wingman-to-take-australias-airpower-into-the-next-era/#:~:text=The%20Loyal%20Wingman%20was%20unveiled%20in%20front%20of,implications%20for%20the%20future%20of%20Australia%E2%80%99s%20defence%20industry., 7 March 2019.

[7] M. E. Rowan, C. P. Allain, S. A. Pontzer, B. D. Tillman and J. P. Tekell, "Flight Test Evaluation of the AFRL Automated Wingman Functions (Project HAVE RAIDER)," Air Force Material Command, Edwards AFB, CA, 2015.

[8] F. Meyer, J. Bearce, R. Meyer, E. M. Sink and R. E. Chrash, "Flight Test Evaluation of the HAVE RAIDER II Autonomous Wingman Architecture," Air Force Material Command, Edwards AFB, CA, 2017.

[9] "NAVMC 3500.50C. FA-18 Training and Readiness Manual," United States Marine Corps Training and Education Command, Marine Corps Base Quantico, VA, 2012.

[10] *F-16 Aircraft Fundamentals*, Joint Base Langley-Eustiss, VA: United States Air Force, Air Combat Command, 1996.

[11] Naval Air Training Command, Basic Fighter Maneuvering Section Engaged Maneuvering, Naval Air Station Corpus Christi, 2012.

[12] F. Blesse, "No Guts, No Glory!," Nellis AFB, NV.

[13] J. Dean, "Vertical Energy-Maneuverability," in *Society of Experimental Test Pilots, West Coast Symposium*, San Diego, CA, 2015.

[14] "PF803B: Energy," United States AIr Force Test Pilot School, Edwards Air Force Base, CA, 2002.

[15] K. Ayling, Combat Aviation, Harrisburg, PA: Military Service Publishing Company, 1943.

[16] E. A. Sims, Fighter Tactics and Strategy: 1914-1970, Harper and Row, 1972.

[17] T. A. Keaney and E. Cohen, "Gulf War Air Power Survey," U.S. Government Printing Office, Washington, D.C., 1993.

[18] R. L. Shaw, Fighter Combat: Tactics and Maneuvering, Annapolis, MD: Naval Institute Press, 1985.

[19] P. Bonanni, The Art of the Kill: A Comprehensive Guide to Modern Air Combat, Spectrum, 1993.

[20] E. Rutowski, "Energy Approach to the General Aircraft Performance Problem," 1954.

[21] J. Boyd, "Aerial Attack Study," U.S. Air Force, 1964.

[22] D. Johnson, "Evaluation of Energy Maneuverability Procedures in Aircraft Flight Path Optimization and Performance Estimation," Air Force Flight Dynamics Laboratory, Wright-Patterson Air Force Base, OH, 1972.

[23] W. P. Lane, C. D. Eliason, D. P. Glenn and R. W. Terry, "Air Combat Maneuvering Performance Measurement State Space Analysis," Air Force Human Resources Laboratory, 1982.

[24] A. Paranjape and N. Ananthkrishnan, "Combat Aircraft Agility Metrics - A Review," *Journal of Aerospace Sciences and Technologies*, vol. 58, no. 2, 2005.

[25] A. Tewari, Atmospheric and Space Flight Dynamics, Boston, MA: Birkhauser, 2007.

[26] B. L. Stevens and F. L. Lewis, Aircraft Control and Simulation: Dynamics Controls Design, and Autonomous Systems 3rd Ed, Wiley Blackwell Publishing, 2015.

[27] E. D. Medagoda and P. W. Gibbens, "Synthetic Waypoint Guidance Algorithm for Following a Desired Flight Trajectory," *Journal of Guidance, Control, and Dynamics,* vol. 33, no. 2, pp. 601-606, 2020.

[28] J. Dean, "Defining the Control Zone in Basic Fighter Maneuvering," Unpublished Academic Work, University of Texas at Arlington, 2014.

[29] C. Silvestre, A. Pascoal and I. Kaminer, "On the Design of Gain-Scheduled Trajectory Tracking Controllers," *Internal Journal of Robust and Nonlinear Control,* vol. 12, pp. 797-839, 2002.

[30] L. Walter, S. Fleischmann, G. Schloffel and S. Theodoulis, "Real-Time Optimal Gain Scheduling for Nonlinear Dynamic Inversion," French-German Research Institue of Saint-Louis, Jan 2014.

[31] D. J. Leith and W. E. Leithead, "Survey of Gain-Scheduling Analysis and Design," *International Journal of Control,* 2000.

[32] K. Mehran, "Takagi-Sugeno Fuzzy Method for Process Control," Newcastle University, 2008.

[33] Y. Elhalwagy and M. Tarbouchi, "Three-Dimensional Missile Guidance Laws Design Using Fuzzy Schemes," Royal Military College, Kingston Ontario, Canada.

[34] C.-H. Wang and K.-N. Hung, "Intelligent Adaptive Law for Missile Guidance Using Fuzzy Neural Networks," *International Journal of Fuzzy Systems,* vol. 15, pp. 182-192, June 2013.

[35] M. D. Davis, Game Theory: A Nontechnical Introduction, Dover Books, 1970.

[36] W. L. Othling, "Application of Differential Game Theory to Pursuit-Evasion Problems of Two Aircraft," Air Force Institute of Technology, 1970.

[37] J. Sprinkle, M. Eklund, H. J. Kim and S. Sastry, "Encoding Aerial Pursuit/Evasion Games with Fixed Wing Aircraft into a Nonlinear Model Predictive Tracking Controller," in *Conference on Decision and Control*, University of California - Berkeley, 2004.

[38] K. Moritz, R. Polis and K. Well, "Pursuit-Evasion in Medium-Range Air-Combat Scenarios," *Comput. Math. Applic.,* vol. 13, no. 1-3, pp. 167-180, 1987.

[39] T. S. Anderson and R. Kristiansen, "Path-Following in Three dimensions Using Quaternions for a Fixed-Wing UAV," in *Conference on Control Technologies and Applications*, Copenhagen, 2018.

[40] R. Isaacs, "Games of Pursuit," RAND, 1951.

[41] S. Ghasemi, M. Nikravesh, M. Menhaj and S. Akbari, "Fuzzy Model for Human's Performance for Guarding Territory in an Air Combat," *AUT Journal of Modeling and Simulation,* 2010.

[42] G. H. Burgin and A. J. Owens, "An Adaptive Maneuvering Logic Computer Program for the Simulation of One-On-One Air-To-Air Combat," NASA, Washington, DC, 1975.

[43] W. Hankins, "Computer Automated Opponent for Manned Air to Air Combat Simulations," NASA Technical Report, 1979.

[44] G. Olsder and J. Breakwell, "Role Determination in an Aerial Dogfight," *Intl. Journal of Game Theory,* vol. 3, no. 1, pp. 47-66, 1974.

[45] R. Ghasemi, S. Nikravesh, M. Menhaj and S. Akbari, "A 3-D Fuzzy Modeling opf Pilot's Performance in the Dogfight," Amirkabir University, Tehran, 2004.

[46] R. Ghasemi, S. Nikravesh, M. Menhaj and S. Akbari, "Near Optimal Fuzzy Modeling of Pursuit-Evasion in an Air Combat," Amirkabir University, Department of Electrical Engineering.

[47] S. Akbari and M. B. Menhaj, "A Fuzzy Guidance Law for Modeling Offensive Air-To-Air Combat Maneuver," in *Joint 9th FSA World Congress and 20th NAFIPS International Conference*, 2001.

[48] H. Park, B.-Y. Lee, M.-J. Tahk and D.-W. Yoo, "Differential Game Based Air Combat Maneuver Generation Using Scoring Function Matrix," *International Journal of Aeronautical & Space Sci.,* vol. 17, no. 2, pp. 204-213, 2016.

[49] K. N. Ure and G. Inalhan, "Autonomous Control of Unmanned Combat Air Vehicles," *IEEE Control Systems Magazine*, pp. 74-95, October 2012.

[50] M. B. Pearce, Artist, *Autonomous Aerobatics: A Linear Control and Implenetation For a Slow Roll.* [Art]. North Carolina State University.

[51] R. A. Oberle, "An Air Combat Maneuver Conversion Model," Center for aval Analyses, Arlington, VA, 1974.

[52] G. Burgin and L. Sidor, "Rule-Based Air Combat Simulation," Titan Systems, Inc., La Jolla, CA, 1988.

[53] K. Virtanen and T. Ralvio, "Modeling Pilot's Sequential Maneuvering Decisions by a Multistage Influence Diagram," *Journal of Guidance Control and Dynamics,* vol. 27, no. 4, 2004.

[54] K. Virtanen, "Optimal Pilot Decisions and Flight Trajectories in Air Combat," Helsinki University of Technology, 2005.

[55] K. Virtanen, J. Karelahti and T. Raivio, "Modeling Air Combat by a Moving Horizon Influence Diagram Game," *Journal of Guidance, Control, and Dynamics,* vol. 29, no. 5, pp. 1080-1093, 2006.

[56] J. Kaneshige and K. Krishnakumar, "Artificial Immune System Approach for Air Combat Maneuvering," NASA Ames Research Center, Moffett Field, CA, 2007.

[57] Y. Wang, C. Huang and C. Tang, "Research on Unmanned Combat Aerial Vehgicle Robust Maneuvering Decision Under Incomplete Target Information," *Advances in Mechanical Engineering,* vol. 8, pp. 1-12, 2016.

[58] J. N. Hall, J. H. Hayes, J. Jurado, B. Karlow, D. Koeniguer and M. D. Pacini, "Initial Dynamic Engagement Demonstration of the Automatic Air Collision Avoidance System (Project Have POSIT II)," Air Force Material Command, Edwards AFB, CA, 2013.

[59] J. Dean, C. M. Bell, A. Hafez, P. Dolce and D. Nelson, "Initial Demonstration of Autonomous Formation Flying Utilizing Variable Stability System," Air Force Material Command, Edwards AFB, CA, 2014.

[60] E. Y. Rodin and S. M. Amin, "Maneuver Prediction in Air Combat Via Artificial Neural Networks," *Computers Math. Applic.,* vol. 24, no. 3, pp. 95-112, 1992.

[61] T.-H. Teng, A.-H. Tan, Y.-S. Tan and A. Yeo, "Self-organizing Neural Networks for Learning Air Combat Maneuvers," in *IEEE World Congress on Computational Intelligence*, Brisbane, Australia, June 2012.

[62] R. W. Schvaneveldt and A. E. Benson, "Neural Network Models of Air Combat Maneuvering," Air Force Material Command, Williams AIr Force Base, AZ, 1992.

[63] X. Zhang, G. Liu, C. Yang and J. Wu, "Research on Air Combat Maneuver Decision-Making Method Based on Reinforcement Learning," *Electronics,* vol. 7, 2018.

[64] W. Kong, D. Zhou, Z. Yang, Y. Zhao and K. Zhang, "UAV Autonomous Aerial Combat Maneuver Strategy Generation with Observation Error Based on State-Adversarial Deep Deterministic Policy Gradient and Inverse Reinforcement Learning," *Electronics,* vol. 9, no. 1121, 2020.

[65] Z. Wang, H. Li, H. Wu and Z. Wu, "Improving Maneuver Strategy in Air Combat by Alternate Freeze Games with a Deep Reinforcement Learning Algorithm," *Mathematical Problems in Engineering,* 2020.

[66] W. B. Powell, "What You Should Know About Approximate Dynamic Programming," Wiley InterScience, Inc., 2008.

[67] J. S. McGrew, "Real-Time Maneuvering Decisions for Autonomous Air Combat," Massachusetts Institute of Technology, 2008.

[68] J. S. McGrew, J. P. How, L. A. Bush, B. Williams and N. Roy, "Air Combat Strategy Using Approximate Dynamic Programming," *Journal of Guidance, Control, and Dynamics,* vol. 33, pp. 1641-1654, 2010.

[69] Y. Ma, X. Ma and X. Song, "A Case Study on Air Combat Decision Using Approximated Dynamic Programming," *Mathematical Problems in Engineering,* 2014.

[70] N. R. Lopez and R. Zbikowski, "Effectiveness of Autonomous Decision Making for Unmanned Combat Aerial Vehicles in Dogfight Engagements," *Journal of Guidance, Control, and Dynamics*, vol. 41, no. 4, pp. 1021-1024, 2018.

[71] E. Berglund, "Technologies for Future Precision Strike Missile Systems," Swedish Defence Research Agency, Stockholm, Sweden.

[72] D.-I. You and D. H. Shim, "Design of an Aerial Combat Guidance Law Using Virtual Pursuit Point Concept," in *Proceedings of the Institution of MEchanical Engineers*, 2015.

[73] F. Gavilan, R. Vazquez and E. Camacho, "An Iterative Model Predictive Control Algorithm for UAV Guidance," *IEEE Transactions on Aerospace and Electronic Systems*, vol. 51, no. 3, 2015.

[74] F. Balampanis, P. Aguiar, I. Maza and A. Ollero, "Path Tracking for Waypoint Lists Based on a Pure Pursuit Method for Fixed Wing UAS," in *Workshop on Research, Education and Development of Unmanned Aerial Systems*, 2017.

[75] H. Shin, J. Lee, D. H. Shim and D.-I. You, "Design of a Virtual Fighter Pilot and Simulation Environment for Unmanned Combat Aerial Vehicles," in *AIAA Guidance, Navigation, and Control Conference*, Grapevine, TX, 2017.

[76] "MIL-STD-1797B: Flying Qualities of Piloted AIrcraft," Department of Defense, Wright Patterson Air Force Base, OH, 2006.

[77] K. Huenecke, Modern Combat Aircraft Design, Naval Institue Press, 1983.

[78] R. Leifer, J. Valasek and D. Eggold, "Fighter Agility Metrics, Research, and Test," University of Kansas Flight Research Laboratory, Lawrence, Kansas.

[79] B. Etkin, Dynamics of Atmospheric Flight, New York, NY: Dover Books, 2000.

[80] C. Cotting, "Flight Controls and Handling Qualities Cheat Sheet," U.S. Air Force Test Pilot School, Edwards AFB, CA, 2013.

[81] "Stability Derivatives," in *Flying Qualities Testing*, United States Air Force, pp. 7-1 through 7-13.

[82] R. E. Ball, The Fundamentals of AircraftCombat Survivability Analysis and Design, American Institute of Aeronautics and Astronautics, 1984.

[83] R. Whitford, Design for Air Combat, United Kingdom: Jane's Information Group, 1989.

[84] D. P. Raymer, Aircraft Design: A Conceptual Approach 3d Ed, Reston, VA: American Institute of Aeronautics and Astronautics, 1999.

[85] Flying Qualities Testing, Edwards Air Force Base, CA: U.S. Air Force Flight Test Center, pp. 14-9 through 14-11.

[86] B. L. Stevens and Frank L. Lewis, Aircraft Control and Simulation, 2d Edition, New York, NY: Wiley, 2003.

[87] A. Rehmann, "A Handbook of Flight Simulation Fidelity Requirements for Human Factors Research (DOT/FAA/CT-TN95/46)," National Technical Information Service, Springfield, VA, 1995.

[88] G. W. Stimson, Introduction to Airborne Radar, Edison, NJ: Scitech Publishing, 2014.

[89] C. Dever, B. Mettler, E. Feron and J. Popovic, "Nonlinear Trajectory Generation for Autonomous Vehicles via Parameterized Maneuver Classes," *Journal of Guidance, Control, and Dynamics*, vol. 29, no. 2, pp. 289-302, March-April 2006.

[90] K. N. Ure and G. Inalhan, "Auto Control of UCAVs," *IEEE Control Systems Magazine*, pp. 74-95, October 2012.

[91] R. K. Wilcox, Scream of Eagles: The Dramatic Account of the U.S. Navy's Top Gun Fighter Pilots and How They Took Back the Skies Over Vietnam, New York, NY: Pocket Star Books, 2014.

Appendix B

MATLAB Script and Functions

```
clear all;

%%%%%%%%%%%%   Initial Conditions  %%%%%%%%%%%%%%%%

load Ps.mat;

IC_set=6; %Set initial conditions to 1 = perch, 2 = high yo-yo, 3=roller, 4 =
abeam, 5 = Def Perch, 6 = HA BFM

k_roll=5; %Constant gain.  Applies to fighter roll.
k_cz=1; %Initialized Constant.  Adjusted dynamically, based on
offensive/defensive.
k_nz=0.1667; %Constant gain.  Applies to ftr nz.
k_v = 1500; %Constant gain.  Applies to ftr bleed rate.

%Set fighter characteristics
nz_max_ftr=7.5;    %Load factor limit
C_lp_ftr=0.5;
ftr_bleed_rate_corr=0;
Iy_ftr=55814;      %Iyy
S=300;
c_bar=30;

%Define 3 sets of initial conditions, each with r0, v0, and angles0

if IC_set==1;
V_bdt(1) = 800;
V_ftr(1) = 800;
r_i_bdt(1,:)=[3500 2000 5000];
r_i_ftr(1,:)=[-5500 2200 5000];
nz_bdt(1)=6.3;  a_bdt=32.2*nz_bdt(1);
nz_max_bdt=7.5;
nz_ftr(1)=1;  a_ftr=32.2*nz_ftr(1);
angles_bdt(1,:)=deg2rad([acosd(1/nz_bdt) 0 -40]);
angles_ftr(1,:)=deg2rad([0 0 0]);
time=24;
end

if IC_set==2;
V_bdt(1) = 600;
V_ftr(1) = 800;
r_i_bdt(1,:)=[-2000 0 5000];
r_i_ftr(1,:)=[-2700 -700 5000];
nz_bdt(1)=5.3;  a_bdt=32.2*nz_bdt(1);
nz_max_bdt=7.5;
nz_ftr(1)=1;  a_ftr=32.2*nz_ftr(1);
angles_bdt(1,:)=deg2rad([acosd(1/nz_bdt) 0 0]);
angles_ftr(1,:)=deg2rad([0 0 120]);
time=18;
end

if IC_set==3;
V_bdt(1) = 450;
V_ftr(1) = 690;
```

```
r_i_bdt(1,:)=[-4000 2000 8500];
r_i_ftr(1,:)=[-4000 2000 5200];
nz_bdt(1)=5.0;  a_bdt=32.2*nz_bdt(1);
nz_max_bdt=7.5;
nz_ftr(1)=1;  a_ftr=32.2*nz_ftr(1);
angles_bdt(1,:)=deg2rad([0*acosd(1/nz_bdt) 180 90]);
angles_ftr(1,:)=deg2rad([0 0 0]);
time=27;
end

if IC_set==4;
V_bdt(1) = 500;
V_ftr(1) = 550;
r_i_bdt(1,:)=[0 -4000 5000];
r_i_ftr(1,:)=[-2000 -4000 5000];
nz_bdt(1)=1;  a_bdt=32.2*nz_bdt(1);
nz_max_bdt=7.5;
nz_ftr(1)=1;  a_ftr=32.2*nz_ftr(1);
angles_bdt(1,:)=deg2rad([acosd(1/nz_bdt) 0 90]);
angles_ftr(1,:)=deg2rad([0 0 90]);
time=15;
end

if IC_set==5;
V_bdt(1) = 800;
V_ftr(1) = 800;
r_i_bdt(1,:)=[-3000 2000 5000];
r_i_ftr(1,:)=[3000 2000 5000];
nz_bdt(1)=1;  a_bdt=32.2*nz_bdt(1);
nz_max_bdt=7.5;
nz_ftr(1)=1;  a_ftr=32.2*nz_ftr(1);
angles_bdt(1,:)=deg2rad([acosd(1/nz_bdt) 0 0]);
angles_ftr(1,:)=deg2rad([0 0 -40]);
time=21;
end

if IC_set==6
V_bdt(1) = 800;
V_ftr(1) = 550;
r_i_bdt(1,:)=[0 3500 5000];
r_i_ftr(1,:)=[0 3000 5000];
nz_bdt(1)=5;  a_bdt=32.2*nz_bdt(1);
nz_max_bdt=7.5;
nz_ftr(1)=1;  a_ftr=32.2*nz_ftr(1);
angles_bdt(1,:)=deg2rad([acosd(1/nz_bdt) 0 0]);
angles_ftr(1,:)=deg2rad([0 0 -180]);
time=24;
end

%Constants
g=32.2;
crnr_arspd=500;
min_ftr_radius=crnr_arspd^2/(g*nz_max_ftr(1));

%Time constants for simulation
dt=0.02;
```

```
run_time = time/dt;
cz_dim=10;

%Initialize
ftr_roll_rate(1)=0;
nz_onset_rate(1)=0;
nz_onset(1)=0;

%%%%%%%%%%%%   Bandit Geometry   %%%%%%%%%%%%%%%%
%%%%  These are open-loop maneuvers,  %%%%%%%%%%%%
%%%%  based on initial conditions.    %%%%%%%%%%%%

for i=1:run_time
%Option to add noise to system
r_i_bdt(i,:) = r_i_bdt(i,:);
V_bdt(i)=V_bdt(i);
%Set magnitude of bdt velocity in body/radial frame (U=V_bdt)
v_b_bdt=[V_bdt(i) 0 0];
%calculate rotation matrix from inertial to body
rbi_bdt=R_BI(angles_bdt(i,1),angles_bdt(i,2),angles_bdt(i,3));

%EOMs (T, Dp, and Di are accounted for in Ps bleed rates)
axg=-g*sin(angles_bdt(i,2));
ayg=g*cos(angles_bdt(i,2))*sin(angles_bdt(i,1));
azg=g*cos(angles_bdt(i,2))*cos(angles_bdt(i,1));
a_b_bdt(i,:)=-[axg ayg azg-nz_bdt(i)*g];
a_b_max_bdt(i,:)=-[axg ayg azg-nz_max_bdt*g]';

%rotation matrix from body to radial
rrb_bdt=R_RB(norm(a_b_bdt(i,:))/g,angles_bdt(i,2),angles_bdt(i,1));

%Angular rates in body frame
w_b(i,:)=cross(v_b_bdt,a_b_bdt(i,:))/(norm(v_b_bdt)^2);
wskew=skew(w_b(i,:));
r_b_double_dot=wskew*v_b_bdt'*dt+2*wskew*v_b_bdt'+wskew*wskew*v_b_bdt'*dt;
%Incremental change in position, body frame
dr=v_b_bdt'*dt + 0.5*r_b_double_dot*dt^2;
%Rotate dr back to inertial frame
dr_i=rbi_bdt'*dr;
%Newtonian calculations complete, increment bdt position, inertial frame
r_i_bdt(i+1,:)=r_i_bdt(i,:)+dr_i';
%Increment Euler angles
omega_dot(i,:)=R_Eul(angles_bdt(i,:),w_b(i,:));
angles_bdt(i+1,:)=angles_bdt(i,:) + omega_dot(i,:)*dt;

%For IC sets 1 and 2, nz_bdt remains constant
nz_bdt(i+1)=nz_bdt(i)+0*randn(1);

%Define reversal(s) for IC set 2
if IC_set==2
if i==200
     angles_bdt(i+1,1)=-angles_bdt(i,1); %Reversal, S-turn
end
if i==700
     angles_bdt(i+1,1)=-angles_bdt(i,1); %Reversal, S-turn
```

```
end
end

%Define bandit lag for IC set 5
if IC_set==5
if i>150
    nz_bdt(i+1)=6.9;
    angles_bdt(i+1,1)=acos(1/nz_bdt(i+1));
end
end

%Define rolling scissors geometry for bandit
if IC_set==3;
    angles_bdt(i+1,:)=angles_bdt(i,:) + omega_dot(i,:)*dt +
[abs(0.0052*sin(angles_bdt(i,2))) 0 0];
    nz_bdt(i+1)=0.01*V_bdt(i)+0*randn(1);
end

% Determine bleedrate for bandit, f(nz, V, h)
bleed_rate_bdt(i)=0*Ps(round(nz_bdt(i)*5),max(20,min(90,round(V_bdt(i)/10))),
round(r_i_bdt(i,3)/1000));
dh=r_i_bdt(i+1,3)-r_i_bdt(i,3);
bleed_rate_bdt(i)=bleed_rate_bdt(i)*32.2/V_bdt(i);
V_bdt(i+1)=max(200,sqrt(V_bdt(i)^2-2*g*dh)+bleed_rate_bdt(i)*dt);

%Total specific energy, bandit
Es_bdt(i)=r_i_bdt(i,3)+V_bdt(i)^2/(2*g);
end

%%%% Fighter Response to Bandit Maneuvers %%%%

for j=1:run_time
    Es_ftr(j)=r_i_ftr(j,3)+V_ftr(j)^2/(2*g);

    %Initial relationship between fighter and bandit
    r_i_ftr_bdt(j,:)=r_i_bdt(j,:)-r_i_ftr(j,:);
    range_bdt(j)=norm(r_i_ftr_bdt(j,:));
    %Store values to be used in calculating the CZ
    rbi_bdt=R_BI(angles_bdt(j,1),angles_bdt(j,2),angles_bdt(j,3));
    rrb_bdt=R_RB(norm(a_b_bdt(j,:))/g,angles_bdt(j,2),angles_bdt(j,1));
    nr_bdt_norm=norm(a_b_bdt(j,:))/32.2;
    nr_max_bdt_norm(j)=norm(a_b_max_bdt(j,:))/32.2;

%This line allows for an aadjustable aimpoint.  k_cz_bias is calculated at
%end.
    k_cz_bias(j)=k_cz(j);

%Otheriwse, this line keeps the k_cz constant
%     k_cz_bias(j)=1;

    %Calculate the aimpoint
    radius_bdt(j)=V_bdt(j)^2/(nr_bdt_norm*32.2);
    radius_min_bdt(j)=V_bdt(j)^2/(g*nr_max_bdt_norm(j));
    tau_ap(j)=k_cz_bias(j)*nr_bdt_norm/nr_max_bdt_norm(j);
```

```
    rho_r_ap(j,:)=([-radius_bdt(j)*sin(tau_ap(j)); 0; -radius_bdt(j)*(1-
cos(tau_ap(j)))]);
    rho_i_ap(j,:)=rbi_bdt'*rrb_bdt'*rho_r_ap(j,:)';

    if nz_bdt(j)==1
    rho_r_ap(j,:)=[-k_cz_bias(j)*radius_min_bdt(j) 0 0];
    rho_i_ap(j,:)=rbi_bdt'*rrb_bdt'*rho_r_ap(j,:)';
    end

    if j>1
    ap_VEM_corr(j)=((V_ftr(j)-550)-(V_bdt(j)-650))*(abs(ATA_bdt(j-
1))+abs(TA(j-1))+1);
    else
    ap_VEM_corr(j)=0;
    end
    r_i_bdt_ap(j,:)=r_i_bdt(j,:)+rho_i_ap(j,:)+[0 0 ap_VEM_corr(j)];
    %Protect aimpoint from going below 0' AGL
    r_i_bdt_ap(j,3)=max(0,r_i_bdt_ap(j,3));

    %Calculate the control zone (not necessarily the same as aimpoint)
    for k=1:cz_dim+1
    tau_cz(j)=(1+1.5*(k-1)/cz_dim)*nr_bdt_norm/nr_max_bdt_norm(j);
    rho_r_cz(j,:)=([-radius_bdt(j)*sin(tau_cz(j)); 0; -radius_bdt(j)*(1-
cos(tau_cz(j)))]);
    rho_i_cz(j,:)=rbi_bdt'*rrb_bdt'*rho_r_cz(j,:)';
    if nz_bdt(j)==1
    rho_r_cz(j,:)=[-(1+1.5*(k-1)/cz_dim)*radius_min_bdt(j) 0 0];
    rho_i_cz(j,:)=rbi_bdt'*rrb_bdt'*rho_r_cz(j,:)';
    end
    r_i_bdt_cz(j,:,k)=r_i_bdt(j,:)+rho_i_cz(j,:);
    end

    %Relationship between fighter and aimpoint/CZ
    if j>1
    r_i_ftr_ap(j,:)=r_i_bdt_ap(j,:)-r_i_ftr(j,:);
    r_i_ftr_bdt_cz(j,:)=r_i_bdt_cz(j,:,1)-r_i_ftr(j,:);
    else
    r_i_ftr_ap(j,:)=r_i_bdt_ap(j,:)-r_i_ftr(j,:);
    r_i_ftr_bdt_cz(j,:)=r_i_bdt_cz(j,:,1)-r_i_ftr(j,:);
    end
    range_ap(j)=norm(r_i_ftr_ap(j,:));
    range_cz(j)=norm(r_i_ftr_bdt_cz(j,:));


    %Set magnitude of bdt velocity in body/radial frame
    v_b_ftr=[V_ftr(j) 0 0];


    %calculate rotation matrix from inertial to body
    rbi_ftr=R_BI(angles_ftr(j,1),angles_ftr(j,2),angles_ftr(j,3));
    %EOMs
    axg=-g*sin(angles_ftr(j,2));
    ayg=g*cos(angles_ftr(j,2))*sin(angles_ftr(j,1));
    azg=g*cos(angles_ftr(j,2))*cos(angles_ftr(j,1));
    a_b_ftr=-[axg ayg azg-nz_ftr(j)*g];
```

```
    w_b(j,:)=cross(v_b_ftr,a_b_ftr)/(norm(v_b_ftr)^2);
    wskew=skew(w_b(j,:));

r_b_double_dot=wskew*v_b_ftr'*dt+2*wskew*v_b_ftr'+wskew*wskew*v_b_ftr'*dt;
    %Incremental change in position, body frame
    dr=v_b_ftr'*dt + 0.5*r_b_double_dot*dt^2;
    %Rotate dr back to inertial frame
    dr_i=rbi_ftr'*dr;
    %Newtonian calculations complete, increment ftr position, inertial frame
    r_i_ftr(j+1,:)=r_i_ftr(j,:)+dr_i';

    %Relationship between fighter and bandit
    r_b_ftr_bdt(j,:)=r_i_ftr_bdt(j,:)*rbi_ftr';
    r_b_ftr_ap(j,:)=r_i_ftr_ap(j,:)*rbi_ftr';
    r_bbdt_ftr_bdt(j,:)=-r_i_ftr_bdt(j,:)*rbi_bdt';

    %Increment Euler angles
    omega_dot(j,:)=R_Eul(angles_ftr(j,:),w_b(j,:));
    angles_ftr(j+1,:)=angles_ftr(j,:) + omega_dot(j,:)*dt;

    rrb_ftr=R_RB(norm(a_b_ftr)/g,angles_ftr(j,2),angles_ftr(j,1));
    r_r_ftr_bdt(j,:)=rrb_ftr*r_b_ftr_bdt(j,:)';
    r_r_ftr_bdt_cz(j,:)=rrb_ftr*r_b_ftr_ap(j,:)';

    %Start developing command signal for fighter roll
    brg_t(j)=wrapToPi(atan2(r_i_ftr_ap(j,2),r_i_ftr_ap(j,1)));
    brg_r(j)=wrapToPi(angles_ftr(j,3)-brg_t(j));
    phi_nr(j)=atan2(norm(r_i_ftr_ap(j,1:2))*sin(brg_r(j)),r_i_ftr_ap(j,3));

    norm_nr_max_cmd(j)=7.5-
abs(cos(angles_ftr(j,2)))*(cos(phi_nr(j))+abs(sin(phi_nr(j))*(7.5-
7.5*sin(acos(1/7.5)))));
    nr_i_max(j,:)=[norm_nr_max_cmd(j)*sin(phi_nr(j))
norm_nr_max_cmd(j)*cos(phi_nr(j))];
    nr_z_max(j,:)=[norm_nr_max_cmd(j)*sin(phi_nr(j))
norm_nr_max_cmd(j)*cos(phi_nr(j))+cos(angles_ftr(j,2))];

    %Identified nr_max, now calculate the desired nr_cmd
    %Antenna Train Angle to bandit
    ATA_bdt(j)=asin(norm(r_b_ftr_bdt(j,2:3))/range_bdt(j));
    if r_b_ftr_bdt(j,1)<0
        ATA_bdt(j)=pi-ATA_bdt(j);
    end

    %Target Aspect
    TA(j)=asin(norm(r_bbdt_ftr_bdt(j,2:3))/range_bdt(j));
    if r_bbdt_ftr_bdt(j,1)>0
        TA(j)=pi-TA(j);
    end

    %Antenna Train Angle to aimpoint
    ATA(j)=asin(norm(r_b_ftr_ap(j,2:3))/range_ap(j));
    if r_b_ftr_ap(j,1)<0
        ATA(j)=pi-ATA(j);
```

```
    end

    %%%% Variable Gain: nr_ftr is function(ATA, V, Range_ap, roll_cmd) %%%%
    norm_nr_cmd(j) = abs(ATA(j)*rad2deg(k_nz))*exp(1-
(range_bdt(j)/(2*radius_min_bdt(j)))^.333);
    if V_ftr(j) < crnr_arspd
        norm_nr_cmd(j)=(V_ftr(j)/(crnr_arspd))^4*norm_nr_cmd(j);
    end
    norm_nr_cmd(j) = max(0,min(norm_nr_cmd(j),norm_nr_max_cmd(j)));
    nr_cmd(j,:)=nr_i_max(j,:)*norm_nr_cmd(j)/norm_nr_max_cmd(j);%
    nz_cmd(j,:)=nr_cmd(j,:)+[0 cos(angles_ftr(j,2))];
    norm_nz_cmd(j)=norm(nz_cmd(j,:));
    norm_nz_cmd(j)=min(nz_max_ftr(1),norm_nz_cmd(j));

    %%%% Start calculating angles to generate roll command
    d_phi(j)= asin(r_b_ftr_ap(j,2)/norm(r_b_ftr_ap(j,2:3)));
    d_phi2(j)=(atan2(real(nr_cmd(j,1)),real(nr_cmd(j,2)))-
atan2(real(nz_cmd(j,1)),real(nz_cmd(j,2))));
    d_phi3(j)=wrapToPi(d_phi(j)-d_phi2(j));

    %%%% Variable Gain: roll_cmd is function(Range_Bdt) %%%%
    ftr_roll_rate_cmd(j)=k_roll*d_phi3(j)-
ftr_roll_rate(j);%*min(1,(range_ap(j)/1500)^2);
    ftr_p_dot(j)=(V_ftr(j)/600)^2*(1/C_lp_ftr)*(ftr_roll_rate_cmd(j)-
ftr_roll_rate(j));

ftr_roll_rate(j+1)=ftr_roll_rate(j)+ftr_p_dot(j)*dt;%min(pi,abs(ftr_p_dot(j)*
dt))*sign(ftr_p_dot(j));
    angles_ftr(j+1,1)=angles_ftr(j,1)+ftr_roll_rate(j)*dt;


bleed_rate_ftr(j)=ftr_bleed_rate_corr+Ps(round(nz_ftr(j)*5),max(20,min(90,rou
nd(V_ftr(j)/10))),max(1,round(r_i_ftr(j,3)/1000)));
    dh=r_i_ftr(j+1,3)-r_i_ftr(j,3);
    V_bleed_rate_ftr(j)=bleed_rate_ftr(j)*32.2/V_ftr(j);

    V_ftr(j+1)=max(100,sqrt(V_ftr(j)^2-2*g*dh)+V_bleed_rate_ftr(j)*dt);

    %%%% Variable Gain: Bleed Rate Cmd is function(ATA_bdt, Range_Bdt )%%%%
    if r_b_ftr_ap(j,1)>0
    bleed_rate_ftr_cmd(j)=(V_bdt(j)-
V_ftr(j))*cos(abs(TA(j)))*(1/((abs(((range_cz(j))/k_v))^3)*((abs(ATA_bdt(j))/
.785)+1)));
    else
    bleed_rate_ftr_cmd(j)=0;
    end

bleed_rate_ftr_cmd(j)=min(0,bleed_rate_ftr_cmd(j))*nz_ftr(j)/nz_max_ftr(1);

    if V_ftr(j) > V_bdt(j)
    V_ftr(j+1)=V_ftr(j+1) + bleed_rate_ftr_cmd(j)*dt;
    end

    nz_ftr_cmd(j)=max(0.5,norm_nz_cmd(j)*min(1,abs(.3/d_phi3(j))));
```

```
    wsp=sqrt(S*c_bar*(.5*V_ftr(j)^2*0.002048)*0.7/Iy_ftr);

    nz_onset_rate(j)=wsp^2*nz_ftr_cmd(j-min((j-1),5))-wsp^2*nz_ftr(j)-
2*wsp*0.8*nz_onset(j);
    nz_onset(j+1)=nz_onset(j)+nz_onset_rate(j)*dt;
    nz_ftr(j+1)=nz_ftr(j)+nz_onset(j+1)*dt;

    ftr_radius(j)=V_ftr(j)^2/(g*nz_ftr(j+1));

    if V_ftr(j) < 500
        nz_max_ftr(j+1) = V_ftr(j)^2/(g*min_ftr_radius);
    else
        nz_max_ftr(j+1)=nz_max_ftr(1);
    end


    %%% This is an experimental section to deal with offesnive vs defensive
    ang_adv(j)=(pi-abs(ATA_bdt(j))-abs(TA(j)))/(2*pi);
    nrg_adv(j)=(exp(-Es_bdt(j)/Es_ftr(j))-exp(-1));
    k_cz(j+1)=(ang_adv(j)+nrg_adv(j));
end

%%%%%%%%%%%%   Plot Functions   %%%%%%%%%%%%%%%%


angles_bdt(:,1)=wrapTo180(rad2deg(angles_bdt(:,1)));
angles_bdt(:,2)=wrapTo180(rad2deg(angles_bdt(:,2)));
angles_bdt(:,3)=wrapTo360(rad2deg(angles_bdt(:,3)));
angles_ftr(:,1)=wrapTo180(rad2deg(angles_ftr(:,1)));
angles_ftr(:,2)=wrapTo180(rad2deg(angles_ftr(:,2)));
angles_ftr(:,3)=wrapTo360(rad2deg(angles_ftr(:,3)));
ATA(:)=rad2deg(ATA);
ATA_bdt(:)=rad2deg(ATA_bdt);
TA(:)=rad2deg(TA);


figure;
subplot(6,1,1);
plot([0:dt:time],angles_bdt(:,1),'r','linewidth',2); hold;
plot([0:dt:time],angles_ftr(:,1),'b','linewidth',2);
ylabel('AOB','fontsize',8);
grid on; axis ([0 time -180 180]);%1.2*min(angles_ftr(:,1))-10
1.2*max(angles_ftr(:,1))+10]);
subplot(6,1,2);
plot([0:dt:time],-angles_bdt(:,2),'r','linewidth',2); hold;
plot([0:dt:time],-angles_ftr(:,2),'b','linewidth',2);
ylabel('Pitch','fontsize',8);
grid on; axis ([0 time min(angles_ftr(:,2))-120 max(angles_ftr(:,2))+120]);
subplot(6,1,3);
plot([0:dt:time],angles_bdt(:,3),'r','linewidth',2); hold;
plot([0:dt:time],angles_ftr(:,3),'b','linewidth',2);
ylabel('Heading','fontsize',8);
grid on; axis ([0 time 1.1*min(angles_ftr(:,3))-20
1.1*max(angles_ftr(:,3))+20]);
subplot(6,1,4);
```

```
plot([0:dt:(time-dt)],ATA_bdt,'b','linewidth',2); hold;
plot([0:dt:(time-dt)],TA,'r','linewidth',2);
ylabel('ATA / TA','fontsize',8);
grid on; axis ([0 time min(ATA_bdt)-10 max(ATA_bdt)+30]);
subplot(6,1,5);
plot([0:dt:time],V_bdt,'r','linewidth',2); hold;
plot([0:dt:time],V_ftr,'b','linewidth',2);
plot([0:dt:time],crnr_arspd*ones(length(V_ftr)),'b--');
grid on; axis ([0 time .9*min(min(V_ftr(:)),min(V_bdt(:)))
1.1*max(max(V_ftr(:)),max(V_bdt))]);
ylabel('Velocity','fontsize',8);
subplot(6,1,6);
plot([0:dt:time],nz_bdt,'r','linewidth',2); hold;
plot([0:dt:time],nz_ftr,'b','linewidth',2);
grid on; axis ([0 time 0 10]);
ylabel('Nz Command','fontsize',8);
xlabel('Time (sec)');
xlabel('Time (sec)');



figure;
grid on;
axis([-5000 5000 -5000 5000 0 10000]);
% axis([-5000 5000 -1000 9000 0 10000]); %For abeam scenario
xlabel('Xi (ft)');
ylabel('Yi (ft)');
zlabel('Zi (ft)');

hbdt = animatedline('color','r','linewidth',2);
hbdtmkr = animatedline('color','r','linewidth',2,'marker','o');
hftr = animatedline('color','b','linewidth',2);
hftrmkr = animatedline('color','b','linewidth',2,'marker','o');
hcz = animatedline('color','k','linewidth',1,'marker','x');

for y = 1:run_time
for k=1:cz_dim+1
addpoints(hcz,r_i_bdt_cz(y,1,k),r_i_bdt_cz(y,2,k),r_i_bdt_cz(y,3,k));
end
addpoints(hbdt,r_i_bdt(y,1),r_i_bdt(y,2),r_i_bdt(y,3));
addpoints(hftr,r_i_ftr(y,1),r_i_ftr(y,2),r_i_ftr(y,3));
drawnow limitrate;
clearpoints(hcz);
end
hold;
for k=2:cz_dim
plot3(r_i_bdt_cz(end,1,k),r_i_bdt_cz(end,2,k),r_i_bdt_cz(end,3,k),'kx','linew
idth',1);
end
plot3(r_i_bdt_ap(end,1,1),r_i_bdt_ap(end,2,1),r_i_bdt_ap(end,3,1),'ko','linew
idth',2)
plot3(r_i_bdt(end,1),r_i_bdt(end,2),r_i_bdt(end,3),'ro','linewidth',2);
plot3(r_i_ftr(end,1),r_i_ftr(end,2),r_i_ftr(end,3),'bo','linewidth',2);

if time>=3
```

```
plot3(r_i_bdt(150:150:end,1),r_i_bdt(150:150:end,2),r_i_bdt(150:150:end,3),'r
o','linewidth',2);

plot3(r_i_ftr(150:150:end,1),r_i_ftr(150:150:end,2),r_i_ftr(150:150:end,3),'b
o','linewidth',2);
end


r_i_ftr(end,:)
angles_ftr(end,:)
V_ftr(end)
nz_ftr(end)
ATA_bdt(end)
r_i_bdt(end,:)
angles_bdt(end,:)
V_bdt(end)
nz_bdt(end)
TA(end)
r_i_bdt_ap(end,:)
ATA(end)
norm_nr_cmd(end)

%%%% Supporting functions %%%%

% Calculate skew matrix
function [s] = skew( w )
s=[0 -w(3) w(2);...
    w(3) 0 -w(1);...
    -w(2) w(1) 0];
end

% Rotation matrix from inertial-frame to body-frame
function rbi = R_BI(phi, theta, psi)
    rbi=[[(cos(theta)*cos(psi)) (cos(theta)*sin(psi)) (-sin(theta))];
    [(sin(phi)*sin(theta)*cos(psi)-cos(phi)*sin(psi)) ...
    (sin(phi)*sin(theta)*sin(psi)+cos(phi)*cos(psi)) ...
    (sin(phi)*cos(theta))];
    [(cos(phi)*sin(theta)*cos(psi)+sin(phi)*sin(psi)) ...
    (cos(phi)*sin(theta)*sin(psi)-sin(phi)*cos(psi)) ...
    (cos(phi)*cos(theta))]];
    rbi=[1 0 0; 0 -1 0; 0 0 -1]*rbi;
end

% Rotation matrix from body-frame to radial-frame
function rrb = R_RB(nr, theta, phi)
    nr=max(nr,0.0000001);
    mu=asin(sin(theta)/nr);
    nu=asin(sin(phi)/nr);
    R_mu=[[(cos(mu)), 0, (-sin(mu))];
    [0 1 0];
    [(sin(mu)) (0) (cos(mu))]];
    R_nu=[[1 0 0];
    [0 (cos(nu)) (sin(nu))];
    [0 (-sin(nu)) (cos(nu))]];
    rrb=R_nu*R_mu;
```

```
end

%Calculate Euler angles, w_dot
function [ omega_dot ] = R_Eul(angles,omega)
phi=angles(1);
theta=angles(2);
psi=angles(3);
P=omega(1);
Q=omega(2);
R=omega(3);
omega_dot=[1 sin(phi)*tan(theta) cos(phi)*tan(theta);...
    0 cos(phi) -sin(phi);...
    0 sin(phi)*sec(theta) cos(phi)*sec(theta)]*[P Q R]';
end

%Full EOM
function [kin_output] = kin_input(angles,u,v,w,lift,T,D,m)
u_dot=r*v-q*w-32.2*sin(angles(2))+(D+T)/m;
v_dot=-r*u*p*w+32.2*sin(angles(1))*cos(angles(2));
w_dot=q*u-p*v+32.2*cos(angles(1))*cos(angles(2))+lift/m;
kin_output=[u_dot; v_dot; w_dot];
end

function [mom_output] = mom_input(omega,omega_dot,Ix,Iy,Iz,Ixz)
P_dot=omega_dot(1);
Q_dot=omega_dot(2);
R_dot=omega_dot(3);
T = Ix*IZ-Ixz^2;
roll_l=Ix*P_dot-Ixz*(R_dot-P*Q)+(Iz-Iy)*R*Q;
pitch_m=Iy*Q_dot+Ixz*(P^2-R^2)+(Ix-Iz)*P*R;
yaw_n=Iz*R_dot-Ixz*(P_dot-Q*R)+(Iy-Ix)*P*Q;
end
```

Appendix C

Table C-1. P_s Modeling Data (Sea Level)

	Airspeed (ft/sec)									
G	0	100	200	300	400	500	600	700	800	900
0	-1200	250	300	400	500	600	700	900	900	700
1	-1200	50	100	300	400	490	520	840	740	600
2	-1200	-300	-100	100	150	330	460	650	650	590
3	-1200	-1200	-600	-100	50	250	300	470	550	490
4	-1200	-1200	-1200	-600	-700	150	180	300	370	290
5	-1200	-1200	-1200	-1000	-900	-700	100	230	150	100
6	-1200	-1200	-1200	-1200	-1200	-1000	-100	100	50	0
7	-1200	-1200	-1200	-1200	-1200	-1200	-800	-300	-300	-300
8	-1200	-1200	-1200	-1200	-1200	-1200	-1200	-800	-800	-800
9	-1200	-1200	-1200	-1200	-1200	-1200	-1200	-1200	-1200	-1200

Table C-2. P_s Modeling Data (5k')

	Airspeed (ft/sec)									
G	0	100	200	300	400	500	600	700	800	900
0	-1300	150	200	300	400	500	600	800	800	600
1	-1300	-50	0	200	300	390	420	740	640	500
2	-1300	-400	-200	0	50	230	360	550	550	490
3	-1300	-1300	-700	-200	-50	150	200	370	450	390
4	-1300	-1300	-1300	-700	-200	50	80	200	270	190
5	-1300	-1300	-1300	-1100	-700	-200	0	130	50	0
6	-1300	-1300	-1300	-1300	-1300	-600	-200	0	-50	-100
7	-1300	-1300	-1300	-1300	-1300	-1300	-600	-400	-400	-400
8	-1300	-1300	-1300	-1300	-1300	-1300	-1300	-800	-800	-800
9	-1300	-1300	-1300	-1300	-1300	-1300	-1300	-1300	-1300	-1300

Table C-3. P_s Modeling Data (10k')

	Airspeed (ft/sec)									
G	0	100	200	300	400	500	600	700	800	900
0	-1350	100	150	250	350	450	550	750	750	550
1	-1350	-100	-50	150	250	340	370	690	590	450
2	-1350	-450	-250	-50	0	180	310	500	500	440
3	-1350	-1350	-750	-250	-100	100	150	320	400	340
4	-1350	-1350	-1350	-750	-250	0	30	150	220	140
5	-1350	-1350	-1350	-1150	-750	-250	-50	80	0	-50
6	-1350	-1350	-1350	-1350	-1350	-650	-250	-50	-100	-150
7	-1350	-1350	-1350	-1350	-1350	-1350	-650	-450	-450	-450
8	-1350	-1350	-1350	-1350	-1350	-1350	-1350	-850	-850	-850
9	-1350	-1350	-1350	-1350	-1350	-1350	-1350	-1350	-1350	-1350

Table C-4. P_s Modeling Data (15k')

	Airspeed (ft/sec)									
G	0	100	200	300	400	500	600	700	800	900
0	-1400	50	100	200	300	400	500	700	700	500
1	-1400	-150	-100	100	200	290	320	640	540	400
2	-1400	-500	-300	-100	-50	130	260	450	450	390
3	-1400	-1400	-800	-300	-150	50	100	270	350	290
4	-1400	-1400	-1400	-800	-300	-50	-20	100	170	90
5	-1400	-1400	-1400	-1200	-800	-300	-100	30	-50	-100
6	-1400	-1400	-1400	-1400	-1400	-700	-300	-100	-150	-200
7	-1400	-1400	-1400	-1400	-1400	-1400	-700	-500	-500	-500
8	-1400	-1400	-1400	-1400	-1400	-1400	-1400	-900	-900	-900
9	-1400	-1400	-1400	-1400	-1400	-1400	-1400	-1400	-1400	-1400

Table C-5. P_s Modeling Data (20k')

	Airspeed (ft/sec)									
G	0	100	200	300	400	500	600	700	800	900
0	-1470	-20	30	130	230	330	430	630	630	430
1	-1470	-220	-170	30	130	220	250	570	470	330
2	-1470	-570	-370	-170	-120	60	190	380	380	320
3	-1470	-1470	-870	-370	-220	-20	30	200	280	220
4	-1470	-1470	-1470	-870	-370	-120	-90	30	100	20
5	-1470	-1470	-1470	-1270	-870	-370	-170	-40	-120	-170
6	-1470	-1470	-1470	-1470	-1470	-770	-370	-170	-220	-270
7	-1470	-1470	-1470	-1470	-1470	-1470	-770	-570	-570	-570
8	-1470	-1470	-1470	-1470	-1470	-1470	-1470	-970	-970	-970
9	-1470	-1470	-1470	-1470	-1470	-1470	-1470	-1470	-1470	-1470

Table C-6. P_s Modeling Data (25k')

	Airspeed (ft/sec)									
G	0	100	200	300	400	500	600	700	800	900
0	-1540	-90	-40	60	160	260	360	560	560	360
1	-1540	-290	-240	-40	60	150	180	500	400	260
2	-1540	-640	-440	-240	-190	-10	120	310	310	250
3	-1540	-1540	-940	-440	-290	-90	-40	130	210	150
4	-1540	-1540	-1540	-940	-440	-190	-160	-40	30	-50
5	-1540	-1540	-1540	-1340	-940	-440	-240	-110	-190	-240
6	-1540	-1540	-1540	-1540	-1540	-840	-440	-240	-290	-340
7	-1540	-1540	-1540	-1540	-1540	-1540	-840	-640	-640	-640
8	-1540	-1540	-1540	-1540	-1540	-1540	-1540	-1040	-1040	-1040
9	-1540	-1540	-1540	-1540	-1540	-1540	-1540	-1540	-1540	-1540

Appendix D

BIOGRAPHICAL STATEMENT

Jeff Dean was born in Arlington, Texas in 1979. He attended the United States Naval Academy and graduated with a B.S. in Control Systems Engineering in 2002. Upon graduation, he was commissioned a Second Lieutenant in the United States Marine Corps. He flew F/A-18 Hornets for several years and graduated from the Navy Fighter Weapons School (TOPGUN) and the Marine Corps Weapons and Tactics Instructor (WTI) Course. In 2014, then-Major Dean graduated from the United States Air Force Test Pilot School in Edwards Air Force Base, where he received a M.S. in Flight Test Engineering. He is now a Captain for FedEx Express, and he continues to serve in the United States Marine Corps Reserve. Jeff has flown more than 4,000 hours in 39 different types of aircraft.